Deutsches Biomasseforschungszentrum
gemeinnützige GmbH

Tagungsband 2

Workshop CFD

Computational Fluid Dynamics (CFD) and biomass thermochemical Conversion

September 30, 2014 | Leipzig

Computational Fluid Dynamics (CFD) and biomass thermochemical Conversion

September 30, 2014

- Conference Proceedings -

Organizer:

DBFZ Deutsches Biomasseforschungszentrum gemeinnützige GmbH
Torgauer Straße 116
04347 Leipzig, Germany
Phone: +49 (0)341 2434 - 112
Fax: +49 (0)341 2434 - 133
info@dbfz.de
Internet: www.dbfz.de

Scientific Contact:

Fouzi Tabet
Phone: +49 (0)341 2434-495
E-Mail: fouzi.tabet@dbfz.de

Imprint

Computational Fluid Dynamics (CFD) and biomass thermochemical Conversion at September 30, 2014

Published by:
Prof. Dr. mont. Michael Nelles

DBFZ Deutsches Biomasseforschungszentrum gemeinnützige GmbH, Leipzig, an enterprise of the German Governement with funding from the Federal Ministry of Food and Agriculture pursuant to a resolution by the German Bundestag.

Federal Ministry
of Food
and Agriculture

DBFZ Deutsches Biomasseforschungszentrum
gemeinnützige GmbH
Torgauer Straße 116
04347 Leipzig
Germany
Phone: +49 (0)341 2434-112
Fax: +49 (0)341 2434-133
info@dbfz.de
www.dbfz.de

General Management:
Prof. Dr. mont. Michael Nelles
(Scientific Managing Director)
Daniel Mayer
(Administrative Managing Director)

ISSN: 2199-9384

Responsibility for the content lies with the publishers.

Pictures: DBFZ, © davis - Fotolia.com

Editing & DTP: Paul Trainer
Frontpage: Stefanie Bader/Steffen Kronberg

Editorial deadline: September 30, 2014
Date of Publication: December 09, 2014

Table of content

KEYNOTES (ABSTRACTS)

FULL PAPER

POSTER

ANNEX

Words of welcome

Dear Participants of the 1. CFD-Workshop,

Fouzi Tabet (DBFZ)

DBFZ Deutsches Biomasseforschungzentrum gemeinnützige GmbH is actively involved in several areas of CFD (Computational Fluid Dynamics) with an emphasis on biomass thermochemical conversion.

Given the high importance of CFD application to biomass thermochemical conversion, DBFZ has decided to organize every year an international workshop on this topic with the aim to provide a forum for researchers around the world to share practical experiences and address the current opportunities and limitations of CFD in the field of biomass thermochemical conversion.

The 1st edition of the workshop took place at DBFZ in September the 30th, 2014.

The workshop gave an exposure to the major areas of research in CFD applications to biomass thermochemical conversion with special focus on the following topics:

- Small scale combustion
- Medium and large scale combustion
- Co-firing
- Gasification

Several sessions covering the above topics including guest plenary and poster exhibitions of research work were organized.

The workshop was a great success with high level of participation from countries like Norway, Germany, Austria, the Netherlands, France, Belgium, etc. The presenters did an outstanding job of sharing their expertise. During this first edition, 11 contributed papers were presented in addition to 2 plenary lectures and 5 posters. The papers corresponding to the workshop contributions are being published in this proceedings. I would like to thank the participants (committees members and authors) for their contribution to the 1st international workshop on CFD (Computational Fluid Dynamics) and biomass thermochemical conversion.

Sincerely,

F. TABET

KEYNOTES (ABSTRACTS)

Øyvind Skreiberg (SINTEF, Norway)

Keynote: Biofuels of the future and modelling implications

SINTEF Energy Research
Kolbjørn Hejes vei 1A, Trondheim, Norway
Oyvind.Skreiberg@sintef.no

KEYWORDS: Biofuels, torrefaction, carbonization, combustion, modelling.

The most challenging biofuels are the solid biofuels. Within the solid biofuels a fuel quality ladder can be defined, where low-quality and cheaper solid biofuels typically will require more plant investments and downstream cleaning efforts. Low-quality solid biofuels can be upgraded through various processes to give better quality fuels. Biofuels of the future may include a number of fuels, from very low quality heterogeneous and high moisture content fuels to high quality biocarbon.

Untreated low quality fuels have inherent properties that makes modelling more challenging. Fuel mixtures are more demanding with respect to the need for separate sets of input data for each fuel in the mixture, however, they behave “independently”. Upgraded, e.g. using torrefaction or carbonization, low quality biofuels have fuel characteristics demanding a completely new set of input parameters in modelling. Benefits of torrefied and carbonized fuels that also makes modelling easier are loss of moisture, loss of volatiles and to some extent ash (especially catalytic elements), loss of the fibrous structure and smaller and more uniform particles when grinded. However, more focus needs to be put on heterogeneous reactions for upgraded fuels. A major challenge is the increased lack of knowledge of fuel type and pretreatment conditions.

Fouzi Tabet (DBFZ, Germany)

Keynote: Towards efficient and environmental friendly heating using CFD

Fouzi Tabet, Andrea Dernbecher, Andreas Ortwein
DBFZ Deutsches Biomasseforschungszentrum gemeinnützige GmbH
Torgauer Straße 116, D-04347 Leipzig, Germany
fouzi.tabet@dbfz.de, andera.dernbecher@dbfz.de, andreas.ortwein@dbfz.de

KEYWORDS: Biomass, combustion, CFD modelling, NO_x emissions, Ash related problems

CFD modelling is a powerful and reliable tool to design, analyze and optimize operating conditions. Its application to biomass combustion enables to solve numerous technical issues in particular those related to operating. This presentation provides a review on CFD modelling of emissions from biomass combustion, with a particular focus on NO_x and ash related problems modelling. The models are provided for small scale biomass combustion technologies.

The prediction of NO_x in biomass combustion is, mainly, based on two approaches. The first one, often applied in post-processing, consists of solving transport equations for NO_x precursors. The second one, more expensive in terms of computing time, combines detailed or reduced chemical mechanisms of NO_x formation with gas phase kinetics models.

Formation process of fly ash leads to bimodal particle size distribution (inorganic fly ash and coarse fly ash). Ash related problems modelling account for inorganic fly ash formation and transport, coarse fly ash entrainment from the fuel bed and deposition of ash particles inside the boiler. Two types of models are available. The first category of models uses Eulerian approach for inorganic fly ash and Lagrangian approach for coarse fly ash while the second one considers the GDE (General Dynamic Equation) equation for the whole fly particles spectrum. Solving the GDE equation enables to predict particles size distribution which is not the case with first category models.

FULL PAPER

Martin Miltner (Institute of Chemical Engineering, Vienna University of Technology, Austria)

Application of CFD methods to the optimization of an innovative combustion apparatus for baled biomass

Martin Miltner, Michael Harasek, Anton Friedl
Institute of Chemical Engineering, Vienna University of Technology
Getreidemarkt 9/166,
1060 Vienna, Austria
martin.miltner@tuwien.ac.at, michael.harasek@tuwien.ac.at, anton.friedl@tuwien.ac.at

The current work presents the application of CFD for the development and optimisation of a novel combustion apparatus based on compressed biomass bales. A commercial CFD solver is combined with a proprietary FVM-solver to extend the capabilities towards the description of heterogeneous combustion steps. A detailed description of the applied modelling approaches covering mainly mass but also heat transfer aspects is provided. The results presented clearly indicate that CFD is a powerful tool for qualitative and quantitative description of biomass combustion. The application of this tool allows for a significant reduction of time and costs for the development of innovative chemical engineering concepts.

KEYWORDS: Biomass, Combustion, Emission reduction, NO_x, Straw, CFD

1. INTRODUCTION

Biomass combustion for the combined production of electrical power and heat is a field of ever growing importance in consideration of GHG abatement and the foreseeable depletion of fossil fuels. Despite the extensive knowledge already publicly available, substantial R&D efforts are still undertaken. These works typically focus on the development and implementation of novel combustion concepts as well as on the optimisation of existing processes. CFD is accepted to be a tool of great practical value during these steps of development and optimisation.

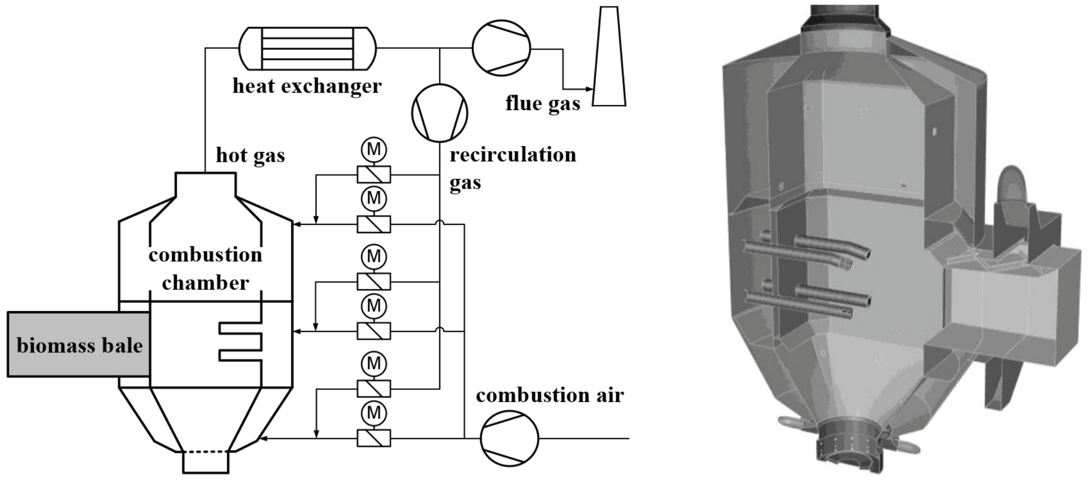

Figure 1: Basic flow sheet of the combustion cycle and geometrical overview of the novel combustion chamber

In the present study, CFD is used for the development and optimisation of an innovative combustion chamber for a solid biofuel in the form of non-disintegrated bales of whole crop maize. The novel design makes use of combustion air staging during combustible gas and residual char burnout as well as substantial flue gas recirculation for combustion temperature control. A flow sheet of the combustion cycle and a drawing of the combustor geometry are given in Figure 1. The main objective of this investigation is the minimisation of the gaseous emissions such as volatile organic components (VOCs), carbon monoxide and nitrogen oxide. Furthermore, the thermal output of the apparatus shall be maximised by an optimisation of the bale burnout. The theoretical analysis takes advantage of the accompanying pilot test operation carried out at a medium scale pilot plant with 2 MW thermal output. Experimental results are used for model development, validation and parameter optimisation.

2. METHODS

CFD modelling and simulations have been performed applying the commercial FVM-solver ANSYS FLUENT© 6.3 and extending the capabilities especially towards the description of heterogeneous combustion steps. The solid biomass fuel phase has been modelled in a separate proprietary FVM-solver environment applying a dual grid approach for spatial discretisation. Geometry pre-processing has been conducted using ANSYS GAMBIT© 2.4 tool with a special focus on a high percentage of hexahedral cells, low geometrical distortion and local refinement in regions of higher gradients anticipated. The size of the used computational grids ranges from 0.64 to 3.93 million cells depending on the degree of details.

Stationary simulations of the fluid phase have been performed applying the segregated solution of continuity equation, energy equation, species conservation equations and Reynolds-averaged Navier-Stokes-equation. Menter's widely accepted SST-k-ω-model [05] has been chosen for the description of the turbulence effects within the combustion chamber. The performance of this model has been compared against experimental results and literature data for the test cases of straight and slightly rotating turbulent free jets in a preliminary study [06]. It has been decided that these free jets comprise the most relevant features of the turbulent flow field within the combustion chamber. It is widely accepted that turbulent free shear flows are very well described by the k-ε-approach. Nevertheless, also wall-bounded shear flows seemed to be of importance for the combustion chamber simulation which are better described by the k-ω-formulation. Thus, the application of the blending SST-k-ω-model was substantially justified.

The gaseous composition inside the combustor is described by the 'species transport'-approach defining ten 'command' species of molecular type (H_2, H_2O, CO, CO_2, C_xH_y, O_2, NH_3, HCN, NO and N_2). C_xH_y is used as a lumped species representing hydrocarbons from C1 to C3. These species participate in overall seven homogeneous gas phase reactions which are assumed to describe the combustion process sufficiently. Authors followed the suggestions of Zhou et al. [11] to keep the reaction scheme as simple as possible to enhance the numerical stability and the convergence behaviour. The considered reactions together with their respective rate expressions have been reported by Miltner et al. [07]. The reaction scheme considers oxidation of H_2, C_xH_y and CO and four additional reactions comprising the model for estimation of NO_x-emissions from fuel-bound nitrogen containing the two NO_x-precursor species NH_3 and HCN. For the coupling of chemical reaction kinetics with reactant mixing due to turbulent diffusion the Eddy-Dissipation-Concept (EDC) by Magnussen and Hjertager has been chosen [04].

Gaseous species are released during the heterogeneous processes of moisture evaporation, volatilisation and residual char combustion. The development of this model was extensively supported by thermogravimetric analysis (TGA) of the considered biomass for different reaction regimes. For modelling purposes, the solid fuel has then been subdivided into the pseudo-components cellulose, hemicellulose, lignin and moisture (initial contents 54.6 wt%dm, 16.4 wt%dm, 29.0 wt%dm and 8.9 wt%raw respectively). The volatilisation behaviour of the analysed biomass fuel has then been approximated by a first-order kinetic scheme with a lumped-parameter approach. Volatile and residual fractions of the pseudo-components as well as pre-exponential factors and activation energies of the Arrhenius approach have been linearly optimised to reproduce the TGA results with high quality. The non-volatile fractions for cellulose, hemicellulose and lignin constitute the residual amount of char which is gradually formed during volatilisation. The respective conversion rate formulation and parameter set is given in Eqs. (1) - (4) below. Final parameters have been compared to literature data and very good correlation has been found [03, 09, 10]. Furthermore, the rate formulations for moisture evaporation and lignin volatilisation have been extended by additional functions to improve the predictions at lower solid fuel temperatures. The release rate of gaseous components is connected to the mass-loss of solid fuel and the ratio of considered gas species is kept constant throughout the volatilisation process.

$$\frac{\partial \dot{m}_{\mathrm{H2O,\,p}}}{\partial t} = -\frac{\partial \dot{m}_{\mathrm{H2O,\,gas}}}{\partial t} = -2.291 \cdot 10^{-4} \cdot \left|T_{\mathrm{p}} - 470\right|^{7} \cdot \exp\left(-\frac{84{,}767}{\mathrm{R}T_{\mathrm{p}}}\right) \cdot \dot{m}_{\mathrm{H2O,\,p}} \tag{1}$$

$$\frac{\partial \dot{m}_{\mathrm{Cell,p}}}{\partial t} = -3.497 \cdot 10^{11} \cdot \exp\left(-\frac{124{,}158}{\mathrm{R}T_{\mathrm{p}}}\right) \cdot \left(\dot{m}_{\mathrm{Cell,p}} \cdot \frac{100 - 0.535}{100}\right) \tag{2}$$

$$\frac{\partial \dot{m}_{\mathrm{Hcell,p}}}{\partial t} = -1.073 \cdot 10^{5} \cdot \exp\left(-\frac{74{,}796}{\mathrm{R}T_{\mathrm{p}}}\right) \cdot \left(\dot{m}_{\mathrm{Hcell,p}} \cdot \frac{100 - 42.566}{100}\right) \tag{3}$$

$$\frac{\partial \dot{m}_{\mathrm{Lign,p}}}{\partial t} = -0.002254 \cdot \exp\left(-\frac{3{,}413}{\mathrm{R}T_{\mathrm{p}}}\right) \cdot \left(\dot{m}_{\mathrm{Lign,p}} \cdot \frac{100 - 41.891}{100}\right) \cdot \left(0.5 \cdot \mathrm{tanhyp}\left(\frac{T_p - 405}{0.145 \cdot 100}\right) + 0.5\right) \tag{4}$$

The oxidation of the residual char fraction has been modelled as a combination of oxygen adsorption from the gas to the carbon surface (film diffusion approach using the Colburn-factor) and a subsequent Arrhenius-type oxidation reaction to CO and CO_2. This approach has been adapted from literature and has already been reported in a previous work [07]. The char combustion reaction rate in the kinetic-dominated regime is determined by Eqs. (5) and (6) below. This formulation contains a non-constant pre-exponential factor for the carbon oxidation reaction in order to capture the effect of thermal char deactivation at higher temperatures. Thermal deactivation of the char oxidation has been considered to be a function of the volatilisation temperature as reported by Zolin et al. [12]. An exponential function has been developed to properly fit the experimental data published in this literature study.

$$\left(\frac{\partial \dot{m}_{\mathrm{char}}}{\partial t}\right)_{kinetic} = -k_{char,kinetic} \cdot p_{\mathrm{O2,surface}} \cdot \dot{m}_{\mathrm{char}} = A_{\mathrm{char}} \cdot \exp\left(-\frac{135{,}000}{\mathrm{R}T_{\mathrm{p}}}\right) \cdot p_{\mathrm{O2,surface}} \cdot \dot{m}_{\mathrm{char}} \tag{5}$$

$$A_{\mathrm{char}} = A_{\mathrm{char}}(T_{\mathrm{vol}}) = \begin{cases} 1.44773460 \quad \text{for} \quad T_{\mathrm{vol}} < 1{,}000\,\mathrm{K} \\ \exp\left(\begin{array}{l} 4.3349 \cdot 10^{-10} T_{\mathrm{vol}}^{4} - 2.1935 \cdot 10^{-6} T_{\mathrm{vol}}^{3} \\ + 4.0778 \cdot 10^{-3} T_{\mathrm{vol}}^{2} - 3.3089 T_{\mathrm{vol}} + 991.48 \end{array}\right) \\ 0.00273239 \quad \text{for} \quad T_{\mathrm{vol}} > 1{,}520\,\mathrm{K} \end{cases} \tag{6}$$

The reaction rate in the diffusion-dominated regime is calculated following the works of Dwivedi and co-author [01] by utilisation of the Colburn-factor and its dependence on dimensionless Sh, Sc and Re numbers. The complete derivation of this model is provided in a former publication of the author [07]. Making use of gas properties (density, viscosity, diffusion coefficient, and mean velocity), char properties (molar mass and surface area) and the stoichiometric ratio of CO/CO_2 denoted as Φ the reaction rate is determined by Eq. (7). The stoichiometric ratio of CO/CO_2 for the char combustion is depending on the particle temperature in an Arrhenius-type approach as provided by Zhou at al. [11]. This stoichiometric ratio is also used in the calculation of oxygen depletion and carbon monoxide/dioxide generation in the adjacent gas phase. The diffusion coefficient of oxygen in air which is used in the heterogeneous char combustion model has been calculated using the equations of Wilke and Lee given in Poling et al. [8].

$$\begin{aligned} \left(\frac{\mathrm{d}\dot{m}_{\mathrm{char}}}{\mathrm{dt}}\right)_{\mathrm{diffusion}} &= -k_{\mathrm{char,diffusion}} \cdot \frac{p_{\mathrm{O2,bulk}} - p_{\mathrm{O2,surface}}}{\mathrm{R} \cdot T_{\mathrm{p}}} \cdot \Phi \cdot \mathrm{M}_{\mathrm{char}} \cdot A_{\mathrm{char}} \\ \textit{where} \quad k_{\mathrm{char,diffusion}} &= \frac{D^{2/3} \cdot v_{\mathrm{s,gas}} \cdot \rho_{\mathrm{gas}}^{2/3}}{\eta_{\mathrm{gas}}^{2/3} \cdot \varepsilon_{\mathrm{solid\,bed}}} \cdot \left(\frac{0.765}{Re_{\mathrm{d}}^{0.82}} + \frac{0.365}{Re_{\mathrm{d}}^{0.386}}\right) \end{aligned} \tag{7}$$

Joining both rate expressions leads to a combined model for kinetic/diffusion-controlled regimes. Introducing an effective mass transfer coefficient calculated as a series of mass transfer resistances this complete model is given by Eq. (8). Heat transfer has been accounted for by a mixed model considering convective and conductive heat transport within the porous solid fuel regions as well as the heat transfer between solids and gaseous phases due to convection and radiation. A detailed description of the applied approach is given in Miltner et al. [07]. Another sub-model has been developed for the description of the fluid dynamic behaviour of the solid biomass (pressure drop as a function of gas velocity and degree of solid burnout). A combination of the well-accepted Ergun equation with an estimation of the Forchheimer parameters for packed beds has been adapted from literature [02] and complemented by own experimental findings.

$$\begin{aligned} \left(\frac{\partial \dot{m}_{\mathrm{char}}}{\partial t}\right)_{\mathrm{effective}} &= -k_{\mathrm{char,effective}} \cdot p_{\mathrm{O2,bulk}} \cdot \dot{m}_{\mathrm{char}} \\ \textit{where} \quad k_{\mathrm{char,effective}} &= \frac{1}{\dfrac{1}{k_{\mathrm{char,kinetic}}} + \dfrac{1}{k_{\mathrm{char,diffusion}}} \cdot \dfrac{\dot{m}_{\mathrm{char}}}{\mathrm{M}_{\mathrm{char}}} \cdot \dfrac{\mathrm{R} \cdot T_{\mathrm{p}}}{\Phi \cdot A_{\mathrm{char}}}} \end{aligned} \tag{8}$$

3. RESULTS

The heterogeneous combustion model has been validated against a number of experimental TGA results. Drying and volatilisation has been examined under nitrogen atmosphere at different heating rates and different inert gas flow rates. Residual char burnout has been analysed at constant temperature (800 °C) for different reactive gas flow rates and different oxygen contents. The results of this validation are given in Figure 2. The agreement for drying and volatilisation is remarkably good for the entire analysed operational range while char combustion shows small deviations especially for lower oxygen contents. Nevertheless, it can be concluded that the model quality is sufficient for the intended purposes.

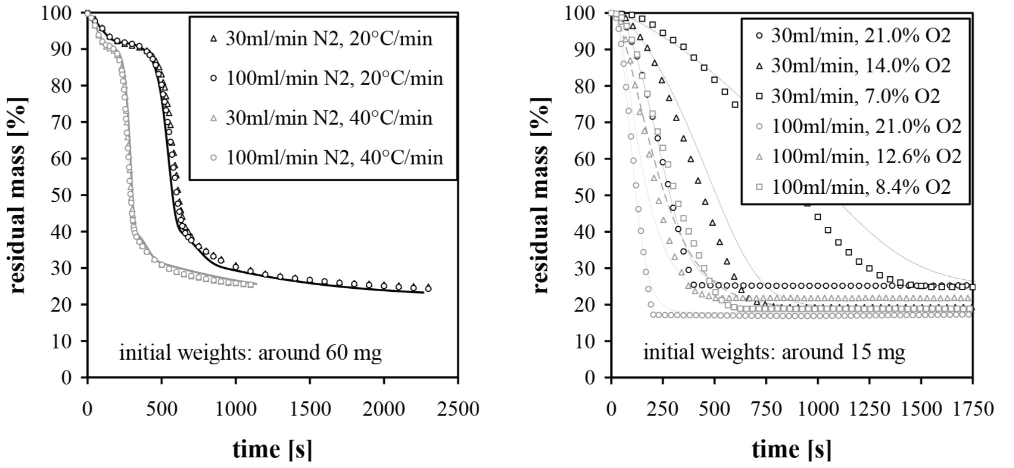

Figure 2: Model prediction vs. experimental TGA results: biomass drying and volatilisation at different inert gas flows and heating rates (left); residual char combustion at different reactive gas flows and oxygen contents (right)

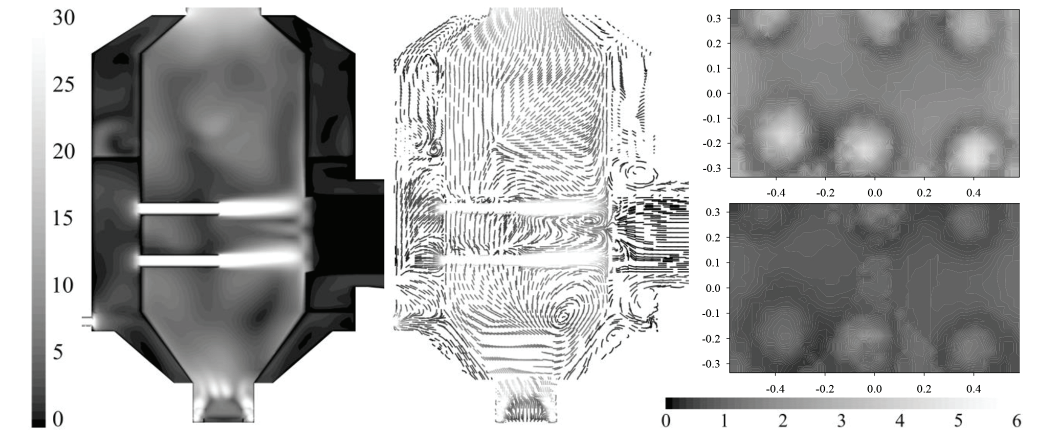

Figure 3: Contours of gas velocity magnitude and gas streamlines (0 – 30 m/s) in the bulk phase; contours of gas velocity magnitude (0 – 6 m/s) in the biomass bale region (top: bale surface, bottom: 12cm below bale surface)

Figure 3 gives a short impression of the gas flow field within the bulk phase as well as the porous biomass bale region. The impinging turbulent free jets arising from the primary air nozzles are clearly observable and lead to noticeable heterogeneous conditions at the biomass bale and non-ideal coverage of the bale surface. Figure 4 shows some exemplary simulation results for the solid biomass fuel phase. It can be concluded that the heterogeneous incident flow results in a partially unbalanced solid burnout. The high flow velocity and oxygen content of the primary air jets induce local 'hot spots' of particle temperature, volatilisation (minor extent) and char burnout rates. This inhomogenity leads to a non-ideal utilisation of the whole primary combustion zone for volatilisation as well as char burnout from the reaction engineering point of view. The resulting 'burn holes' in the bale surface have also been experimentally observed and are a starting point for primary air nozzle optimisation.

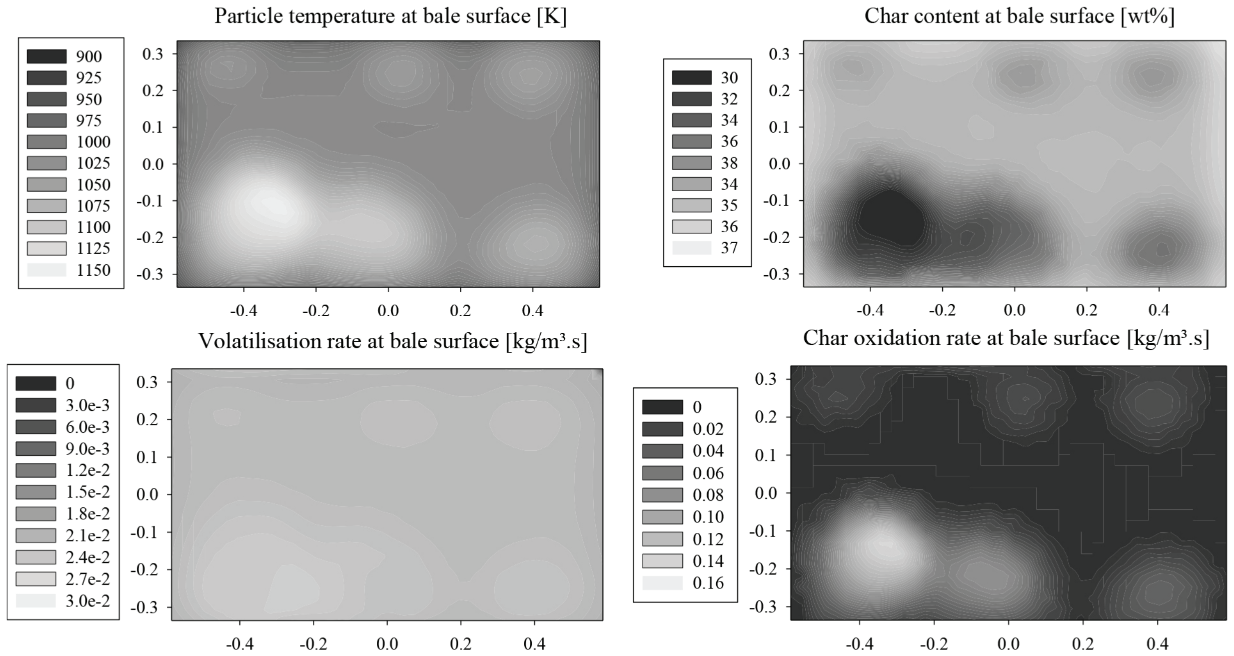

Figure 4: Simulation results of the solid biomass fuel phase at the bale surface

4. CONCLUSIONS

A complex three-dimensional model for the detailed description of heterogeneous biomass combustion has been implemented within a CFD simulation environment. The developed tools have been applied for the optimization of an innovative combustion chamber based on baled herbaceous biomass. Results clearly indicate the benefits of a deeper insight into the heterogeneous combustion steps. The analysis of the solid phase simulation results revealed a significantly unbalanced bale burnout induced by the non-ideal design and positioning of the primary air nozzles. It is expected that a more even coverage of the burning bale surface with impinging primary air jets would lead to a nameable improvement of the utilisation of the combustion chamber. Thus, the thermal load of the apparatus could be increased, unburnt carbon in the ash fraction as well as in the flue gas (CO, VOCs) could be decreased. This geometry optimisation can be performed in a very structured way by the application of the presented CFD approach. A high number of geometrical variations can be analysed by simulation avoiding time- and cost-intensive experimental work. As only pre-optimised combustor designs would have to be analysed in combustion experiments, the overall time-to market and the development costs of innovative combustion concepts such as the currently investigated would be significantly reduced.

5. ACKNOWLEDGEMENTS

The authors gratefully acknowledge the financial support from the European Union (NNE5-2001-00517), the Austrian Research Promotion Agency (FFG-818597) as well as the support from project partners WTI GmbH and Federspiel Oekotechnology Consulting GmbH.

6. REFERENCES

[01] Dwivedi P N, Upadhyay S N (1977). Particle-Fluid Mass Transfer in Fixed and Fluidized Beds. Industrial & Engineering Chemistry Process Design and Development 16, pp. 157-165.
[02] Eric A et al. (2012). Experimental determination thermo physical characteristics of balled biomass. Energy 45, pp. 350-357.
[03] Grammelis P, Kakaras E (2005). Biomass Combustion Modeling in Fluidized Beds. Energy & Fuels 19, pp 292-297.
[04] Magnussen B F, Hjertager B H. (1977). On mathematical modeling of turbulent combustion with special emphasis on soot formation and combustion. Symposium (International) on Combustion 16, pp. 719-729.
[05] Menter F R. (1994). Two-equation eddy-viscosity turbulence models for engineering applications. AIAA journal 32, pp. 1598-1605.
[06] Miltner M, Harasek M, Jordan C. (2014). On the Applicability of RANS-Turbulence Models in CFD Simulations for the Description of Turbulent Free Jets during Biomass Combustion. Chemical Engineering Transactions 39, pp. 913-918.
[07] Miltner M et al. (2008). Computational fluid dynamic simulation of a solid biomass combustor: modelling approaches. Clean Technologies and Environmental Policy 10, pp. 165-174.
[08] Poling B E, Prausnitz J M, O´Connell J P. (2001). The Properties of Gases and Liquids, 5th Edition, McGraw-Hill, New York, USA.
[09] Raveendran K, Ganesh A, Khilar K C. (1995). Influence of mineral matter on biomass pyrolysis characteristics. Fuel 74, pp. 1812-1822.
[10] Skodras G et al. (2006). Pyrolysis and Combustion Characteristics of Biomass and Waste-Derived Feedstock. Industrial & Engineering Chemistry Research 45, pp. 3791-3799.
[11] Zhou H et al. (2005). Numerical modeling of straw combustion in a fixed bed. Fuel 84, pp. 389-403.
[12] Zolin A et al. (2002). Experimental study of char thermal deactivation. Fuel 81, pp. 1065-1075.

Mateusz Szubel (AGH University of Science and Technology, Krakow, Poland)

The numerical methods as an essential tool for optimization of energy conversion degree in 180 kW biomass boiler

Mateusz Szubel, Mariusz Filipowicz
AGH University of Science and Technology
30 Mickiewicza Av. 30-059, Krakow, Poland
mszubel@agh.edu.pl, filipow@agh.edu.pl

Because of international regulations in range of pollutants emission, producers of heating devices are forced to conduct permanent process of optimization of manufactured boilers and furnaces. In the near future, in many european countries, the process of implementation of the newest international documents, which regulate properties of the solid fuels small combustion instalations will be started. Thanks to the experience, it was possible to define the most important areas of control, as the emission of carbon monoxide and dust. For producers of the boilers (and furnaces), new regulation means necessity of the new approach to design of offered devices. With the rapid advancement of digital computers, CFD is poised to remain at the forefront of cutting-edge research in the science of fluid dynamics and heat transfer. Also, the emergence of CFD as a practical tool in modern engineering practise is steadily attracting much interests [01].

The paper presents the analysis of possibility to use numerical modeling of the EKOPAL RM40 biomass boiler operation. The heating device, which is studied, is batch boiler, dedicated to combust straw and waste wood. In the RM 40 thermal decomposition of biomass occurs autothermally in primary chamber, in presence of moisture from fuel and controlled insufficiency of air. Major product of gasification is carbon monoxide (CO), which is transported to secondary chamber. In this part of evice the afterburning of CO occurs.

In some cases the method of fuel combustion described above is inefficient in given type of boiler, what results in too high CO content in exhaust. The goal of study described in this paper was to investigate selected possibilities to improve the post – combustion efficiency in case of the studied boiler. The relations between operation of the air distribution system and CO afterburning have been presented.

KEYWORDS: Boilers, biomass combustion, CO emission, CFD

1. INTRODUCTION

In the global scale it is possible to extract a series of biomass types. Depending on climatic zone, we can talk about agricultural and forest wastes, various organic residuals and rapidly growing energy crops [02]. Biomass energy utilization is based on different technologies and selection depends on many factors. The conversion of energy from biomass for electricity, heat or fuels can be carried out through direct combustion and processing for liquid and gaseous fuels. Currently, the technologies for distributed energy, that rely on the direct combustion process of the biomass becoming increasingly important. The most commonly used techniques for heating are here: fireplaces, stoves (including the accumulation stoves) and especially heating boilers. Choice of a suitable heating unit depends primarily on the designed power of the system, fuel type and its parameters as well as economic reasons [03]. In the case of rural areas it is always worthwhile to analyze the biomass potential in point of view of heat production. Cost effective heating using own straw is possible not only in case of the houses, but also livestock buildings and greenhouses

Emission of the pollutants from the process of biomass combustion can be divided into two groups. The first group includes chemicals produced in the incomplete combustion process. Such a group contains inter alia carbon monoxide, tar, polyaromatic hydrocarbons (PAHs), CxHy and soot. The second group includes pollutants, which depend on the fuel properties [05]. To provide efficient use of the energy, the combustion process has to be characterised by complete and total combustion of the fuel and lack of generation of the environmentally adverse substances.

Optimal process conditions can be achieved without construction of costly prototypes and long-term investigations, using numerical methods, such as computational fluid dynamics - CFD. Proper designing of the CFD model gives a series of informations, which can be related with flow phenomena, as well as the heat transfer or combustion reactions.

2. IMPACT OF PROPER AIR FEEDING AND DISTRIBUTION ON QUALITY OF THE BIOMASS COMBUSTION PROCESS

The number of parameters important from the combustion point of view, such as temperature of combustion, feeding and fragmentation of fuel, heat transfer as well as control and regulation have to be listed [05]. Despite this, appropriate air distribution in the area of the combustion seems to be particularly important and difficult issue. Air supply to the combustion chamber can be realised by the natural or forced way. In the bigger heating units the blowing fans are applied. It is popular solution inter alia in case of batch boilers based on straw combustion. The straw, as a kind of the biomass, is characterised by the high content of volatiles. In the batch boilers with relatively big combustion chamber, devolatilization may proceed unevenly, which results in ineffective air and volatiles mixing and consequently incomplete combustion (high CO emission) [05]. Incomplete combustion can be reduced thanks dedicated solution of the air distribution system, which allow to conduct the combustion process in two stages.

In the first step, the process of the straw thermal decomposition (gasification, devolatilization) occurs. In the second step, the combustible gas, which has been produced can be post-combusted in the second area. Practically it means, that air has to be divided into two regions: the primary and the secondary combustion chamber areas. Such a method of the combustion allows to reduce the emission of not only CO, but also hydrocarbons, PAHs, and unburned residues of the straw.

3. CHARACTERISTIC OF THE CONCERNED BIOMASS BATCH BOILER AND GOALS OF THE NUMERICAL MODELLING

The heating unit, which has been modelled is the 180 kW EKOPAL RM40 straw boiler (Figure 1a), situated in the experimental laboratory of the Faculty of Energy and Fuels at AGH University (Krakow, Poland). The device operates in two stage air supply system, based on the manifold installed on the back wall (Figure 1b). The primary as well as the secondary air is supplied using the same blowing fan. Seven parallel air ducts (marked at the Figure 1b as R1 to R7) are responsible for providing the air for the gasification, which proceeds in the primary combustion chamber. Two extra pipes (one duct visible in the figure 1b - marked as D1) are connected through the side walls of the secondary combustion chamber, to provide secondary air.

In a process of the numerical simulations of the boiler operation, the flow phenomena and reactions proceed in the secondary combustion chamber were studied. Current state of the air supply system has been analysed as a first step. Then chosen changes in range of air supply system were implemented, to investigate impact on the CO oxidation efficiency. The basic alteration was adding two extra secondary air ducts, situated on different height of the secondary combustion chamber side walls.

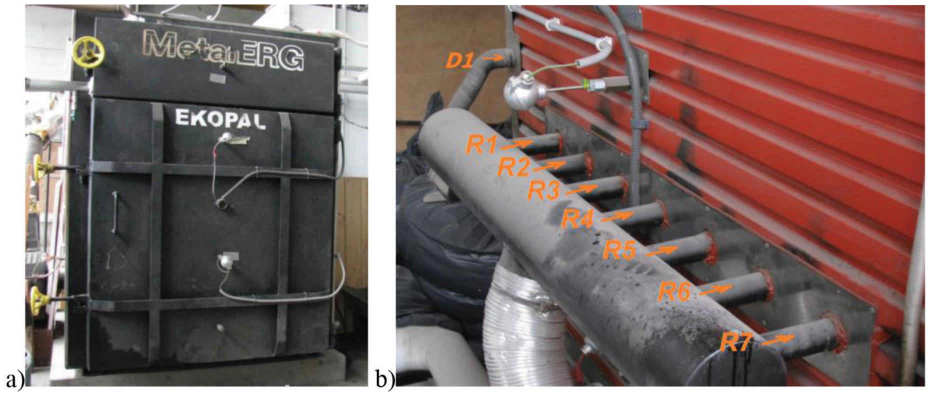

Figure 1: a) General view of the front of the EKOPAL RM 40 biomass boiler, b) air manifold installed on the back wall of the device.

4. PREPARING AND PERFORMANCE OF THE NUMERICAL MODEL

The next part of the paper describes stages of preparing and calculations of the numerical model and its utilization to studies of some flow phenomenons, occurring in the secondary combustion chamber during operation of the biomass boiler system. It was decided, that it is justified to ignore the primary chamber, because the moment, when the chamber is almost full of straw in the form of compressed blocks was considered. Intensity CO source as a results of biomass gasification is treated as constant. The fuel geometry variation as a result of combustion was not considered To simulate above montioned issues, the commercial tool ANSYS CFX has been used.

4.1. Design of the geometry and the computational grid

To perform the computations of the boiler model, the spatial geometry of the secondary combustion chamber has been designed. To create the block of modelled domain Autodesc Inventor 2013 software has been applied. The domain includes the vertical, general area of the post-combustion and the horisontal section of a dust collector.

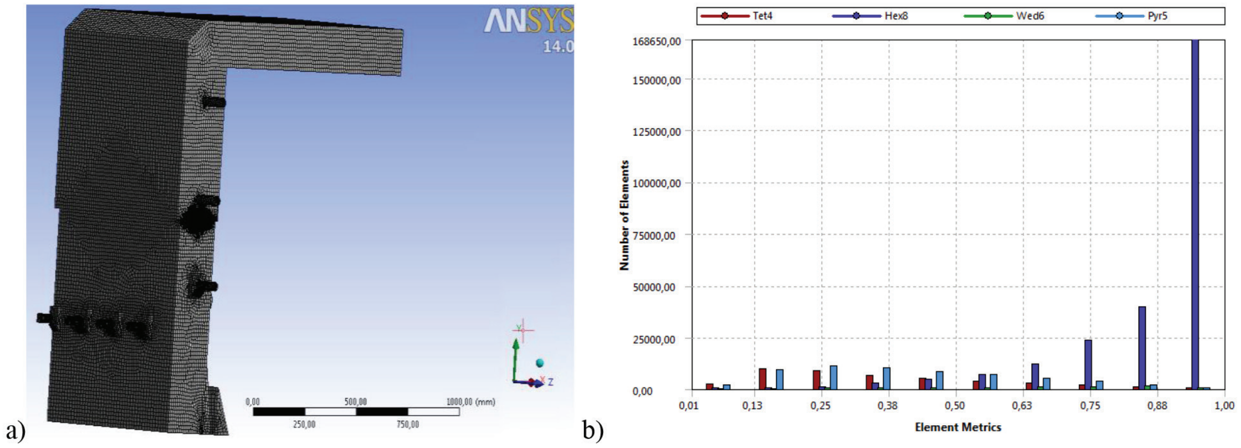

a) b)

Figure 2: a) Design of the geometry and computational grid generated in the ANSYS Meshing tool, b) Diagram representing quality of the grid

Designed geometry was imported into the ANSYS Design Modeler environment, and then transferred to the ANSYS Mesching, when discretization has been carried out.

A fine grid was imposed using the "hex dominant" method, which is one of available meshing modes. Figure 2b presents the number of grid elements characterized by given shape and size. The elements are mostly heksagonal, what is advantage in the computations performance point of view. The total number of the computational grid elements was 3,65x10^5.

4.2. Assumptions and boundary conditions

Because of non homogeneous air distribution along the pipes of the air manifold, the primary and secondary air inlets have been set as an individual parameters. The values of mass flow rates were calculated based on the measurements performed using thermoanemometers. The highest value of the mas flow was assumed for the central duct, situated on the symmetry plane of the geometry (R4, see Fig. 1b) and for the secondary air duct (D1?), 0,0237 kg/s and 0,0239 kg/s, respectively. The mass flow for other ducts (R1-R3 and R6-7) oscillate around 0,0235 kg/s. The mechanism of the chemical reaction of CO and O$_2$ was based on the Arrhenius equation, which is presented below (Equation 1).

$$k = Ae^{\frac{-E_a}{RT}} \tag{1}$$

where: k – reaction rate
A – pre exponential factor
E_a – energy of activation
R – universal gas constant
T – absolute temperature

The products of the biomass gasification have been limited to CO. Additional process of water evaporation has been included. The assumed source of CO and H_2O is marked in Figure 3,

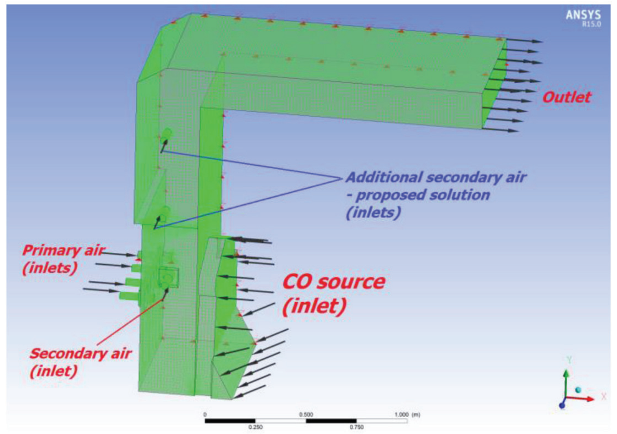

Figure 3: Boundary conditions and assumptions of the designed model

which shows all boundary conditions 3. Initial temperature of the domain has been set on the 1000 K level. The O$_2$ (0,21 mass %) and N$_2$ (0,79 mass %) were included as the only components of the air supplied by the inlet ducts. The two cases of air supply system are considered: a) without and b) with two extra supply ducts, indicated in Figure 3 by blue arrows. The aim of additional secondary air is to improve CO burn-up.

5. RESULTS AND DISCUSSION

In frames of described analysis, three simulations with application of the two different air supply systems have been performed. The results are presented in Figure 4 for chosen cross-sectional planes of the secondary chamber. Case I presented in Figure 4.I presents visualisation of the CO fraction in the secondary chamber in the current state of the analysed device. CO fraction shown in Figure 4.II is not significantly better comparing to 4.I. The secondary air has been provided using two extra ducts, but the air mass was still the same. Significant improvement of the combustion conditions is observed in the third example – see 4.III, where the air distribution in the basic ducts has been preserved, but with additional supply of the air mass (0,023kg/s per each of two pipes). The essentials reduction of the CO fraction is clearly visible, especially at the top of the secondaty chamber

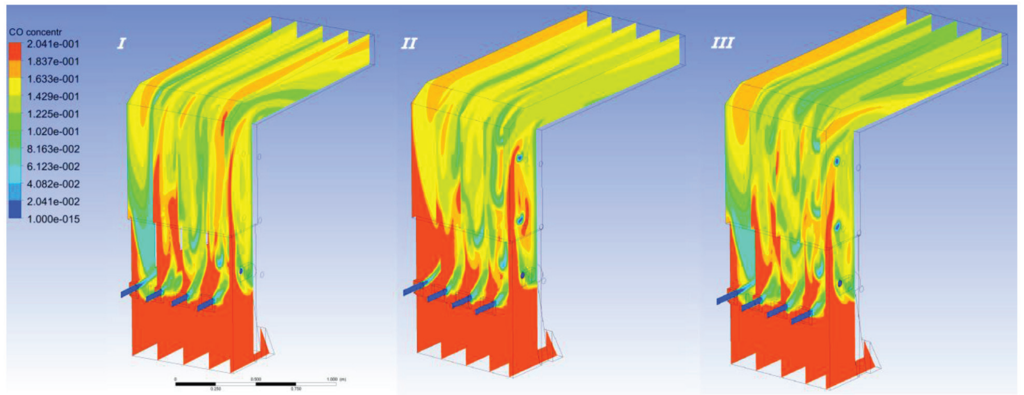

Figure 4: Three cases of the CO volume fraction considered in simulation. Different air supply system design and air flow conditions were applied (view of chosen cross-section planes of the secondary chamber and the symmetry plane).

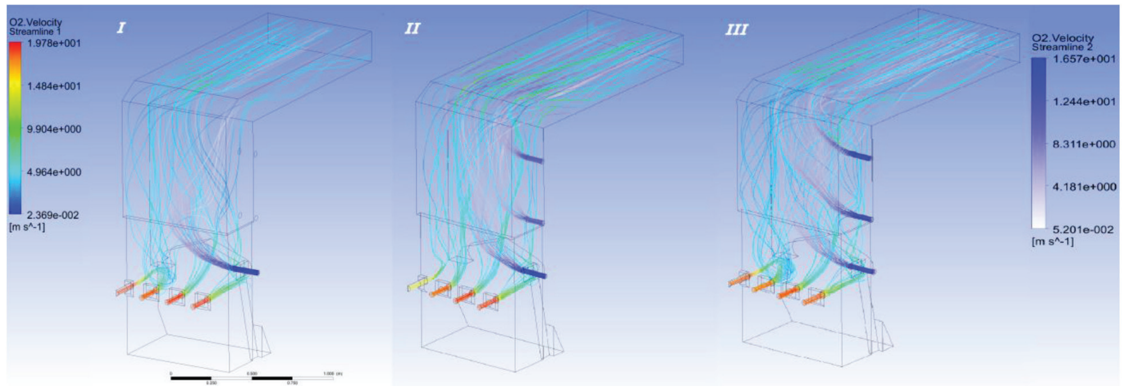

Figure 5 : *Comparison of the air distribution in considered cases (so-called velocity streamlines, primary air velocity – left legend, secondary air velocity – right legend)*

The reason of this phenomenon is stabilisation of the exhaust flow (more laminar). Such effect is clearly visible in the Figure 5, which presents considered cases of the air flow conditions: I – state of art, II – with two additional air ducts, but the total volume of the air is the same, III – as in II but with additional air volume. The region of the most intensive oxidation is the middle of the chamber. In this area two important processes occur. Firstly, mixing of the fuel and oxygen is the most efficient, which not occurs below the air feeders. Secondary, temperature of gases in such region of the chamber is relatively high – in III between 600 and 700˚C).

The highest content of the CO near to the level of the chamber floor is actually not problem, because entire gas is forced to move up, so it is pointless to attach importance to the air distribution in such part of installation.

6. CONCLUSION

In frames of the partially described works, the investigation of impact of parameters of the air supply system in the EKOPAL RM40 boiler on the efficiency of the combustion process and the emission of chosen pollutants has been performed. The appropriate position of the air supply inlets determines efficient mixing and reacting of CO and the oxidant (oxygen from the air). As a result of add the secondary air supply ducts, the reduction of the CO content in the exhaust has been reached. Thanks to the additional portion of the oxidant, increase of the combustion efficiency in the middle part of the secondary chamber is possible. The mixing degree of the combustible gases and oxygen, appropriate excess air ratio and temperature in the reaction area have been identified as the major factors influencing the environmental effect and efficiency of the combustion.

The numerical analysis presented in the paper are general and early stage of the more detailed investigation of the RM40 biomass boiler operation, aimed to develop a serie of recommendations related with the device optimization process.

7. ACKNOWLEDGEMENTS

The work done in frames of the Bio-Eco-Matic project: Construction of small to medium capacity boilers for clean and efficient combustion of biomass for heating

8. REFERENCES

[01] Chaoqun L, Jiyuan T, Guan-Heng Y (2013). Computational Fluid Dynamics. A practical Approach. Butterworth-Heinemann, Oxford.
[02] Bocian P, Golec T, Rakowski J (2010). Nowoczesne Technologie pozyskiwania i energetycznego wykorzystywania biomasy. Instytut Energetyki. Warszawa (in Polish).
[03] Szubel M, Haracz A, Wesołowski W, Podlasek P, Kopeć J (2014). Analiza wpływu warunków prowadzenia procesu spalania biomasy. Dokonania Młodych Naukowców 3. Digital document ISSN 2300-4436.
[04] Producer information materials, available in the Internet: http://www.metalerg.pl/index.php/ekopal-rm, access: 1.08.2014
[05] Rybak W (2006). Spalanie i współspalanie biopaliw stałych. Oficyna Wydawnicza Politechniki Wrocławskiej. Wrocław (in Polish).

Abdallah Elorf (ICARE-CNRS, Orléans, France)

Combustion of pulverized pomace olive

A. Elorf, N. Mrad-koched, S. Bostyn, B. Sarh, I. Gökalp, B. Izrar
ICARE, UPR 3021 du CNRS,
Université d'Orléans, France
abdallah.elorf@cnrs-orleans.fr

J. Chaoufi
LETSMP Faculté des sciences,
Université Ibn Zohr Agadir, Maroc

This paper presents a CFD simulation of pulverised pomace olive (PO) combustion in a 3D furnace using RANS methods for turbulent flow. Air is introduced through the lower base of the furnace. The particles of PO are injected perpendicularly to the central axe of furnace near the lower base. The mean size particle diameter is 100 µm. The PO is represented in the model as a solid hydrocarbon material containing moisture and ash, which undergoes drying, pyrolysis, and char combustion. The results obtained show that recirculation zone is deeply involved in the flame stabilization.

KEYWORDS: Biomass, combustion, non-premixed flam, pulverized pomace olive, 3D RANS simulation

1. INTRODUCTION

Biomass is an important fuel for heating and power generation. An understanding of the physical and chemical processes involved in biomass combustion is important for any application in which biomass combustion is required, including stoves, boilers, and large-scale burners [01] [02]. Substituting traditional fossil fuel with biomass in large scale combustion facilities is not only of significant importance for meeting society's energy needs, but can also make a huge contribution towards the reduction of greenhouse gases emitted into the atmosphere. Furthermore, the development of new technologies for utilization of biomass raises new opportunities for economic re-vitalization and growth [03] [04] [05].

Pomace Olive (PO), which is a waste of olive oil-mill, is an important biomass generated in Mediterranean countries and is available in large amounts at a very low cost. By-product of vegetable oils such us PO can be considered as alternative fuels [06]. PO actually is a waste and like other wastes can cause problems if suitable and acceptable disposal measures are not taken. Efficient use of PO in energy production solves the two problems in one step: clean energy production and acceptable disposal of olive-mill wastes. PO can be burned alone or can be combined with other combustible materials, like low calorific value lignite coals. Morocco is rich in olive trees. Annually, about 1.5 million tons of olive is used in olive oil production and approximately 675,000 tons of PO are produced. The calorific value (LHV) of this PO is about 12,500- 22,000 kJ/kg [6]. It is comparable with the calorific values of wood and soft coal, which are 17,000 and 23,000 kJ/kg, respectively. The sulfur content of PO is about 0.05- 0.1 wt%. Therefore, it is of prime importance to be able to burn this waste for producing clean energy in the regions where olive trees are raised. However, an appropriate technology must be employed to avoid the production of pollutants and other problems while maximizing process efficiency [06] [07].

Combustion of biomass waste is a promising technology being researched by the "Institut de Combustion Aérothermique Réactivité et Environnement". The project developed in the laboratory, called "VERA", is focused on the combustion of PO for heat and power generation.

The project links three complementary parts; (i) CFD simulation of pulverised PO combustion in a 3D furnace using RANS methods for turbulent flow, (ii) experimental study of PO combustion, (iii) ASPEN Plus simulation of the process. In this paper, our goal is to present the CFD simulation of PO combustion. Indeed, CFD simulation is a good way for understand the PO combustion processes. Not all the relevant phenomena in a combustion system are described in depth, but CFD calculations give an approximate overview of the system, helping to troubleshoot and fine-tune the system's operation, as well as give assistance when dealing with new designs. At present, there are still only a very few numerical simulations of biomass combustion systems using detailed models for both the bed and gas phases [01] [05].

2. POMACE OLIVE CHARACTERISTICS

Pomace olive was used as biomass feeding material taken from a Moroccan traditional unit of olive extraction. The initial moisture content of the PO was 18 %, which was reduced by drying. Drying process was carried out at 60°C air temperature in a convective dryer at airflow rate of 300 m^3/hr. PO composition is described by its ultimate and proximate analysis presented in table 1. The ultimate analysis was experimentally obtained using a organic elemental analyser whereas proximate analysis was calculated based on the thermogravimetric analysis showed in figure 1.

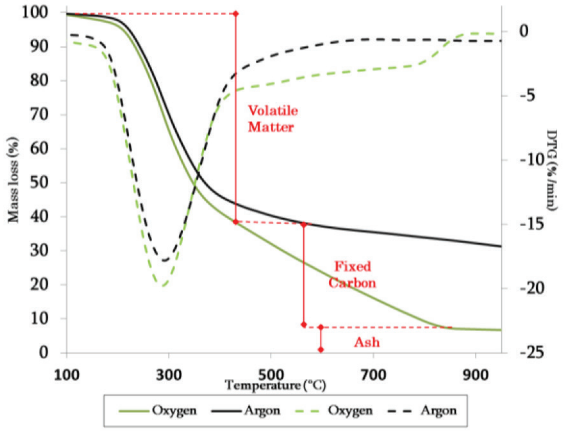

Proximate Analysis Wt%, dry - DAF	
Volatile Matter	64
Fixed Carbon	23,2
Ash	6,5
Moisture	6,5
Ultimate analysis (Wt %, dry)	
Carbon	59
Hydrogen	8,5
Nitogen	1,5
Sulphur	0
Oxygen	31

Figure 1: Thermogravimetric analysis of PO

Table 1: PO composition

PO used in this simulation has a low density of 600 kg/m^3, and a high heating value of 21.0 MJ/kg. The thermal analysis of PO chips TGA results in mass loss evolution and heat balance shown in Figure 6. Where drying, devolatiliztion and combustion of PO particles is demonstrated as a function of temperature.

The initial weight loss (~6 %) corresponds to the moisture not observed in this figure between 50 °C and 100 °C is attributed to the evaporation of the water from the particles. This event corresponds to the drying zone in the downdraft gasifier where heat generated from the exothermic combustion and gasification reactions at the center and bottom of the gasifier is used to supply the necessary sensible and latent heat for the release of moisture. [08]

The second event of the thermal analysis represents the devolatilization process where the volatiles are released at an onset temperature as low as 200 °C and continues till approximately 350 °C. In this model, the volatile content of char is assumed to decompose further into CO, H_2, H_2O, and N_2 by virtue of the fuels' proximate, ultimate, and heating value. The last event in the TGA thermal analysis represents the gasification of the char into H_2, CO, and CH_4 through reactions with hot gases and water vapor produced along the gasifiers upper zones [8]. This last event divided into two parts the first one represents fixed carbon (~23 %) and ash presents the second (~6 %).

3. COMPUTATIONAL METHOD AND MODELING

3.1. Geometry and mesh construction:

The burner configuration is developed in the laboratory ICARE. A schematic view of the burner is shown in Figure 2. The air inlet diameter d = 80 mm is used to calculate the non-dimensional data presented in the paper. The combustion chamber is a cylindrical tube with inner diameter of 500mm and total length of 1500mm. The particles of PO are injected perpendicularly to the central axe of burner near the lower base for particles injections.

As sketched in Figure 1, the model combustor is periodic and the computational domain covers a fraction of the total configuration to minimize the rate calculation.

Three computational structured grids (coarse, medium and a fine) are designed, as presented in Table 1. The difference in these three meshes is mainly due to different grid resolution requirements in order to have higher resolution in the injection pipe and in the flame region.

At the inlet the mass flow rate of air inlet and swirl air inlet are respectively m_{air} = 2.83 g/s and m_{swirl} = 4.55 g/s. A ratio of axial and tangential velocities *w/u=0.9* is introduced to give the flow the desired swirling velocity. In the burner the flame operates with a perfect mixing of fuel and air, for a global equivalence ratio $\Phi = 0.58$ at atmospheric pressure, the PO mass flow rate calculated is m_{PO} = 0.561 g/s.

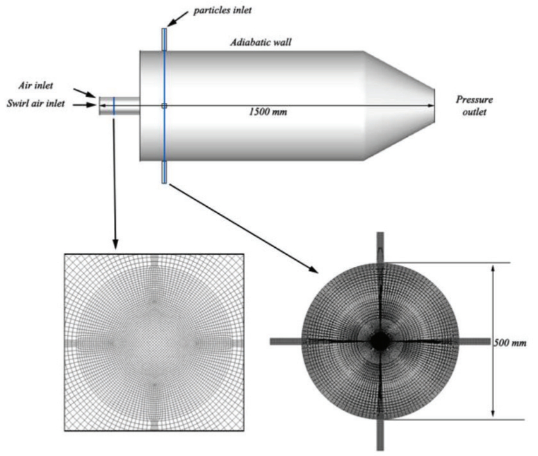

Figure 2: Geometry and computational mesh of 1956384 cells

Grid refinement	Total number of cells
Coarse	1956384
Medium	3960000
Fine	5460528

Table 1: Summary of grid refinement

3.2. Numerical modelling

Simulations were performed using the ANSYS-Fluent 14 CFD software. Turbulence was accounted for using the standard k–ε model; radiation using the P1 model and non-premixed combustion for model of combustion using the mixture fraction/PDF approach due to the greater computational efficiency [08]. In addition to solving transport equation for continuity momentum, energy, turbulence and combustion chemistry fluent simulates the discrete second phase in a lagrangian frame of reference. This second phase consist of spherical PO particles, dispersed in the continuous phase, that follow several heat and mass transfer relationships or laws [08]. Convergence criteria are set to 10^{-5} for all equations.

3.3. Calculation procedure

Study was undertaken to find the modelling procedure that would lead to the fastest convergence. That procedure used throughout the current work is as follows:

a. Solve non-reacting flow with no coupling between discrete and continuous phase.
b. Patch high temperature to burner region and solve for to ignite flame
c. Solve reaction flow performing 50 continuous phase iterations per discrete phase iteration.
d. The particles have uniform distribution and are spherical in shape with mean size diameter is 100 μm. To minimize the statistical errors we use 10 number of diameters model rosin-rammler

4. RESULTS AND DISCUSSION:

4.1. Grid sensitivity analysis

A grid convergence study has been conducted for three meshes discussed in Table 1. This analysis is done by simulating the non-reacting flow using the Standard k-ε model. Comparison of the mean axial velocity radial profiles in the burner is presented in Figure 4. Both profiles of fine and medium grids show the same trend in all axes z/d presented.

The profiles of the coarse grid illustrate a significant difference in the location of axial velocity peaks. Therefore, the medium grid was chosen for all calculation in the present study.

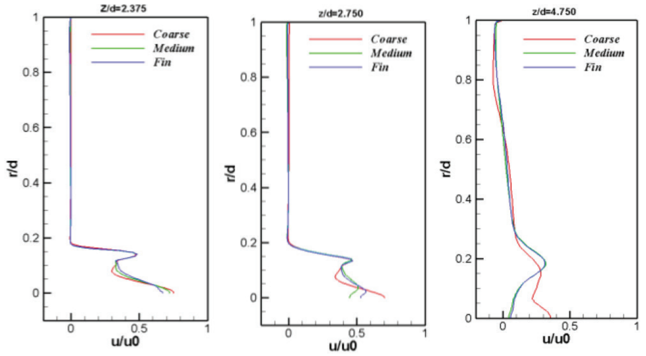

Figure 3: Grid sensitivity solutions of the radial profiles of the axial velocity at several locations.

4.2. Flow structure and temperature distribution in the combustion chamber

The development of the flow field over the combustion chamber is illustrated in Figure 4, using contours of axial velocity and streamline patterns. As expected from a turbulent swirling flow in burner, a recirculation zone was created. This recirculation zone is deeply involved in the flame stabilization process as it constantly puts hot burnt gases in contact with fresh gases allowing permanent ignition.

Figure 5 shows a predicted spatial distribution of temperature in the combustion chamber. The recirculation zone is partially filled with relatively homogenous burned gases, as expected in swirl-stabilized flames, with a maximum temperature of about 1500 K.

The separation of the combustion chamber into five temperatures zones can be observed. Significantly different temperature distribution is obtained for the pulverized PO combustion in air.

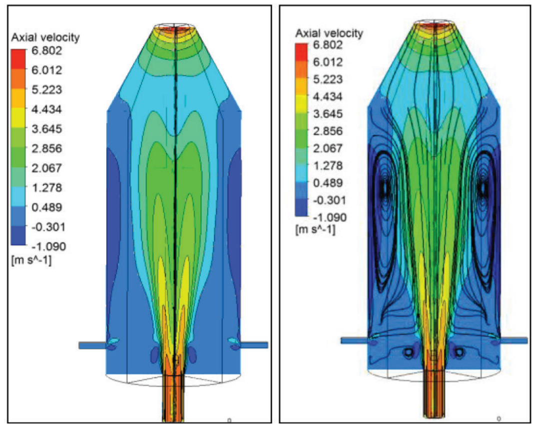

Figure 4: Predicted axial velocity contours (left) and

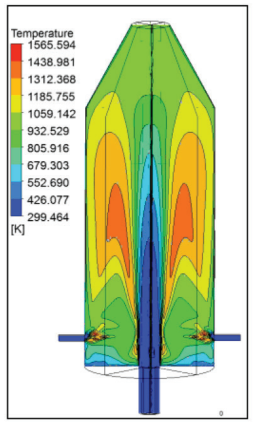

Figure 5: Gas temperature with streamline (right)

The maximum temperature reached is in the vicinity of 1566 K which is a common value for this type of combustion system. Also the ignition process of air-PO mixture appears at the outer border of the recirculation zone, and the combustion process also occurs inside the burner.

The temperature values are also related to the consumption of oxidizer to the interior of the combustion chamber which can be seen better on the temperature and oxygen distribution for four distances from the burner presented in Figure 6.

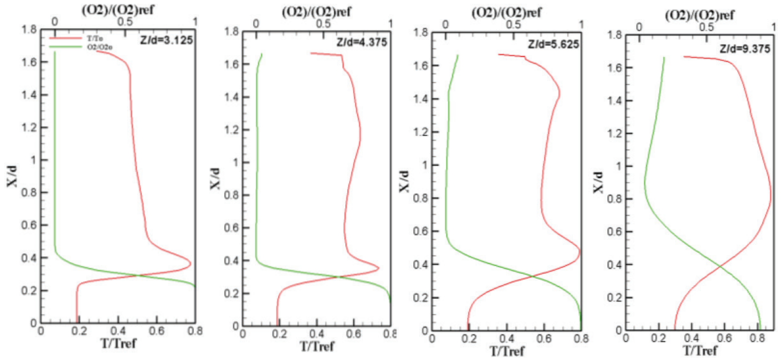

Figure 6: *Temperature radial profiles and mass fraction of* O_2

Figure above shows the strong relationship between the O_2 concentration and the gas temperature distribution. The low O_2 concentration zones in the furnace correspond to the high gas temperature zones.

4.3. Trajectory of particles

Trajectories of PO particles entering the furnace are shown in Figure 9. The averaged residence times of particles go from the 10 s. This not only affects the efficiency of combustion, in terms of unburned PO particles exiting the furnace, but also the distribution of particles through the upper outlet (fly ash).

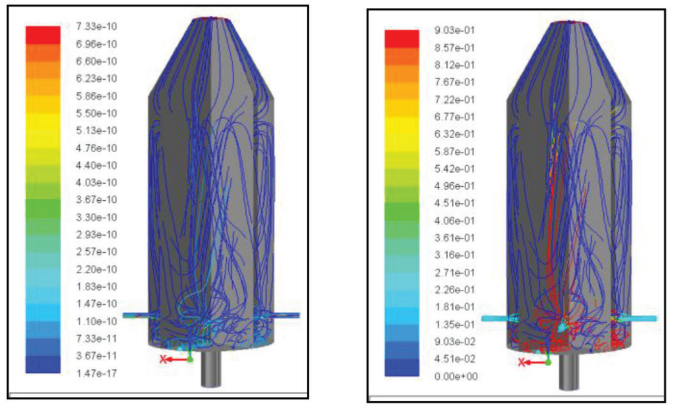

Figure 7: *Particles traces colored by particle mass (left) and particle char mass fraction (right).*

Initially, the PO contains 29.7 % char. This value is based on the total mass of the fixed carbon, which depends on the proximate analysis. As the composition of the particles is char, the mass is reduced with the degradation of the particles along their trajectories.

Also the char fraction of pulverized PO increases up to 91.2 %: devolatilization has ended and the particle has fixed carbon and ash. Thus, decreasing to a zero value indicates that all fixed carbon has been used up, and that only ash remains.

4.4. Gas emissions:

Figure 8 shows a distribution of Mass fraction Radial profiles of the CO_2 and CO for four distances from the burner z/d.

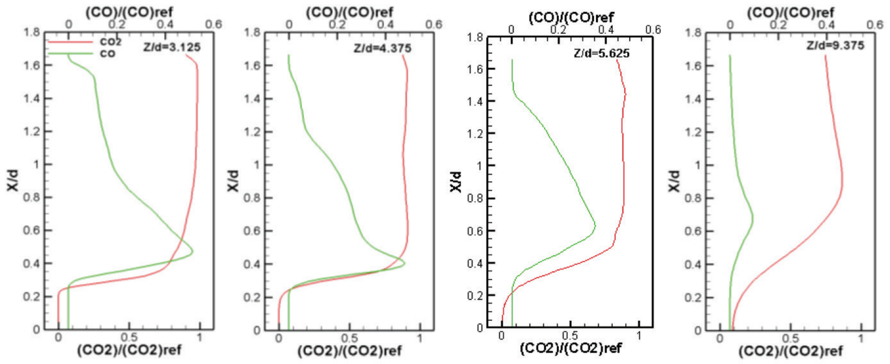

Figure 8: *Mass fraction radial profiles of the* CO_2 *and CO*

For the four face we see that the two evolutions of the mass fraction of CO and CO_2 increase in a similar fashion to a certain diameter in the chamber (X / D = 0.4). After this distance we can see that the emission of CO decreases until these reach 0. As against the CO_2 emissions increases until a maximum value and remains constant up to the walls.

5. CONCLUSION

This work summarized the CFD modeling tool to study combustion of pulverized PO in vertical furnace. The devolatilization of PO particles travelling through gas and char combustion has been simulated. Reaction has been modeled by the mixture fraction/PDF method, this approach which has been specifically developed for turbulent diffusion flames, offer many benefits over the finite rate formulation. There is evidence that CFD can be used as a powerful tool to predict characteristics of fuels and solid biomass during combustion.

6. REFERENCES

[01] Collazo J, Porteiro J (2012). Numerical modeling of the combustion of densified wood under fixed-bed conditions. Fuel 93, pp. 149–159.
[02] Al-attab KA, Zainal ZA (2011). Design and performance of a pressurized cyclone combustor (PCC) for high and low heating value gas combustion. Applied Energy 88, pp.1084–1095.
[03] Yin C, Rosendahl LA, Kær SK (2008). Grate-firing of biomass for heat and power production Progress in Energy and Combustion Science 34, pp. 725– 754.
[04] Zhang X, Ghamari M, Ratner A (2013). Numerical modeling of co-firing a light density biomass, oat (Avena sativa) hulls, and chunk coal in fluidized bed boiler. Biomass and Bioenergy 56, pp. 239-246.
[05] Topala H, Atimtay AT et al. (2003). Olive cake combustion in a circulating fluidized bed. Fuel 82, pp. 1049–1056.
[06] Atimtay AT, Topal H (2004). Co-Combustion of Olive Cake with Lignite Coal in a Circulating Fluidized Bed", Fuel 83, pp. 859-867.
[07] Macphee JE, Selliee M, Jermy M, Tadula E. CFD Modelling of pulverized coal combustion in a rotary lime kiln. Seventh International Conference on CFD in the Minerals and Process Industries CSIRO, Melbourne, Australia 9-11 December 2009
[08] Janarjeh I, AL Sharh M (2013). Numerical and experimental investigation of downdraft gasification of wood chips. Energy Conversion and Management 65, pp. 783–792.

Harold Garcia (Institute of Combustion and Power Plant Technology, University of Stuttgart, Germany)

Adapting a CFD code from coal to biomass combustion

Harold García, Uwe Schnell, Günter Scheffknecht
Institute of Combustion and Power Plant Technology (IFK), University of Stuttgart
Pfaffenwaldring 23, D-70569 Stuttgart, Germany
Harold.Garcia@ifk.uni-stuttgart.de, Uwe.Schnell@ifk.uni-stuttgart.de,
Guenter.Scheffknecht@ifk.uni-stuttgart.de

CFD calculations are widely used nowadays in firing systems to improve the understanding and optimization of the processes. Biomass combustion and co-combustion are attractive ways to reduce the energy dependency on fossil fuels. Existing CFD codes for the simulation of coal combustion need to be adapted to take into account the differences in the process between these solid fuels. Special interest has the pyrolysis, in which the major mass release during biomass combustion takes place; hence this work is focused on this process.

A multi-component, competitive mechanism of pyrolysis based on the three main biomass pseudo-components (cellulose, hemicellulose and lignin) is implemented in a pre-processing step in the CFD code AIOLOS, developed by the IFK (Institute of Combustion and Power Plant Technology) of the University of Stuttgart. Apparent kinetic parameters and reduction of the considered species are utilised to integrate the comprehensive pyrolysis model to the existing single reaction mechanism, without increasing the computational time.

Pyrolysis and combustion of coal and biomass in an entrained flow reactor are evaluated. It can be seen that the kinetic parameters of pyrolysis, as well as the composition of the released products have an important influence on the temperature and species distribution in the reactor. The implemented model improves the description of the biomass pyrolysis in AIOLOS, and offers a flexible and efficient way to evaluate this process and the combustion with different feedstocks under various conditions.

KEYWORDS: Biomass, pyrolysis, CFD

1. INTRODUCTION

One of the major challenges in the field of energy supply is replacing the big energy dependency on fossil fuels with renewable energy sources. Without an important increase of the use of biomass it would be hardly possible to reach the desired targets in terms of sustainable energy use. One of the most attractive ways of using biomass is switching from coal to biomass combustion or co-combustion, due to the already established knowledge and technologies in processes with this solid fuel.

Nowadays, the use of CFD calculations for firing systems is a common practice that helps to understand the physical phenomena and to optimise the overall process. The existing computational fluid dynamics (CFD) codes, developed for coal, can be used for the analysis of biomass combustion; however they need to be adapted, due to its different chemical and physical characteristics. In the combustion of biomass, up to 95 % of the mass release takes place in the pyrolysis; in the case of coal, the released volatile matter is typically less than 60 %. Therefore, a more accurate description of the devolatilisation process is recommendable.

Single one-step models are often utilised to model coal and biomass pyrolysis in CFD codes, with the limitation that the kinetic parameters are only valid for a determined feedstock, under specific operating conditions. It is well known that the characteristics of different biomasses can differ strongly from each other, which reduces the predictive capability of single reaction models. Therefore, the implementation of a more flexible and detailed pyrolysis model is desirable that can provide more appropriate predictions for different fuels under different conditions. At the same time, the model should remain as simple as possible to avoid an increase in computational time.

In this work, the CFD code AIOLOS, developed by the IFK (Institute of Combustion and Power Plant Technology) of the University of Stuttgart for the simulation of coal combustion, is adapted for the use of biomass. The work is specially focused on a better description of the pyrolysis process.

The next section introduces the existing single reaction model followed by the description of a more detailed multi-component, competitive mechanism and its integration in the single model through apparent kinetic parameters and the reduction of the number of considered species. In section 3, AIOLOS is described briefly before simulation results are shown to compare the pyrolysis and combustion of coal and biomass in an entrained-flow reactor.

2. PYROLYSIS OF BIOMASS

2.1. Single reaction model

The primary pyrolysis of coal is modelled with a single step reaction of the raw material decomposing to gas, char and tar:

$$\text{Coal} \rightarrow v_G\text{Gas} + v_C\text{Char} + v_T\text{Tar} \qquad (1)$$

The considered light gaseous species are CO, CO_2, H_2, H_2O and $C_mH_nO_p$ (light hydrocarbons), which is simplified to CH_4. The composition of the released gas is identified using proximate and elementary analysis of the fuel. Assuming that the fuel is mainly composed by the chemical elements C, H and O, three mass balances can be formulated and the amount of three volatile species can be calculated accordingly. Two additional volatile species can be determined using experimentally observed ratios of CO/CO_2 and CH_4/CO_2 [06][12]. The tar fraction is approximated as $C_xH_yO_z$ with an H/C molar ratio of 1.1 and O/C molar ratio that is assumed to be equal to that of the parent coal [05][07].

The devolatilisation rate is calculated using an Arrhenius expression:

$$K = k_0 \exp(-E/RT) \qquad (2)$$

where k_0 is the pre-exponential factor, *E* is the energy of activation and *R* is the ideal gas constant.

2.2. Detailed reaction model

Physical and chemical characteristics of biomasses can differ strongly, which limits the predictive capability of the devolatilisation rate and the composition of the products with single reaction models. For different raw materials and operating conditions (heating rate, temperature, etc.), the kinetic parameters and the composition of the products have to be known à priori and must be set in the code.

These problems can be avoided with the use of multi-component, competitive models. In these models, biomass is described in terms of its three major pseudo-components: cellulose, hemicellulose and lignin. The feedstock can be adapted changing the proportions of those components accordingly. Furthermore, the competitive nature of the scheme allows that the gas, char and tar yields change according to the conditions of the pyrolysis process (temperature, heating rate, etc.).

Several pyrolysis models can be found in the literature, however, very few multi-component mechanisms of biomass pyrolysis are available [03]. Among them, the kinetic scheme proposed in [10] and modified in [02] was chosen. This model incorporates multi-step mechanisms for the three main pseudo-components that includes 19 reactions and considers around 36 species distributed as follows: 10 light gases, 10 lumped tars, 10 intermediate, and 6 solid species. As an example, the scheme of the cellulose decomposition is shown:

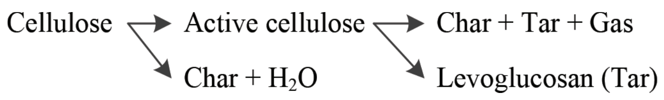

$$\begin{tikzcd}\text{Cellulose} \arrow[r] \arrow[dr] & \text{Active cellulose} \arrow[r] \arrow[dr] & \text{Char + Tar + Gas} \\ & \text{Char} + H_2O & \text{Levoglucosan (Tar)}\end{tikzcd} \qquad (3)$$

Different mechanisms are applied to the other two pseudo-components. A more detailed description of the model can be found in [10].

The relative residual mass and mass release rate of pinewood (cellulose: 0.5, hemicellulose: 0.27, lignin: 0.23 in mass proportions [09]) and its pseudo-components obtained with the detailed model are shown in Figure 2. It can be seen that the hemicellulose decomposes at lower temperatures, cellulose requires higher temperatures, whereas lignin decomposition occurs slowly over a broad range of temperatures.

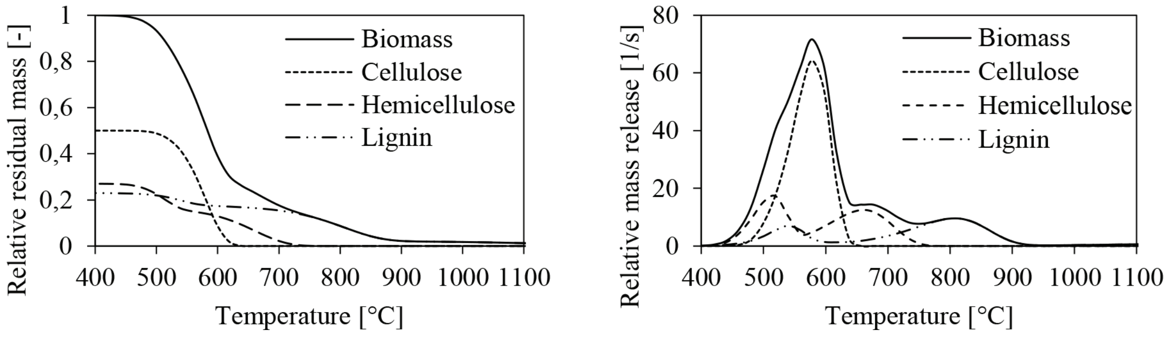

Figure 2: Relative residual mass (left) and relative mass release rate (right) of pinewood and its pseudo-components for a heating rate of 10000 K/s

2.3. Single reaction model with apparent kinetic parameters

The direct implementation of detailed models in CFD codes is often restricted by the increase of computational time and code complexity. One possible way to avoid these difficulties is the inclusion of apparent kinetic parameters to the existing global reaction model [02]. These parameters refer to an optimal set of values (k_0,E), which its replacement in the global reaction model minimizes an established error function. The chosen function is the mean squared error defined as [13]:

$$e = \sqrt{\sum(\widehat{m}_i - m_i)^2/N} \qquad (4)$$

here, N is the number of the data, while $\widehat{m}_i$ and m_i are the relative residual masses calculated with the global and the detailed model, respectively. Figure 3 compares the relative residual mass and relative mass release of pinewood obtained with the detailed model and the single reaction model with the determined apparent kinetic parameters.

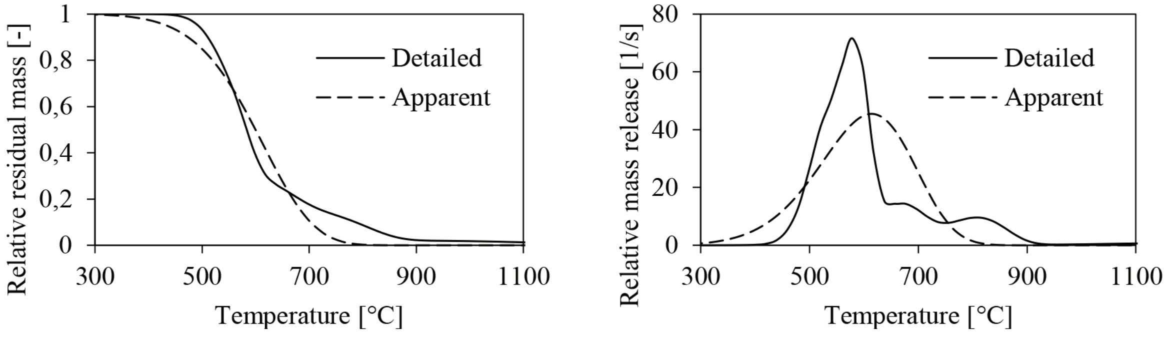

Figure 3: Relative residual mass (left) and relative mass release (right) of pinewood for a heating rate of 10000 K/s calculated with the detailed model and the single reaction model with apparent parameters

In order to reduce the number of considered species and to use the same species contemplated in AIOLOS, mean compositions of the lumped tar and light hydrocarbons are calculated from the detailed model. The resulting composition of the products is supposed to be valid during the whole pyrolysis process. The mean composition of the products for the pyrolysis of pinewood (cellulose: 0.5, hemicellulose: 0.27, lignin: 0.23 in mass proportions [9]), spruce (cellulose: 0.41, hemicellulose: 0.31, lignin: 0.28 in mass proportions [1]) is shown in Figure 4. Additionally, the pyrolysis products composition of a typical brown coal with an assumed ratio of $CO/CO_2 = 0.5$ is shown for comparison. Both biomasses show a very high amount of volatiles release, especially tars, and a low char formation, as is expected for the high heating rate.

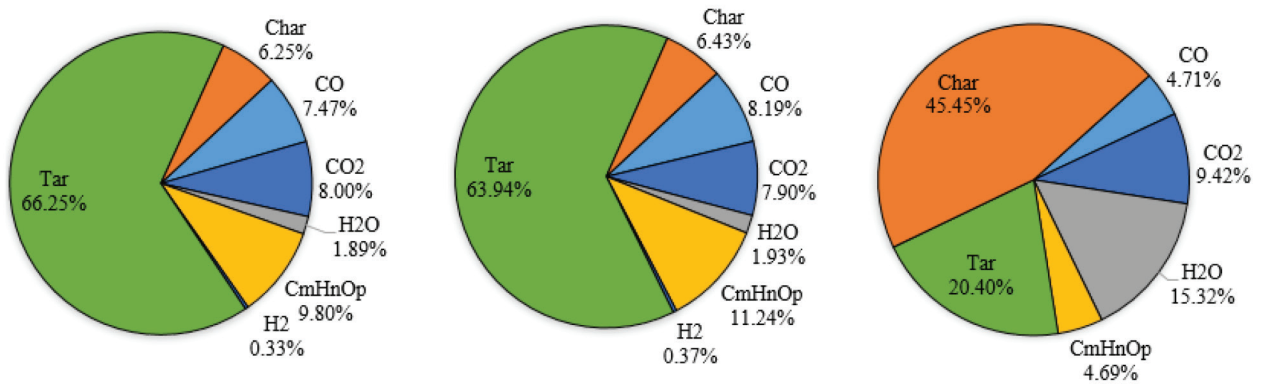

Figure 4: Mean composition of the products for the pyrolysis of pinewood (left), spruce (middle) and a typical brown coal (right) for a heating rate of 10000 K/s

3. MATHEMATICAL MODEL OF THE COMBUSTION PROCESS

The biomass pyrolysis model is coupled with the combustion model implemented in AIOLOS. The code AIOLOS is based on a conservative finite-volume formulation, using the SIMPLEC or SIMPLE method for velocity-pressure coupling, the standard k-ε model, or the differential Reynolds stress model for turbulence. Radiative heat transfer is calculated by either a discrete ordinates method or five other radiation models. Thermal properties of the biomass are taken from [11][12].

Secondary reactions of tar decomposing into carbon monoxide, hydrogen, and soot at high temperatures are considered, as described in [07].

In terms of heterogeneous reactions, char combustion, as well as gasification reactions with carbon dioxide and water vapour are taken into account. The reaction rates are calculated accounting for both, chemical kinetics and physical diffusion. A more detailed description of the char reaction model can be found in [06][07].

Regarding the homogeneous reactions, a two-step model for the oxidation of light hydrocarbons with carbon monoxide as intermediate product, as presented in [04], is chosen, whereas hydrogen from the devolatilisation process is combusted directly to water vapour. Tar and soot oxidation reactions are also considered. Turbulence-chemistry interaction is accounted for by the Eddy dissipation model [08], as described in [07].

4. SIMULATION RESULTS

Simulations for coal and pinewood pyrolysis and the subsequent combustion are done for a 20 kW electrically heated entrained-flow reactor. The reactor tube has a length of 2.5 m and an internal diameter of 200 mm. The carrying air with pulverized fuel enters through the burner centre, surrounded by the primary and the secondary air. The wall temperature is set to 800 °C. For both kinds of fuel, the particle shape is assumed to be spherical, the size distribution is given using typical average diameters and proportions according to experimental measurements. The kinetic parameters of pyrolysis for coal are $k_0=3.15\times10^5\ s^{-1}$ and $E/R=8900$ K , as shown in [06], while the apparent kinetic parameters obtained for the pinewood are $k_0=1.54\times10^6\ s^{-1}$ and $E/R=8873$ K and for spruce $k_0=1.28\times10^5\ s^{-1}$ and $E/R=6963.5$ K.

Figures 5 and 6 show the pyrolysis devolatilisation rate and the temperature distribution along the reactor length. It can be seen that the pyrolysis of the biomasses occurs faster, due to the higher preexponential factor in the case of the pinewood and the lower activation energy for the spruce, as well as the higher temperature in the pyrolysis zone (see Figure 6).

The temperature reached in the reactor for pinewood is higher, as a result of the fast oxidation of the higher percentage of volatiles released in the pyrolysis (pinewood: 93.7 %, spruce: 93.6 %, coal: 54.5 %). The burnout of the higher char fraction obtained in the pyrolysis of coal takes place slower, leading to a smoother heat release and consequently to lower temperatures in the pyrolysis zone.

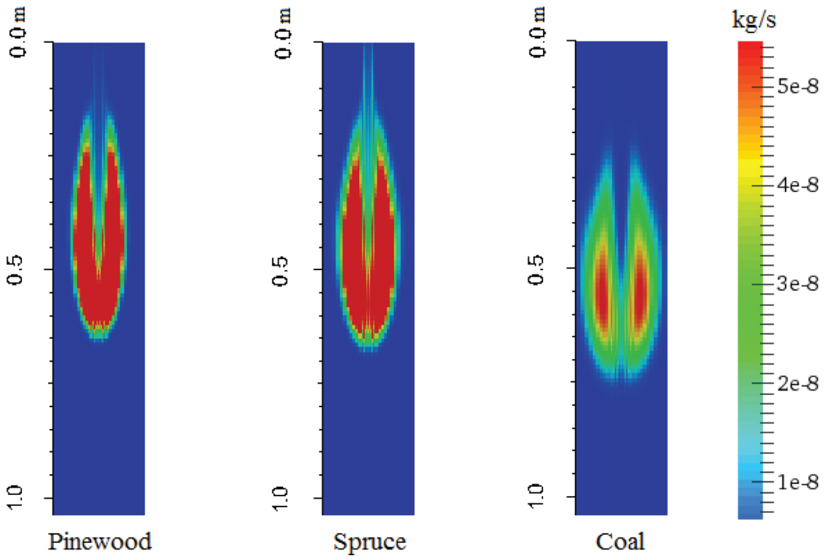

Figure 5: Devolatilisation rate of the pyrolysis of pinewood, spruce and brown coal in an entrained-flow reactor

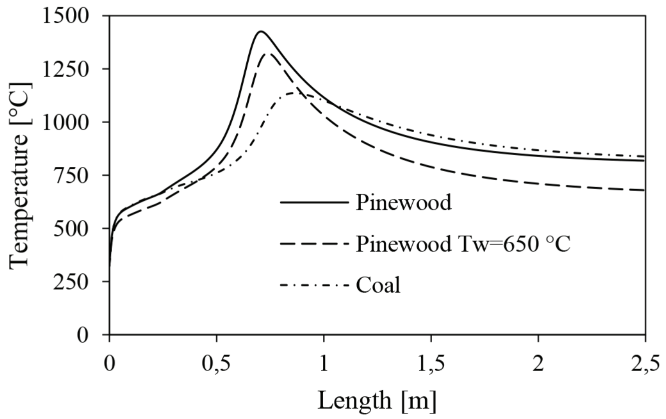

Figure 6: Temperature distribution along the reactor length for the combustion of coal and pinewood

Figure 6 also shows the temperature distribution along the reactor for the combustion of pinewood with a wall temperature of 650 °C. As expected, the temperatures in the reactor are lower than those obtained for a wall temperature of 800 °C, due to the dependency of the reaction rates on temperature.

5. CONCLUSION

In the present work, a detailed model of biomass pyrolysis presented in [10] has been implemented into the CFD program AIOLOS which was developed mainly for pulverized coal combustion. Coal and biomass pyrolysis and combustion were investigated through a large number of CFD simulations. It was found that the kinetic parameters of pyrolysis and the composition of the released products have a big impact, especially on the temperature field which is higher for the biomass, due mainly to the oxidation of the high volatiles amount released in the pyrolysis. The use of the multi-component, competitive scheme to describe the pyrolysis makes the combustion model more flexible, allowing it to be used with different feedstocks under various conditions. The implemented model improves the description of the biomass pyrolysis in AIOLOS and represents an important step in the adaptation of the existing code to biomass combustion, which will continue in the near future.

6. REFERENCES

[01] Antal M et al. (2000). Attainment of the theoretical yield of carbon from biomass. Ind. Eng. Chem. Res. 39, pp. 4024-4031.

[02] Blondeau J, Jeanmart H. (2011). Biomass pyrolysis in pulverized-fuel boilers: Derivation of apparent kinetic parameters for inclusion in CFD codes. Proc. Comb. Inst. 33, pp. 1787-1794.

[03] Di Blasi C. (2008). Modeling chemical and physical processes of wood and biomass pyrolysis. Prog. Energy Combust. Sci. 34, pp. 47-90.

[04] Dryer F, Glassman I. (1973). High-temperature oxidation of CO and CH_4. Symposium (International) on Combustion 14, pp. 987-1003.

[05] Förtsch D. (2003). A kinetic model of pulverized coal combustion for computational fluid dynamics. PhD Thesis, University of Stuttgart.

[06] Kurz D. (2014). Numerische Simulation industrieller Rostfeuerungen nach der Euler-Euler Methode. PhD Thesis, University of Stuttgart.

[07] Leiser S. (2010). Numerical simulation of oxy-fuel combustion. PhD Thesis, University of Stuttgart.

[08] Magnussen B, Hjertager B. (1977). On mathematical modeling of turbulent combustion with special emphasis on soot formation and combustion. Symposium (International) on Combustion 16, pp.719-729.

[09] Miller R, Bellan J. (1997). A generalized pyrolysis model based on superimposed cellulose, hemicellulose and lignin kinetics. Combust. Sci. Technol. 126, pp. 97-137.

[10] Ranzi E et al. (2008). Chemical kinetics of biomass pyrolysis. Energy Fuels 22, pp. 4292-4300.

[11] Ragland K, Aerts D. (1991). Properties of wood for combustion analysis. Bioresource Technology 37, pp. 161-168.

[12] Thunman H et al. (2001). Composition of volatile gases and thermochemical properties of wood for modeling of fixed or fluidized beds. Energy Fuels 15: 1488-1497.

[13] Varhegyi G (1979). Kinetic evaluation of non-isothermal thermoanalytical curves in the case of independent thermal reactions. Thermochim. Acta 28: 367-376.

Florian Sudbrock (Department of Energy Plant Technology, Ruhr-University of Bochum, Germany)

DEM-CFD investigation of drying wood particles in packed and agitated beds

F. Sudbrock, S. Wirtz, H. Kruggel-Emden, V. Scherer
Ruhr-University of Bochum, Department of Energy Plant Technology (LEAT)
Universitätsstr. 150, D-44780 Bochum, Germany
sudbrock@leat.rub.de, wirtz@leat.rub.de

Coupled discrete element (DEM) - computational fluid dynamics (CFD) simulations are a recent development to model thermo-chemical processes in mechanically agitated particle systems exposed to a fluid flow. As an example within this contribution the DEM-CFD methodology is applied to the drying of wood particles in three different configurations: single particle, packed, and agitated particle bed. With this combined approach the advancement of drying can be simultaneously described on the system scale while resolving detailed transport processes on the particle scale. Simulation results are compared to experiments for low-temperature convective drying in all of these configurations.

When the drying of a single wood particle is modelled accounting for the anisotropy of the material and its shape yields a better agreement to experimental data. On the system scale coupled DEM – CFD simulation qualitatively better match experiments in packed and agitated particle beds when resolving inner particle transport three-dimensional. However, integral values of the process are satisfactorily predicted with one-dimensional models as well.

KEYWORDS: drying, wood, DEM-CFD, packed bed, agitated bed, experiments

1. INTRODUCTION

Due to its biogenic origin, biomass designated for combustion, gasification or torrefaction contains moisture contents from 50 to over 150 % (dry basis) in its fresh form [01]. Commonly, biomass requires to be dried initially for fuel handling and storage as well as for increasing the energy efficiency of the conversion process and reducing its pollutant emissions. Industrial drying processes may be grouped as systems with a fixed bed (e.g. packed moving bed dryer) or a mechanically agitated bed (e.g. rotary dryer) of biomass particles. For dryer design continuum approaches like computational fluid dynamics (CFD) are emerging as software tools for detailed process simulation [02]. However, standard CFD models may fail since the material's physical and chemical properties vary to a large extent and process conditions may require that thermal gradients between gas and solid particles and inside each particle (Bi>1) are accounted for. Such as thermo-chemical processes like pyrolysis or torrefaction, drying can be quite accurately described for a single particle under constant boundary conditions and very comprehensive models are available [03]. In this context the integration of the discrete element method (DEM) into CFD simulations is a recent development to couple both scales and model heat and mass transfer in heterogeneous gas-solid systems. In the DEM each particle of the assembly is resolved individually and its mechanical interactions with its surroundings are tracked and solved numerically over time. Thermo-chemical processes and local inhomogeneity can be resolved on the particle scale and on the process scale.

In this contribution a coupled DEM-CFD simulation procedure is presented and applied to study the drying of wood particles in three different configurations: single particle, packed, and agitated particle bed. The inner particle heat and mass transfer is either resolved one- or three-dimensional. The effect of model assumptions and material parameters is analysed on the particle and the process scale by comparing numerical results to experiments.

2. NUMERICAL PROCEDURE

The simulation of the heat, mass and momentum transport in the particulate phase and the fluid phase are carried out in two separate codes. Both simulations apply the same time step and particulate and fluid phases interact with each other by a transient two-way coupling (momentum, energy and mass).

2.1. Fluid Phase

The commercial CFD software package ANSYS FLUENT is applied to solve the governing equations of the fluid phase:

$$\frac{\partial}{\partial t}\left(\varepsilon_f \rho_f\right)+\nabla\left(\rho_f \bar{\mathbf{v}}_f\right)=\sum_k S_{m,k} \tag{1}$$

$$\frac{\partial}{\partial t}\left(\varepsilon_f \rho_f \bar{\mathbf{v}}_f\right)+\nabla\left(\rho_f \bar{\mathbf{v}}_f \bar{\mathbf{v}}_f\right)=-\nabla P+\nabla\left(\bar{\bar{\boldsymbol{\tau}}}\right)+\rho_f \mathbf{g}+\mathbf{f}_{int} \tag{2}$$

$$\frac{\partial}{\partial t}\left(\varepsilon_f \rho_f h_f\right)+\nabla\left(\rho_f h_f \bar{\mathbf{v}}_f\right)=-\frac{\partial \varepsilon_f P}{\partial t}+\nabla\left(K_q \nabla T_f-\sum_k h_k \mathbf{J}_k+\bar{\bar{\boldsymbol{\tau}}}\cdot\mathbf{g}\right)+S_q \tag{3}$$

$$\frac{\partial}{\partial t}\left(\varepsilon_f y_{k,f} h_f\right)+\nabla\left(\rho_f y_{k,f} \bar{\mathbf{v}}_f\right)=\nabla\left(\rho_f K_{m,k} \nabla y_{k,f}\right)+S_{m,k} \tag{4}$$

Since a full spatial resolution of individual particle geometries in the agitated assembly is computationally too expensive, the physical presence of the solid phase is accounted for by an additional interaction force in the momentum equations (2) which is provided by the Ergun equation [04]. Volumetric mass source terms in the continuity (1) species equation (4) and an energy source term in the energy equation (3) account for the convective heat and mass transfer at the particle-fluid interphase. The source terms are integrated over the particle surfaces with the transfer coefficients computed using standard empirical correlations [05].

2.2. Particle Motion

A DEM code developed at the Department of Energy Plant Technology, Ruhr-Universität Bochum computes particle motion by solving Newton's and Euler's laws of motion:

$$m_i \frac{d^2 \mathbf{x}_i}{dt^2}=\sum_{j=1}^{N} \mathbf{F}_{ij}+m_i \mathbf{g} \tag{5}$$

$$\theta_i \frac{d^2 \varphi_i}{dt^2}=\sum_{j=1}^{N} \mathbf{M}_{ij}+\mathbf{M}_i^r=\sum_{j=1}^{N} \mathbf{r}_i \times \mathbf{F}_{ij}+\mathbf{M}_i^r \tag{6}$$

In order to solve the equations (5) and (6) the contact forces are computed. The contact force acting on both particles participating in the contact are split into normal and tangential components. One of the most common models used in DEM simulations is the linear spring dashpot model, a viscoelastic model. The elastic repulsion is proportional to the displacement and the viscous dissipation is proportional to the displacement rate:

$$\mathbf{F}^n=\mathbf{F}_{el}^n+\mathbf{F}_{diss}^n=\left(-k^n \xi-\gamma^n \dot{\xi}\right)\cdot\mathbf{n} \tag{7}$$

Tangential forces are represented by a tangential spring, calculated with the elongation of the spring and the tangential stiffness of a linear spring. The tangential forces are limited by Coulomb's law:

$$\mathbf{F}^t=-min\left(\left|k^t \xi^t\right|,\left|\mu_{dyn}\mathbf{F}^n\right|\right)\cdot\mathbf{t} \tag{8}$$

With the forces of all particle contacts calculated according to equations (7) and (8) the particle's motion can be solved with the equations (5) and (6). The explicit Euler method with constant time steps is used for time-integration.

2.3. Inner particle heat and mass transfer

The particles in the DEM are assumed to be rigid bodies. The transient temperature distribution within each particle computed from the energy balance:

$$\rho c_p \frac{\partial T}{\partial t} = \nabla\left(\lambda \nabla T\right) \tag{9}$$

The moisture distribution within the particle is computed from a diffusion law in terms of the moisture content and an effective transport coefficient:

$$\frac{\partial X}{\partial t} = \nabla\left(\delta_{eff} \nabla X\right) \tag{10}$$

For the internal moisture and energy transport either a radial, one-dimensional or a tree-dimensional spatial resolution is applied. The spatially discretized formulation of (9) and (10) is obtained by the Finite Volume Method and solved implicitly. With the convective transfer coefficients used for integrating the source terms of the fluid phase equations (1-4) defining the boundary condition at the particle surface a strict conservation of the exchange fluxes between both phases is achieved.

3. RESULTS

3.1. Single Particle Drying Behaviour

First, inner particle transport models and parameters are revised and simulation results are compared to drying rates measured with a precision balance for single spherical wood particles exposed to a hot air flow.

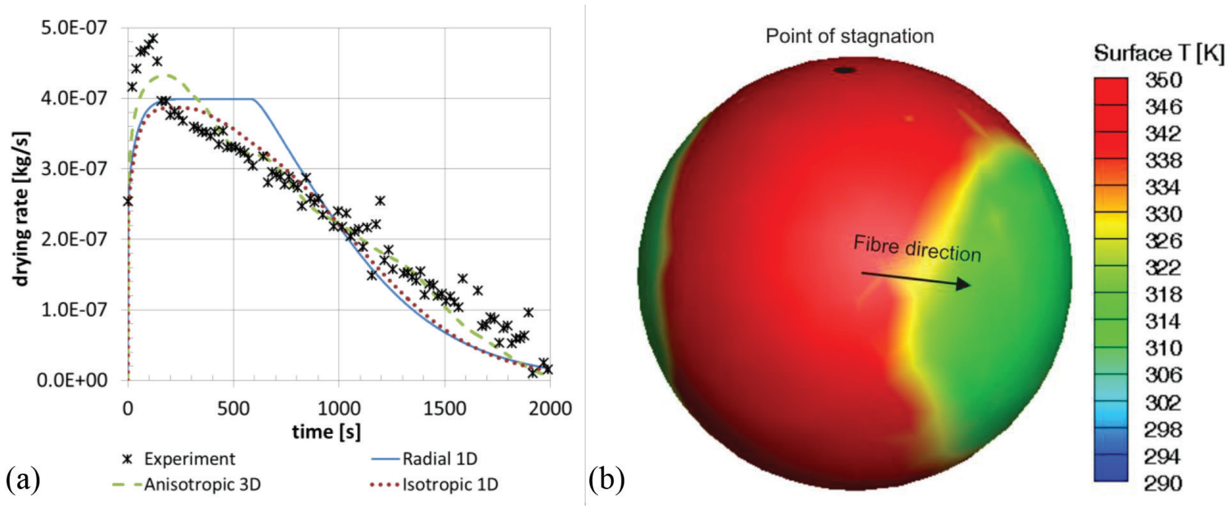

Figure 1: (a) Influence of transport model on drying rate of single wood sphere; (b) surface temperature of wood particle

The best approximation to experimentally determined drying rates is obtained with a three-dimensional spatial resolution (Figure 1 a). If the highly anisotropic transport behaviour of the wood is accounted for the drying rate decreases almost linearly towards the end of the simulation, as it is measured in the experiments. At the surface of the wood particles the drying process advances inhomogeneous. In the direction of the wood fibres the surface stays wetted for a longer time while in axial and radial direction the surface dries out and the temperature increases earlier. Both effects can be observed in experiments as well as in the single particle simulation (Figure 1 b).

3.2. Packed Bed Drying

Packed bed drying was assessed for a cylindrical bed of wood particles passed vertically by a pre-heated ambient air flow. Throughout the experiment the concentration of water vapor (relative humidity) and the air temperature are obtained continuously at different positions by capacitive humidity sensors. Additionally the packed bed is suspended by a tension load cell and its weight is measured continuously. The packed bed consists of beech particles of different size and shape (spheres, cylinders, chips).

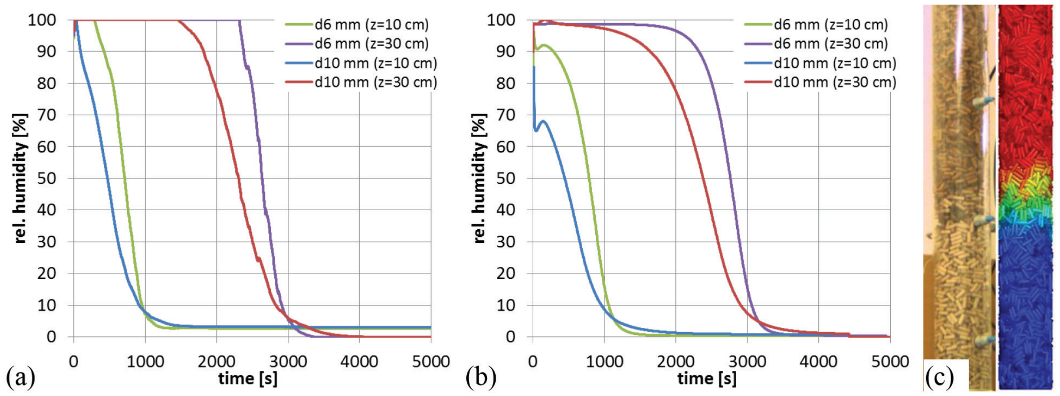

Figure 2: Influence of particle size on propagation of drying front in packed bed: (a) experiment, (b) simulation; (c) drying process in packed of wood cylinders (experiment and simulation)

When considering inner particle temperature and concentration gradients the results of the coupled DEM-CFD simulation are in good agreement with the measured drying rates and the influence of operational parameters, e.g. particle size, inlet temperature of airflow, is computed as it is determined experimentally (Figure 2 a,b). For cylindrical particles, when applying the correlations for the convective transfer coefficient of spheres of equal volume, simulations match the experimental measurements as well (Figure 2 c). The largest deviations are observed when simulating wood chip drying, which is mainly due to the extremely inhomogeneous shape and material parameters.

3.3. Agitated Bed Drying

Agitated bed drying is analyzed for a set-up, which resembles industrial grate systems. The particles are convectively dried by a pre-heated airflow while agitated by moving bars. The overall amount of water transferred from the granular material to the airflow is determined gravimetrically from the initial and final weight of the drying material and the bulk drying rate from the temperature, relative humidity and air flow rate in inlet and outlet. The experiments are recorded by a thermographic system and a digital camera system at the same time. A video analysis on basis of the thermographic and digital images is used to measure the surface temperature of the optically accessible particles in the first layer behind a sapphire observation window.

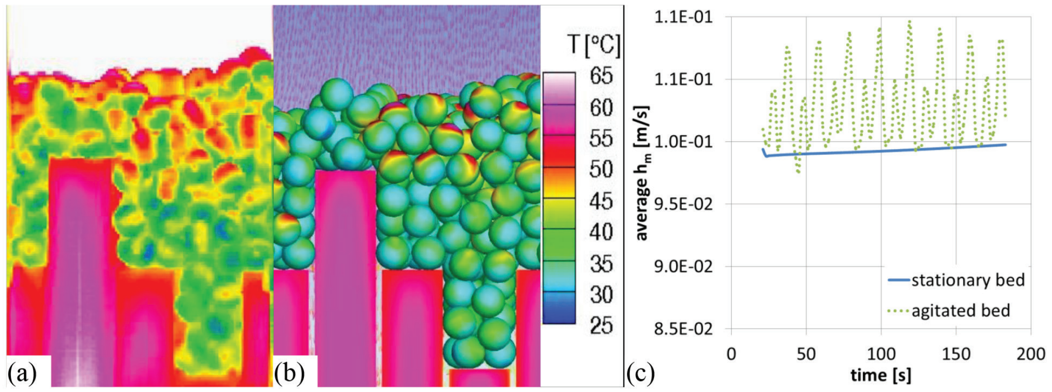

Figure 3: Surface temperatures in agitated particle bed: (a) experiment, (b) simulation; (c) influence of agitation on average mass transfer coefficient of particle bed

The drying rate of the agitated particle bed in the DEM-CFD simulations increased compared to the stationary bed as it was measured in the experiments. A better agreement to the particle surface temperatures determined by the thermographic system (Figure 3 a) is achieved when resolving inner particle transport phenomena three-dimensional (Figure 3 b). However, if the drying process is assessed at a larger scale, also simulations with one-dimensional inner particle models are an adequate approach to predict integral values (e.g. amount of water transferred).

On basis of the simulation data the influence of different agitation effects on the convective heat and mass transfer in the bed can be quantified separately. The moving bars periodically reduce the cross section vertical to the air flow direction and cause a higher flow velocity around the particles positioned between the up-moving bars. This causes the average mass transfer coefficient of all particles to be higher in the agitated particle bed (Figure 3 c).

4. CONCLUSION

The coupled Discrete Element (DEM) - computational fluid dynamics (CFD) approach is a very recent development to model thermo-chemical conversion in moving granular media. Particle motion and one-dimensional or three-dimensional temperature and moisture fields inside each particle are computed within the DEM code. The CFD software package ANSYS FLUENT is applied to solve the transport equations of the interstitial fluid phase. Both codes are interconnected by a transient two-way-coupling (momentum, heat and mass).

Different approaches of modelling inner particle heat and mass transfer were compared for single particle, packed and agitated bed drying. A very good agreement of numerical and experimental results is achieved when resolving inner particle heat and mass transfer three-dimensional and accounting for the anisotropy of the material. For the drying process of the agitated and stationary particle bed also coupled DEM-CFD simulations with numerically less costly models (e.g. 1D) predict integral values to a satisfying extend and provide detailed information on the local conditions for each particle of the assembly. Thus, also coupled DEM-CFD simulations turn out to be a powerful and flexible simulation tool to model thermo-chemical processes of and within granular material and will be applied for numerical studies on different conversion processes in agitated biomass (e.g. combustion, gasification).

5. ACKNOWLEDGEMENTS

Financial support by the German Federal Ministry of Economics and Labor (BMWA) for this work through IGF-project 17949 of the German Federation of Industrial Research Associations „Otto von Guericke“ e.V. (AiF) is gratefully acknowledged.

6. REERENCES

[01] Pang S, Mujumbar A (2010). Drying of Woody Biomass for Bioenergy: Drying Technologies and Optimization for an Integrated Bioenergy Plant. Drying Technology 28, pp. 690.
[02] Kemp I (2007). Drying Software: Past, Present, and Future. Drying Technology 25, pp. 1249.
[03] Perré P (2010). Multiscale Modeling of Drying as a Powerful Extension of the Macroscopic Approach: Application to Solid Wood and Biomass Processing. Drying Technology 28, pp. 944.
[04] Ergun S, Orning, A A (1949). Fluid Flow through Randomly Packed Columns and Fluidized Beds, Industrial & Engineering Chemistry 41, pp. 1179.
[05] Gnielinski V (1978). Gleichungen zur Berechnung des Wärme-und Stoffaustausches in durchströmten ruhenden Kugelschüttungen bei mittleren und großen Pecletzahlen. Verfahrenstechnik 12: 363.

Morten Seljeskog (SINTEF, Norway)

Batch combustion of logs in wood stoves - Transient fuel models and modelling of the fuel decomposition and products composition as input to CFD gas phase calculation

Morten Seljeskog, Øyvind Skreiberg
SINTEF Energy Research,
Kolbjørn Hejes vei 1A, Trondheim, Norway
morten.seljeskog@sintef.no, oyvind.skreiberg@sintef.no

In this paper, a transient modelling approach of the fuel decomposition and products composition in batch combustion of logs in wood stoves as input to CFD gas phase calculations are presented. The single wood log is modelled as a thermally thick particle, which subject to an external heat flux is thermally decomposed as it is heated, releasing water vapour due to drying and volatiles due to pyrolysis of the hemicellulose, cellulose and lignin in the wood, leaving char and ash behind. The volatiles are released to the gas phase, to be combusted, along with the water vapour. Here, no char combustion takes place before all the volatiles have been driven out. The char combustion model is not presented in this paper. The water vapour content and the elemental composition of the volatiles released in the devolatilization phase are used to calculate the transient heat production. The effects of variations in initial moisture content and wood log size on the transient intrinsic moisture content, temperature and volatiles release are presented and discussed. These are essential fuel parameters and their influence on the combustion process and its transient heat production profile is essential to understand to be able to control the batch combustion process of logs in wood stoves in a best possible way, to ultimately achieve a heat release to a room as constant as possible in future's energy efficient buildings. The single wood log model is also useful for parametric studies in an overall transient model for combustion of a batch of logs in wood stoves as well as for implementation as an user defined function in transient or stationary CFD modelling of wood stoves.

KEYWORDS: Biomass, Wood logs, Batch combustion, CFD, Drying, Devolatilization

1. INTRODUCTION

Commercially available CFD codes have long proved their capability of simulating the behaviour of parts of reactive thermal systems like the freeboard or gas phase region in a combustor. However, there are still challenges regarding CFD models simulating the heterogeneous combustion behaviour and in the mass and energy interaction between the zones even for a relatively homogenous fuel as pellets. Most of the modelling work found in the literature is related to continuous grate or fixed bed firing of relatively small homogenous pellet-like biomass particles which usually are considered as a porous bed layer and not single particles, although some recent work endeavour to solve the real physical behaviour. Models which are able to describe the heterogeneous reactions in the bed and the interaction with the gas phase in the freeboard volume do exist. However, they are still complex and require several assumptions in the form of assumed or measured input parameters. They still remain mainly suitable for relatively homogeneous biomass fuels like e.g. pellets. As of today no complete physical models exists which are able to take into account the inhomogeneity of relatively large individual wood logs stacked in some geometry in a wood stove. This means that modelling of the highly transient batch combustion process of log combustion in wood stoves and its emission formation representing real life wood log combustion is still in need of an appropriate heterogeneous solid phase model, i.e. a versatile transient fuel decomposition and products formation model, which efficiently can be coupled with a stationary or transient CFD gas phase model. Such a model, empirical, quasi-empirical or physical, would be helpful both in providing initial conditions as well as to serve as an either one- or two-way coupled boundary condition generator.

Transient empirical or quasi-empirical models for the fuel composition are alternatives to physical models and can be used to estimate transient heat production profiles and for a number of engineering calculations for a wood log batch combustion process. To provide input to CFD calculations it needs to be combined with a model for the fuel decomposition estimating the transient gaseous products composition. A more comprehensive model should be able to consider the individual wood logs and handle both drying, pyrolysis/devolatilization as well as char oxidation/gasification, all including products composition. The driving force for the fuel decomposition model is the transient heat flux to the fuel and its further time-delayed transfer inside the fuel geometry, creating drying, pyrolysis and char reaction fronts with characteristic temperatures at positions in the log dictated by both conditions around the log and the properties of the log itself. The complete oxidation of the fuel, with a certain transient excess air ratio, generates the heat production profile, that together with the properties of the stove materials affect the temperature in the combustion chamber and consequently the heat flux to the fuel. In the present work, a modelling approach for the transient decomposition and products formation of a batch of individually modelled wood logs is presented. This modelling approach depends on an estimated heat flux to the fuel which is the driving external force controlling the fuel decomposition speed. The determination of this heat flux and further transient modelling for generation of other input to CFD modelling of stoves and thermal comfort simulations are presented in [01].

2. WOOD LOG DECOMPOSITION MODEL

Wood logs are so-called thermally thick particles, where internal heat transfer is limiting the drying process and the decomposition rate of the volatile content. Hence, models are needed that can estimate the transient rate of drying and devolatilization, as well as the surface temperature and the gas composition escaping through the surface, and its temperature. In this 1D transient modelling approach the wood log is divided into 50 layers, with mass and energy fluxes passing the layer borders. An external heat flux to the surface is the driving force, which of course in practise will vary greatly through the transient wood log combustion process, since the combustion of the volatiles mainly provides the heat flux. As the surface is heated, the net heat flux to the surface is reduced accordingly. For simplicity, the external heat flux is kept constant here. The internal energy flux taken into account during drying and devolatilization includes heat conduction and preheating of the water vapour from drying and the products of the devolatilization, assumed to be gaseous, before these are leaving the surface, here assumed at the surface temperature. This preheating will slow down the heat transfer into the wood log, together with the heat needed for moisture evaporation. As the incident heat flux on a wood log in a stove may also vary depending on the position of the wood log relative to the radiating flames, the 1D model is made so that two different incident heat fluxes can be applied, opposite each other on the axial sides of the wood log. The length of the wood log is assumed to be significantly longer than the width, making it in principle possible to use a 1D modelling approach. As wood logs are inherently anisotropic with respect to the fibre direction and gases flow more easily in the axial direction, this is of course a significant simplification.

Figure 1 illustrates the modelling approach.

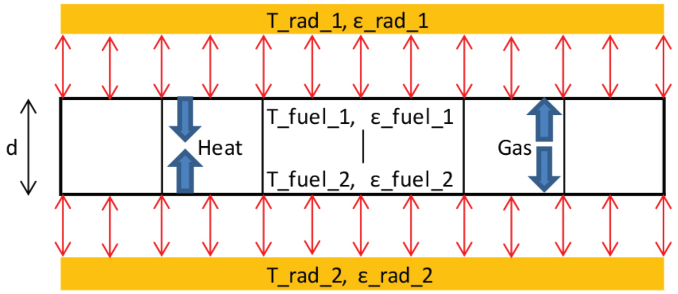

Figure 1: The modelling approach. The wood log has here a square cross section

A number of physical properties need to be included in the modelling approach, as well as kinetic parameters required in the Arrhenius expressions for the decomposition of the hemicellulose, cellulose and lignin in the wood. As previously mentioned, the char combustion model is not presented in this work. Physical properties values used in this work includes; emissivities for the radiation source and the wood log surface; proximate and ultimate composition of the wood, elemental composition of the volatiles and char; chemical composition of the wood (hemicellulose, cellulose, lignin); densities; specific heat capacities; conductivities; and Arrhenius reaction rate constants (activation energy and pre-exponential factor) for hemicellulose, cellulose and lignin.

2.1. Single wood log modelling results

Due to space limitations, in the following only a few selected capabilities of the model is presented and related results are presented in figures and discussed. A base case is defined, and variations are performed for a selected input variable while the other variables are kept constant. The base case is: Radiation temperature (the temperature of the radiation source, which is assumed to account for the heat transfer to the wood log surface): **800°C** (on both sides), initial wood log moisture content: **20 wt%**, wood log width: **50 mm**. Here, wood log shrinkage is not taken into account.

Figure 2 shows the temperature evolution as a function of time and position (layer) for the base case. Here, all layers have the same width. The temperature in the outer layer increases rapidly towards the radiation temperature (their emissivities are assumed equal), while the intrinsic temperatures lags increasingly behind towards the centre of the wood log, due to conductive heat transfer limitations.

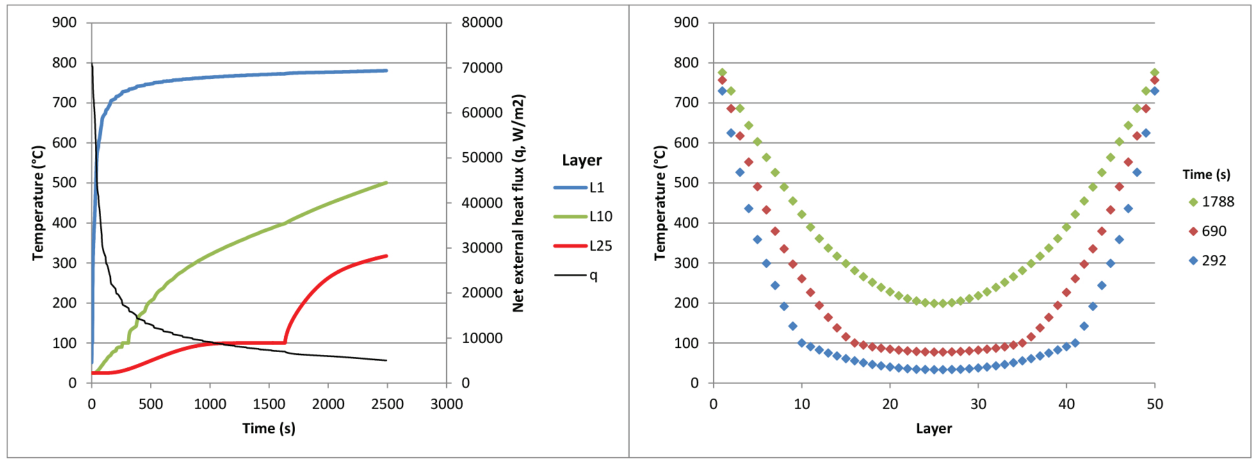

Figure 2: Temperature evolution as a function of time and position (layer) for the base case

Figure 3 shows the mass loss due to drying and devolatilization as a function of time for the base case. More than 1500 s is here needed to completely dry the wood log. Hemicellulose, cellulose and lignin is devolatilizing according to Arrhenius kinetics. Hemicellulose is decomposed earlier (at lower temperatures) than cellulose, while lignin is decomposed in a broad temperature range.

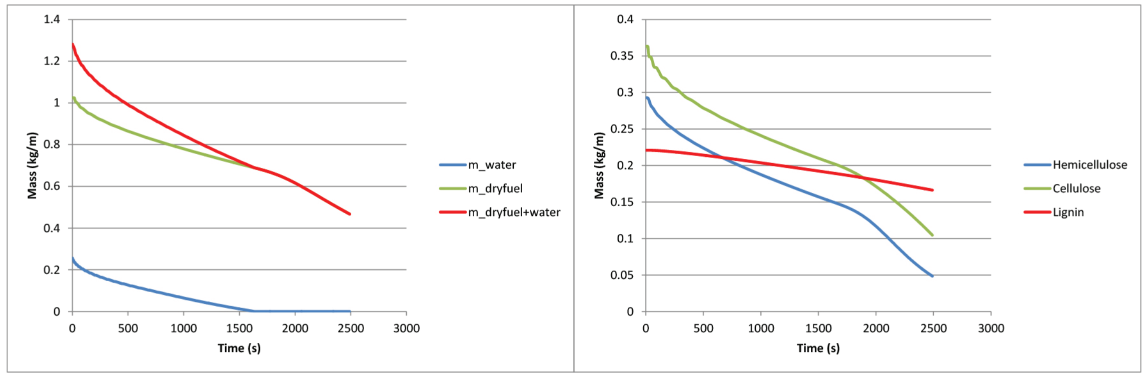

Figure 3: Mass loss due to drying and devolatilization as a function of time for the base case

Figure 4 shows the effect of initial moisture content (0, 10 and 20 wt%) on transient temperature and dry mass loss. As can be seen, the moisture is significantly delaying the heat-up and devolatilization, resulting in an increasing devolatilization delay compared to a case with no moisture. For e.g. layer 10, which here is from 9 to 10 mm inside the wood log, the drying front is delaying the devolatilization with about 500 s for the 20 wt% moisture case, compared to the case with no moisture.

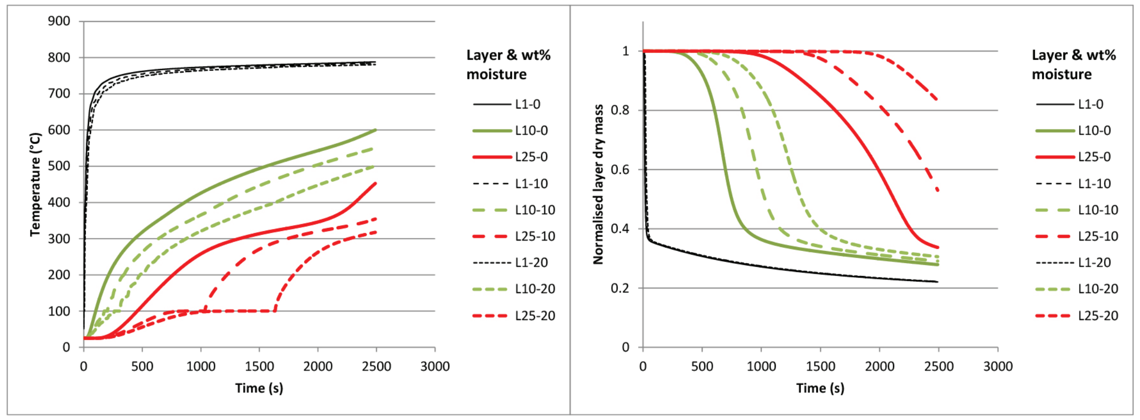

Figure 4: *The effect of initial moisture content (0, 10 and 20 wt%) on transient temperature and dry mass loss*

Figure 5 shows the effect of initial moisture content (5, 10 and 20 wt%) on transient moisture mass loss. In the individual layers, the water is vaporized rather fast. Increasing moisture content demands a longer drying time, and therefore increasingly delays the devolatilization process.

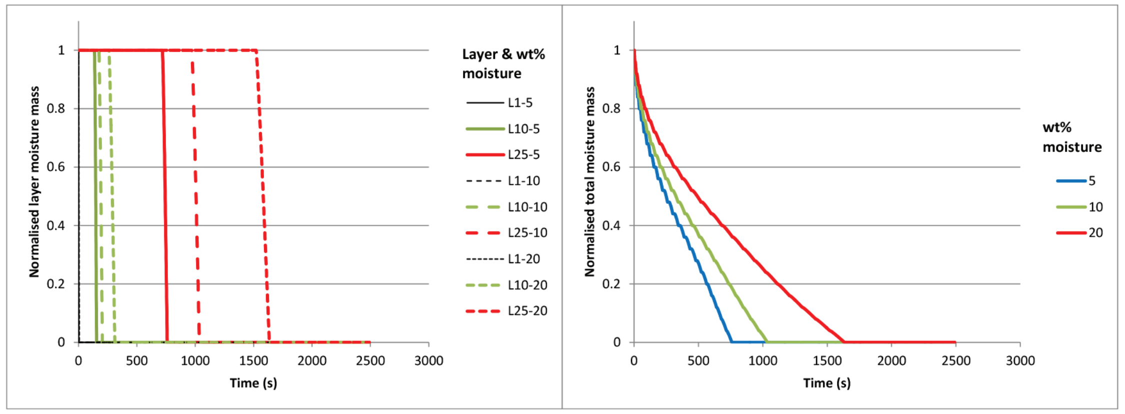

Figure 5: *The effect of initial moisture content (5, 10 and 20 wt%) on transient moisture mass loss*

Figure 6 shows the transient water vapor content and volatiles elemental composition, heating value (MJ/kg wet basis) and heat production (kW). The effect of the discretization approach can be clearly seen, e.g. the drying process in each single layer. The elemental composition of the released volatiles becomes constant for the single wood log. However, the heating value is varying, from negative in the beginning due to high moisture content (100 % initially) and up to the heating value of the volatile fraction of the wood. The heat production also varies, being high for a short period after the initial intensive drying period, due to rapid heating of the outer layers, whereafter it stabilizes due to conductive heat transfer limitation and continuous moisture evaporation, and increases again when all the moisture has evaporated and the temperature of the dry wood rapidly increases.

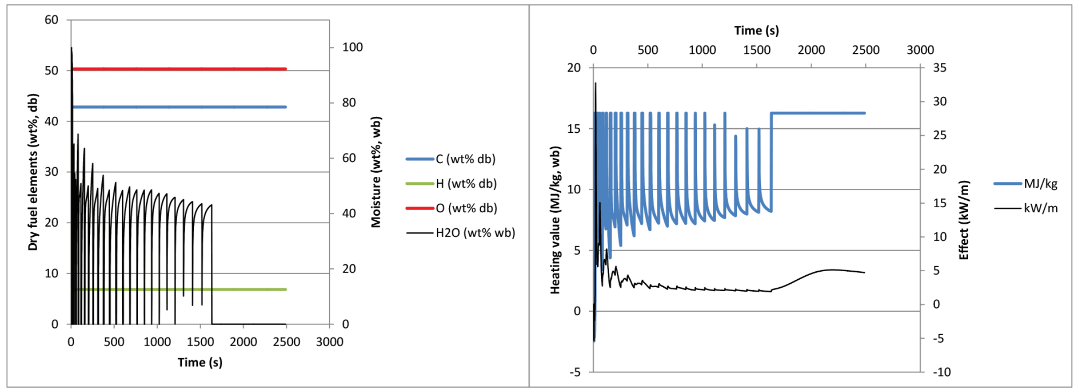

Figure 6: *Transient water vapor content and volatiles elemental composition, heating value and heat production*

Figure 7 shows the effect of wood log width/size on transient layer temperature and mass loss. An increasing wood log size delays the transient temperature evolution and the devolatilization process. The intermediate layer has been selected to enable comparison at close to the same position in the wood log, showing similar behavior until a certain temperature and moment in time have been reached, whereafter the temperature and the mass loss increase more rapidly as the wood log size decreases.

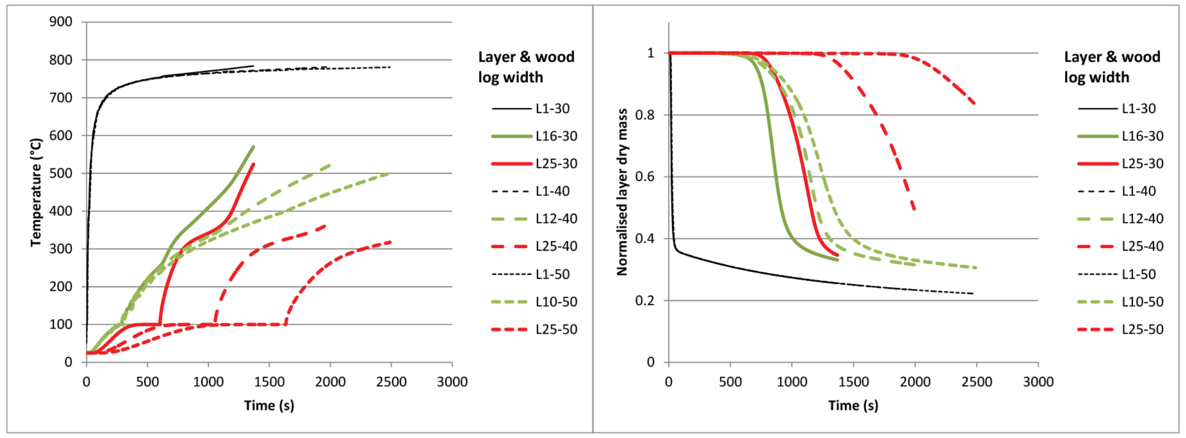

Figure 7: *The effect of wood log width (30, 40 and 50 mm) on transient temperature and mass loss*

Figure 8 shows the effect of initial moisture content (0, 10 and 20 wt%) and wood log width (30, 40 and 50 mm) on transient total dry mass loss, clearly showing higher dry mass loss rate as the moisture content is decreased, but also when the wood log size is reduced. The latter is due to a more rapid temperature increase, as no heat is conducted across the centre line when the same heat flux is applied on the opposite wood log surface. Of course, a smaller wood log will also have a larger surface to volume ratio (this effect is not included in this paper), contributing to an even higher dry mass loss rate when the wood log size decrease. The presented figures underline the importance of understanding the batch combustion of logs in wood stoves, to be able to control it in the best possible way with respect to combustion stability, emissions and energy efficiency.

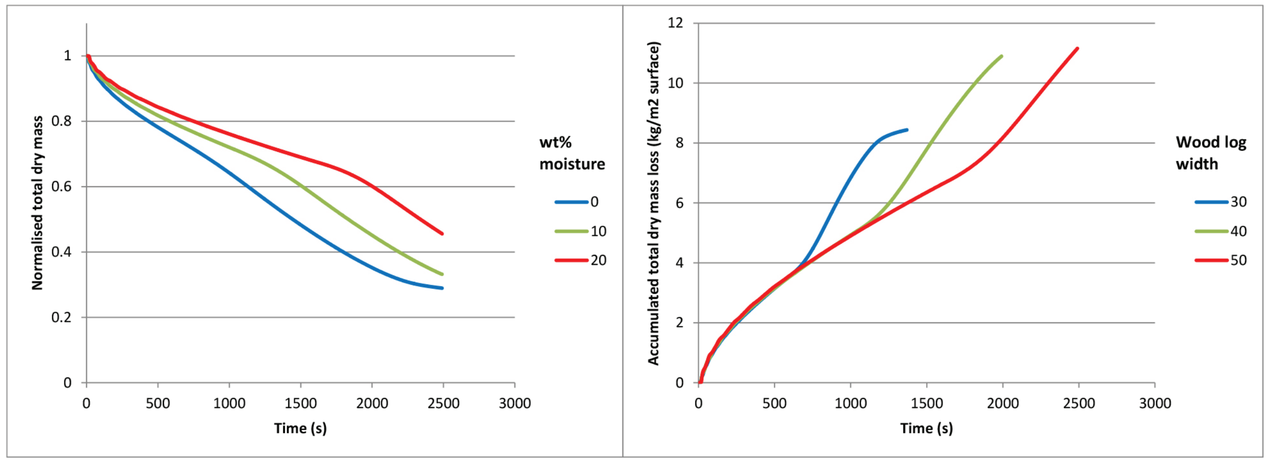

Figure 8: *The effect of initial moisture content (0, 10 and 20 wt%) and wood log width (30, 40 and 50 mm) on transient total dry mass loss*

For simulation of the batch combustion process of logs in wood stoves each log must be treated as a single wood log placed in a specific position and subjected to specific surrounding conditions, resulting in a combined contribution from each individual wood log as input to CFD gas phase simulations.

3. CONCLUSION

The developed wood log thermal decomposition model increases the understanding of the drying and devolatilization process in wood logs, being thermally thick particles. The influence of initial wood log moisture content and wood log size is shown as examples of the capabilities of the model. Increasing moisture content slows down the devolatilization process, while a decreasing particle size accelerates it. Programmed as an user defined function the complete model can provide CFD gas phase simulations of log combustion in wood stoves with necessary fuel input values.

4. ACKNOWLEDGEMENTS

The authors acknowledge the financial support from the Research Council of Norway, and the four industrial partners in the StableWood project:

JØTUL	morsø	DOVRE	1893 GRANIT KLEBER

5. REFERENCES

[01] Skreiberg Ø, Seljeskog M, Georges L. Batch combustion of logs in wood stoves – Transient modelling for generation of input to CFD modelling of stoves and thermal comfort simulations. 1st International Workshop on CFD and Biomass Thermochemical Conversion, 30th September 2014, DBFZ, Leipzig, Germany.

Øyvind Skreiberg (SINTEF, Norway)

Batch combustion of logs in wood stoves - Transient modelling for generation of input to CFD modelling of stoves and thermal comfort simulations

Øyvind Skreiberg, Morten Seljeskog
SINTEF Energy Research,
Kolbjørn Hejes vei 1A, Trondheim, Norway
oyvind.skreiberg@sintef.no, morten.seljeskog@sintef.no

Laurent Georges
Energy and Process Engineering Department,
Norwegian University of Science and Technology, (NTNU),
Trondheim, Norway
laurent.georges@ntnu.no

CFD calculations of wood stoves are a challenge due to the transient behaviour of the combustion process, due to their batch combustion operation principle. Various initial and boundary conditions needs to be specified to carry out a CFD calculation of a wood stove, and many of these will be a result of sub-models that again can be partly based on experimental results. Necessary boundary conditions relates to the fuel and air introduction into the computational domain and the thermal and radiative properties of the surfaces within and enclosing the computational domain. In addition initial conditions must be specified as starting point for the transient models generating the boundary conditions at any time in the batch combustion process. The ultimate goal would be to carry out transient CFD calculations where the boundary conditions are derived for each new stationary calculation based on the results from the previous time step. However, also the choice of models and the degree of detail of these regarding e.g. the handling of the gas phase chemistry are very important. In principle you would like to carry out CFD calculations that are good enough for an increased understanding of the influence of design and process variables on the environmental and energetic performance of the wood stove. As such, CFD calculations of wood stoves is a very useful tool that together with experiments could be used to cost- and time-efficiently design future's high performance wood stoves. In the present work the modelling approach aims at estimating both the transient heat production and release profiles for different design, fuel and operating conditions, as well as generating needed input for CFD calculations, both for the stove itself and for thermal comfort simulations.

KEYWORDS: Biomass, Wood logs, Batch combustion, CFD, Boundary conditions

1. INTRODUCTION

CFD calculations of wood stoves are a challenge due to the transient behaviour of the combustion process, due to their batch combustion operation principle. Various initial and boundary conditions needs to be specified to carry out a CFD calculation of a wood stove, and many of these will be a result of sub-models that again can be partly based on experimental results. This paper deals with these boundary conditions and the generation of representative values for these as input to stationary and transient CFD calculations throughout the batch combustion process as well as thermal comfort simulations. Additionally, heat production profiles and stove wall properties are needed to calculate heat release profiles to the room in which the stove is placed. These heat release profiles are essential input for evaluating the thermal comfort of wood stoves in houses, a subject which has received considerable attention recently as energy efficient houses are increasingly introduced.

Necessary boundary conditions relates to the fuel and air introduction into the computational domain and the thermal and radiative properties of the surfaces within and enclosing the computational domain. In addition initial conditions must be specified as starting point for the transient models generating the boundary conditions at any time in the batch combustion process. The ultimate goal would be to carry out transient CFD calculations where the boundary conditions are derived for each new stationary calculation based on the results from the previous time step. However, also the choice of models and the degree of detail of these regarding e.g. the handling of the gas phase chemistry are very important. In principle you would like to carry out CFD calculations that are good enough for an increased understanding of the influence of design and process variables on the environmental and energetic performance of the wood stove. As such, CFD calculations of wood stoves is a very useful tool that together with experiments could be used to cost-efficiently design future's high performance wood stoves.

2. THE MODELS/SYSTEM

The models that are needed to provide input to stationary or transient CFD calculations of wood stoves are basically connected to a fuel decomposition model [01] taking into account the generation of volatiles from a specified fuel geometry through pyrolysis/devolatilization and the products of heterogeneous char oxidation/gasification. The transient fuel decomposition model must take into account drying, pyrolysis/devolatilization and its products composition and char oxidation/gasification and its products composition. The total products of the fuel decomposition must conform to an overall conservation of each fuel element in the batch combustion process as well to energy conservation.

The driving force for the fuel decomposition model is the transient heat flux to the fuel and its further time-delayed transfer inside the fuel geometry, creating drying, pyrolysis and char reaction fronts with characteristic temperatures at positions in the log dictated by both conditions around the log and the properties of the log itself.

The complete oxidation of the fuel, with a certain transient excess air ratio, generates the heat production profile, where the major fraction of this is transferred through the walls (time-delayed) and the glass (directly by radiation) of the wood stove, to the room in which the stove is placed. This becomes the transient heat release profile to the room, an effect profile which ideally should be as flat as possible. The transient heat storage in the stove walls and their heat storage capacity becomes a possibility to dampen the heat release profile, which is important with respect to thermal comfort in a room/house. However, the stove walls/materials and their properties influence the temperature in the combustion chamber and consequently the heat flux to the fuel.

In the present work the modelling approach aims at estimating both the transient heat production and release profiles for different design, fuel and operating conditions, as well as generating needed input for CFD calculations, both for the stove itself and for thermal comfort simulations.

2.1. Boundary conditions

In [01] a wood log decomposition model was presented for a single wood log. Subject to an incident transient heat flux, drying and devolatilization takes place and water vapour and volatiles are released from the wood log, to be combusted and thus contribute to the heat flux to the fuel. Heterogeneous char oxidation completes the conversion of the wood log, leaving ash behind. This transient conversion of the single wood log results in a transient heat production profile. Each single wood log in a batch can be modelled individually, stacked in some geometry in the combustion chamber, contributing to an overall transient heat production profile.

In a CFD simulation a number of boundary conditions are needed for a stationary simulation, and additional initial conditions for a transient simulation. The boundary conditions concerns temperatures for all boundary surfaces, the surface emissivities, and the flow speed, direction and composition of all streams into the calculation domain. The emissivities of the surfaces must be set, as realistic as possible. Glass surface properties must also be included and set, if a glass is present (as it usually is). The air flow can be calculated for a specific air inlet configuration, knowing all the physical dimensions of the air inlets and the distribution of the air between primary, secondary and (usually) window flushing air, becoming tertiary air. This distribution will depend on the regulation of the air inlet valves, usually two valves, for primary air and secondary/window flushing air. If natural draft is applied it becomes trickier to calculate the amount of air entering the stove, as the draft needs to be established first. Forced draft by a fan makes it possible to set the air flow, to a value corresponding to a desired excess air ratio based on an expected wood log decomposition behaviour, or rather the transient oxygen need matching the desired excess air ratio. The temperatures of the inlet air are trickier when the air is preheated (as it usually is, but to varying degree) before entering the CFD simulation domain. Ideally, the calculation of air preheating should be included in the CFD domain, however, in practise this might be challenging. The single fuel model must provide the fuel gas amount and composition, while the fuel gas flow speed and direction is decided by the amount and the selected dimensions and method of treatment of the wood log surfaces. Of course, mass/elemental and energy balances must be satisfied for the computational domain.

If knowing the heat production from the fuel conversion and the fraction of this that is or needs to be transferred through the walls, you can carry out simplified transient calculations for the (composite) walls of the wood stove, which in addition to providing the transient heat release profile, also provides the wood stove wall temperatures. Such an approach can provide through an user defined function (UDF) the necessary wall temperatures either for transient CFD simulations or for a selected moment in time, for a stationary simulation.

Regarding the gas phase combustion of the fuel gas, chemical kinetics is required. This should be sufficiently detailed to enable pollutant formation studies, e.g. NO_x and soot through soot precursors in the fuel gas. The need for CPU time should also be minimised. In addition a turbulence-chemistry interaction model must be applied, as well as a radiation model.

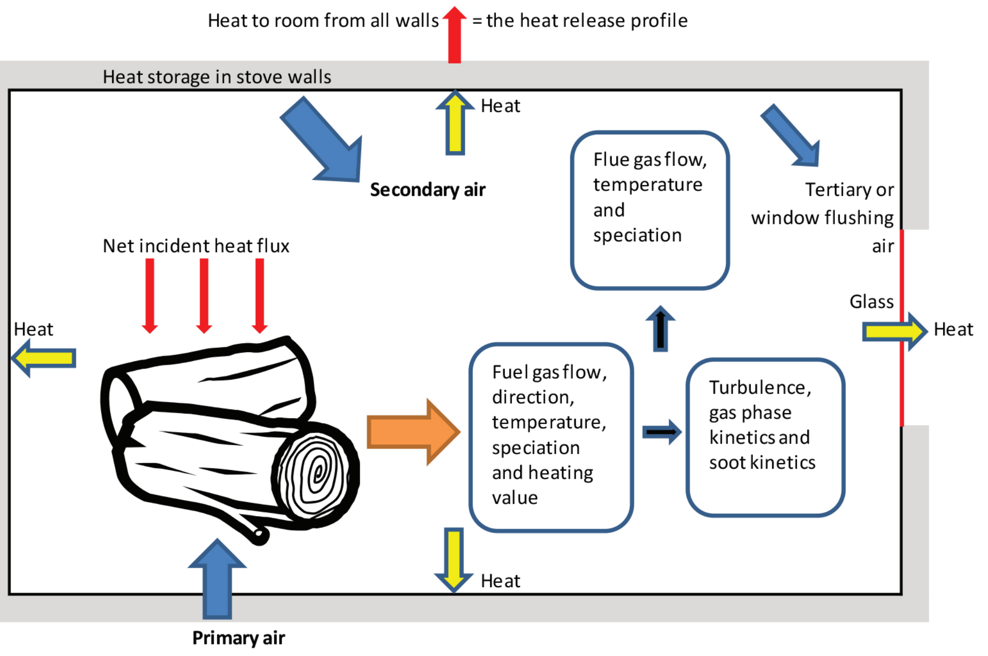

Figure 1: The modelling approach for the combustion chamber

The key factor in such a modelling approach is possibly the accuracy of the fuel model, providing the fuel gas related input. For the other input and models it is more a question of selecting the appropriate model level or detail to be able to carry out the CFD simulation within a reasonable time. The latter means that reduced or simplified models must be used where possible, e.g. for gas phase kinetics. However, simplifying too much gives unreliable results. A trade-off optimum should be sought, which in practise can be rather difficult.

In the following selected results are presented and discussed.

2.2. Transient fuel model output

In [01] single wood log modelling results was presented. Here, this is taken further by modelling the thermal decomposition of a stack of wood logs inside a combustion chamber. For simplicity they are identical and go through an identical decomposition process, however, not at the same time. The wood logs are ignited one after the other, with a certain time interval. For the single wood logs, which are square with sides of 50 mm and having a moisture content of 20 wt% (wet basis), corresponding to the base case in [01], the heat flux is applied on all sides, i.e. the drying, devolatilization and char combustion fronts are moving towards the wood log centre line from each side with equal speeds. Results are shown in Figure 2 and Figure 3 for respectively the transient fuel decomposition rate and heat production profile and the fuel elemental composition for a batch of 9 wood logs placed into a bed of charcoal and igniting in series.

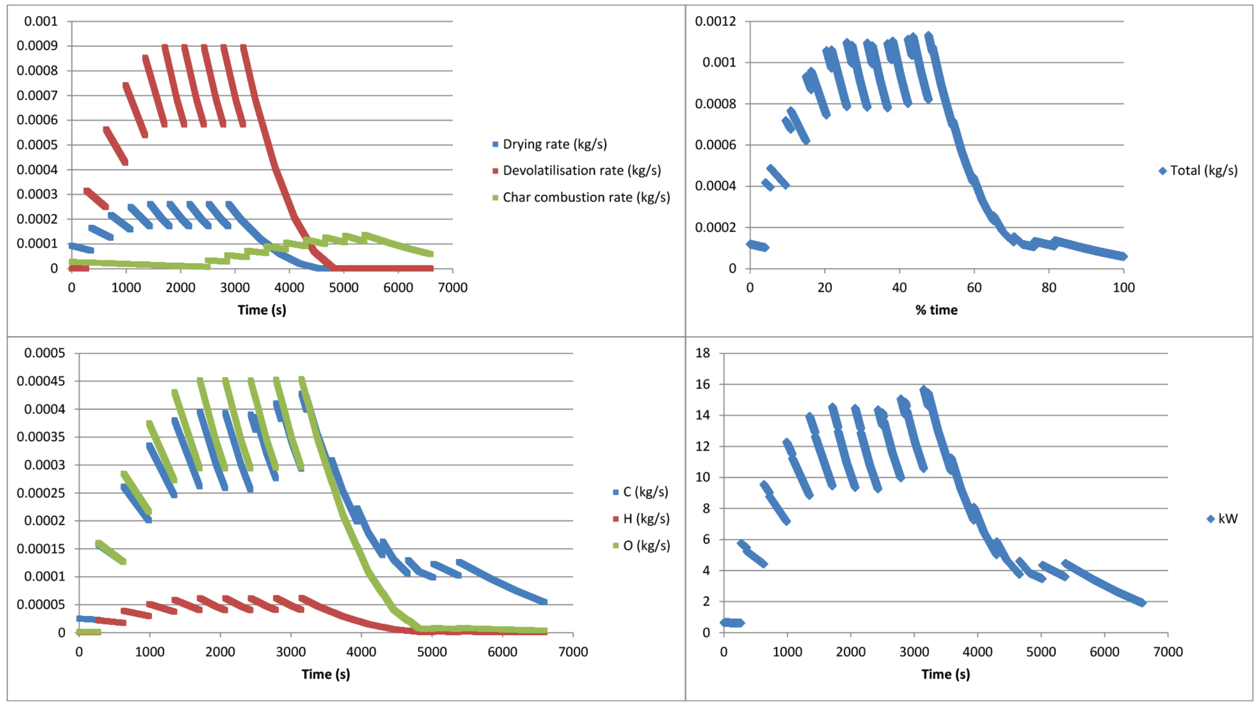

Figure 2: *Transient heat production profile and drying, devolatilization and char combustion rates for a batch of 9 uniform wood logs placed into a bed of charcoal and igniting in series*

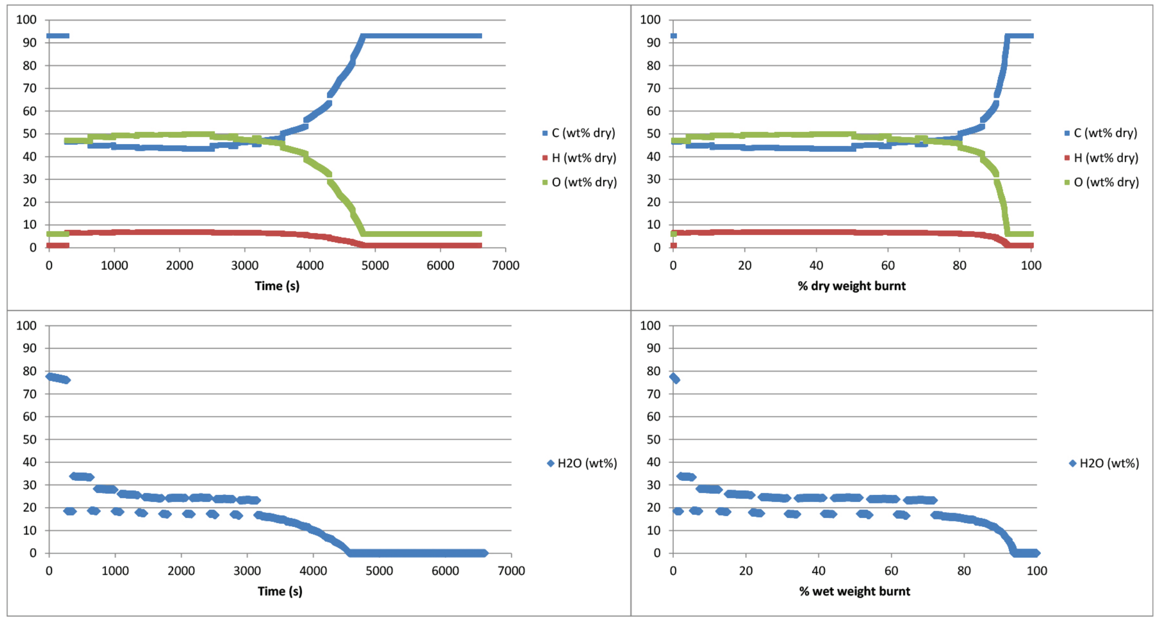

Figure 3: *Transient fuel composition for the case of Figure 2*

2.3. Stove wall calculations

The heat production profile generated by the batch combustion process will be transferred through the stove glass if present and the stove walls, where typically composite walls are used in the combustion chamber and single material walls are used in the downstream heat transfer section. Depending on the heat storage capacity of the walls, there will be a time delay before the heat is released to the room in which the stoves is placed, giving the heat release profile. This heat release profile and the stove surfaces' temperature are essential input to thermal comfort simulations for future's energy efficient residential buildings of the single family type.

A results example is shown in Figure 4 for the transient heat production and release profiles for a stove using phase change material (PCM) as a heat storage material in the outer wall layer [02].

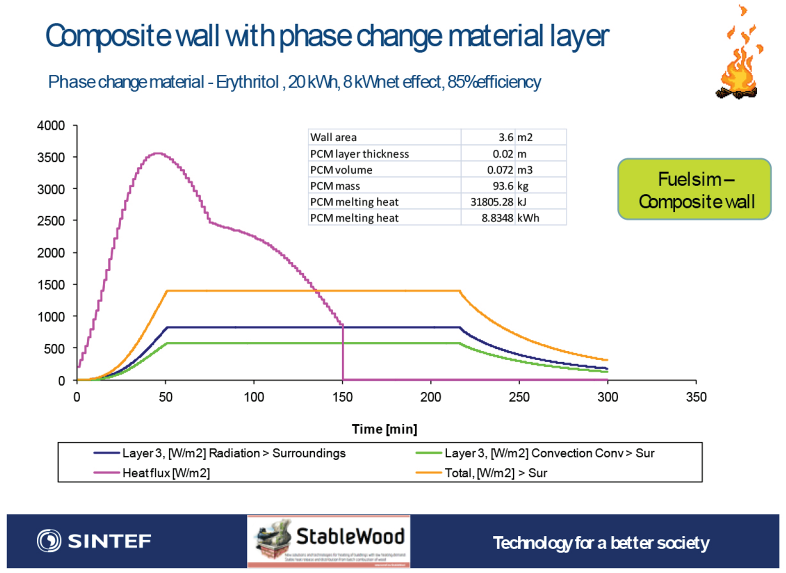

Figure 4: *Transient heat production profile (heat flux) and heat release profile (total = convection + radiation to the room) for a wood stove with a composite wall containing a phase change material*

2.4. Building integration modelling

Representative heat production profiles for wood stoves with different heat storage capacities and combustion cycle lengths have been generated for a large range of stove effects and have been used in two recent publications [03][04] investigating the resulting thermal comfort in passive houses with different thermal inertia in both central European climate (Belgian context) and cold climates (Norwegian context, different climate zones). The results show that wood stoves do have a natural place also in future's energy efficient single family houses, however, proper measures must be taken to prevent overheating in the living room. Reducing the stoves' nominal effect and applying measures to flatten out the heat release profile, through improved combustion control and/or increased heat storage capacity, makes wood stoves very attractive also in this building segment.

3. CONCLUSION

In this paper transient modelling of wood stoves has been discussed, selected results have been presented and the link towards CFD simulations and generation of necessary boundary conditions for these has been discussed. The key factor in the modelling approach is possibly the accuracy of the fuel model, providing the fuel gas related input. For the other input and models it is more a question of selecting the appropriate model level or detail to be able to carry out the CFD simulation within a reasonable time.

4. ACKNOWLEDGEMENTS

The authors acknowledge the financial support from the Research Council of Norway, and the four industrial partners in the StableWood project:

JØTUL	morsø	DOVRE	1893 GRANIT KLEBER

5. REFERENCES

[01] Seljeskog M, Skreiberg Ø. Batch combustion of logs in wood stoves – Transient fuel models and modelling of the fuel decomposition and products composition as input to CFD gas phase calculations. 1st International Workshop on CFD and Biomass Thermochemical Conversion, 30th September 2014, DBFZ, Leipzig, Germany.

[02] Skreiberg Ø, Seljeskog M, Georges L (2013). Transient wood-log stove modelling integrating detailed combustion physics. 21st European Biomass Conference and Exhibition, 3-7 June 2013, Copenhagen, Denmark.

[03] Georges L, Skreiberg Ø, Novakovic V (2013). On the proper integration of wood stoves in passive houses: Investigation using detailed dynamic simulations. Energy and Buildings 59, pp. 203-213.

[04] Georges L, Skreiberg Ø, Novakovic V (2014). On the proper integration of wood stoves in passive houses under cold climates. Energy and Buildings 72, pp. 87-95.

Mette Bugge (SINTEF, Norway)

CFD modelling of NO_x emissions from wood stoves

Mette Bugge, Øyvind Skreiberg, Nils Erland L. Haugen, Morten Seljeskog
SINTEF Energy Research
Kolbjørn Hejesvei 1A, Trondheim, Norway
Mette.Bugge@sintef.no, Oyvind.Skreiberg@sintef.no,
Nils.E.Haugen@sintef.no, Morten.Seljeskog@sintef.no

The present paper addresses NO_x emissions from wood stoves through a CFD modeling approach. The most significant route for NO_x formation in traditional biomass combustion applications is the fuel NO_x mechanism. The formation of fuel NO_x is very complex and sensitive to fuel composition and combustion conditions. Thus, accurate predictions of fuel NO_x formation in wood stoves, which constitute a wide range of compositions and states, rely heavily on the use of chemical kinetics with sufficient level of details. The computational fluid dynamics (CFD) simulations in this work were performed using the realizable k-ε turbulence model and the Eddy Dissipation Concept (EDC) by Magnussen [02][03] for turbulent combustion in conjunction with a detailed chemical reaction mechanism and two skeletal mechanisms recently developed for biomass combustion [04].

This work is a step in the development of a numerical tool required to study concept improvements with respect to NO_x emissions from wood stoves.

KEYWORDS: Wood, combustion, NO_x emissions, CFD, reaction mechanism

1. INTRODUCTION

Today small-scale wood combustion in wood stoves accounts for half of the bioenergy use in Norway, and the use of wood logs in small-scale units and pellets in pellet stoves is expected to increase substantially towards 2020. The national goal is to increase the energy conversion from these units by 8 TWh within 2020 [01]. This means that the energy conversion in these units has to be almost doubled compared with today. This calls for an increased effort with respect to emission reduction, both gaseous emissions due to incomplete combustion, particulates and NO_x.

The present paper addresses NO_x emissions from wood stoves through a CFD modeling approach. The most significant route for NO_x formation in traditional biomass combustion applications is the fuel NO_x mechanism. The formation of fuel NO_x is very complex and sensitive to fuel composition and combustion conditions. Thus, accurate predictions of fuel NO_x formation in wood stoves, which constitute a wide range of compositions and states, rely heavily on the use of chemical kinetics with sufficient level of details. CFD modelling of wood stoves have been published by very few [05][06][07][08][09], for stationary conditions and with considerable simplifications especially when it comes to gas phase chemistry.

In 2009 Scharler et al. [05] wrote a paper on CFD simulations of a commercial wood stove, where the simulations were used to optimize the stove by increasing the thermal efficiency at the same time as the emissions of CO and fine particulates were decreased. They used the realizable k-e turbulence model and the eddy dissipation model with finite rate kinetics for the turbulence-combustion coupling. An extended version of a global 3-step methane mechanism was used for the gas phase chemical kinetics.Scharler et al. (2011) [06] demonstrate how CFD can be used to develop, among other applications, wood stoves. They use a 3-step methane mechanism coupled with EDM for the homogeneous chemistry. The simulations are stationary and post processing with EDC is used in order to obtain predictions for NO_x emissions. Bugge et al. [10] demonstrate the use of the Eddy Dissipation Concept (EDC) for turbulent combustion in conjunction with a skeletal mechanism with 36 species developed for biomass combustion for prediction of NO_x emissions from woodstoves.

2. THE MODELLING APPROACH

2.1. General

Computational Fluid Dynamics (CFD) is the analysis of systems involving fluid flow by means of computer-based simulations. These systems may also involve heat transfer and associated phenomena such as chemical reactions. CFD simulations are based upon a numerical solution of the basic equations of the fluid dynamics; conservation of mass, momentum, and energy, together with mathematical sub-models. The equations can be solved time-dependent and in three-dimensions. Comprehensive modelling of combustion in general requires simulation of turbulent fluid dynamics, chemical kinetics as well as their interactions.

In the current study, the ANSYS FLUENT software is used for the calculations. FLUENT 15 is a general-purpose CFD code, which is based on finite volumes. When using the finite volume method, the region of interest is divided into small sub-regions called control volumes. The equations are discretized and solved iteratively, providing the value of each variable (velocity, temperature, mass fractions etc.) for each control volume throughout the calculation domain. A description of the CFD tool can be found on the ANSYS website (www.ansys.com), and a short description of the various models used is given in the section below.

2.2. Physical models

The computational fluid dynamics (CFD) simulations in this work were performed using the realizable k-ε turbulence model and the Eddy Dissipation Concept (EDC) by Magnussen [02][03] for turbulent combustion in conjunction with chemical reactions from three different reaction mechanisms developed for biomass combustion [04]. The detailed reaction mechanism includes 81 species, while the two skeletal mechanisms reduced from the detailed one includes 49 and 36 species. In this work the discrete ordinates method (DO) is used to model the radiative transfer, and the soot model chosen is the Moss & Brookes model with the soot precursors acetylene and ethylene (C_2H_2 and C_2H_4). The physical models used are described in more detail in previous work [10].

2.3. Geometry and boundary conditions

The wood stove chosen is a 5 kW natural draught wood log stove. The total combustion chamber volume is 0.0266m^3, and the wood amount is 2 kg based on the Norwegian standard NS 3058/3059. Primary air is injected through slots at the bottom of the stove, secondary air through 13 holes from the backside of the stove and flushing air is injected vertically through a slot above the front glass window.

The model is 3-dimensional and in full scale. As the stove is symmetrical, a symmetry boundary is defined through the vertical center plane, which means that the model includes one half of the stove. The geometry has been gridded with the ANSYS meshing platform (AMP). The mesh consists of approximately 256 000 tetrahedral elements. The wood logs are represented as volumes. The thermochemical conversion of the solid fuel is not included in the CFD-calculations. The volatiles are released from the outer surfaces of the wood pile.

Wood-log combustion is a batch process including drying, pyrolysis, gasification, char combustion as well as combustion of the gas components. The release of volatiles from the wood log is time dependent with respect to mass flow and gas composition, and the driving force for the decomposition of the solid fuel is the heat flux to the wood log. A model for the gas release is developed and implemented.

The gas composition and flow is based on Norway spruce, a wood consumption of 1.5 kg/h and the specific excess air ratio (λ_p =0.8). The gas composition has been optimized towards satisfying available relevant pyrolysis gas compositions and char gasification while maintaining the elemental balances for the solid fuel.

Table 1: Composition of the fuel gas/primary air mixture for a primary excess air ratio (λ_p) of 0.8

Specie	wt%	g
CO_2	4.1016	286.2761
H_2O	7.0759	493.8693
CO	12.5715	877.4385
H_2	0.2609	18.2101
CH_4	1.3293	92.7789
C_2H_2	0.0539	3.7646
C_2H_4	0.5811	40.5602
C_2H_6	0.3114	21.7374
NO	0.0011	0.0735
HCN	0.0075	0.5215
NH_3	0.0072	0.5055
O_2	13.3430	931.2863
N_2	59.3434	4141.9418
Ar	1.0122	70.6486
Tot gas	100.0000	6979.6123
Ash		4.9200
Total		6984.5323

Table 1 shows the composition of the fuel gas/primary air mixture based on a primary excess air ratio of 0.8. The amount of primary air injected through the slots corresponds to the excess oxygen in this composition. Increasing the primary excess air ratio will only change the mass of oxygen (O_2) and nitrogen (N_2), diluting the fuel gas. The mass of the combustible components will remain unchanged while the mass flow of primary air injected through the bottom slots will increase. The gas temperature is set to 773K.

The mass flow of volatiles released from the wood logs is determined by the heat flux from the combustion zone which means that the surfaces that are most visible to the flames will have the highest release. In this work the relative ratio between the release velocity for the top, side and end surfaces of the wood pile are 1/0.25/0.375.

The stove has cast iron walls, an insulated combustion chamber and a front glass window. In this work all the walls are treated identical, as isothermal walls with temperature 673K, and hence the radiation heat loss through the front glass window is neglected. In this initial work this is regarded as justifiable assumptions.

In the base case, the total excess air ratio is 1.6, the fraction of primary/secondary/flushing air is 0.5/0.4/0.1, and the air temperatures used are 300, 373 and 623K, respectively. Simulations with two skeletal mechanisms are carried out and compared with the results for the detailed mechanism they originate from. The effect of air distribution on the NO_x emission level is also studied.

3. RESULTS AND DISCUSSION

3.1. Effect of reaction mechanism for the base case

The fuel gas is released from the outer surfaces of the wood pile. The major part is released from the top surface, and the fuel conversion occurs mainly above the wood pile where the secondary air is injected, but also to an extent where the fuel gas from the side and end faces meets the primary air. As shown in Figure 1 the simulations give elevated temperatures in these areas. The maximum temperature is 1600K. The mean outlet temperature obtained in the simulations is 910 K. The three reaction mechanisms used give similar results for the temperature field.

When it comes to NO_x emissions, there are some variations in the predicted results for the three mechanisms. The TFN (total fixed nitrogen)/Fuel-N ratio at the outlet are compared in Figure 2. Four assumptions are used for the TFN ratio; in A0 only the nitrogen in NO is included, while in A3 the TFN includes all the major nitrogen species NO_2, N_2O, HCN and NH_3 in addition to NO. The two other assumptions are A1 including NO, HCN and NH_3, and A2 including NO, NO_2 and N_2O.

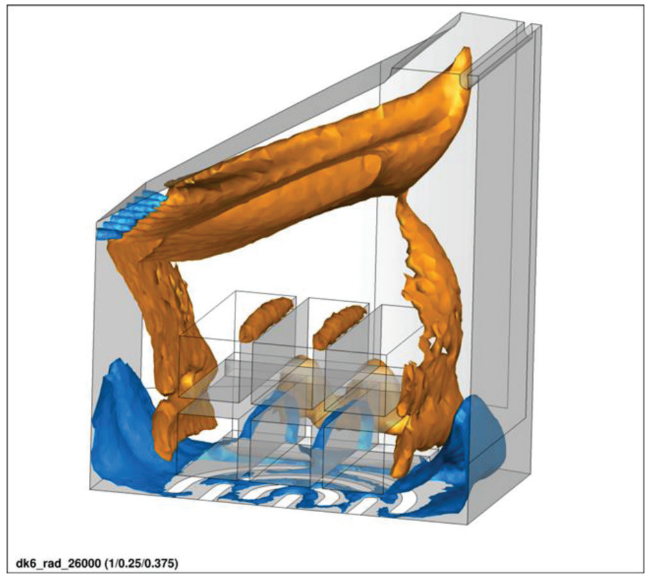

Figure 1: *Iso-surfaces for temperatures of 600 and 1100K for base case*

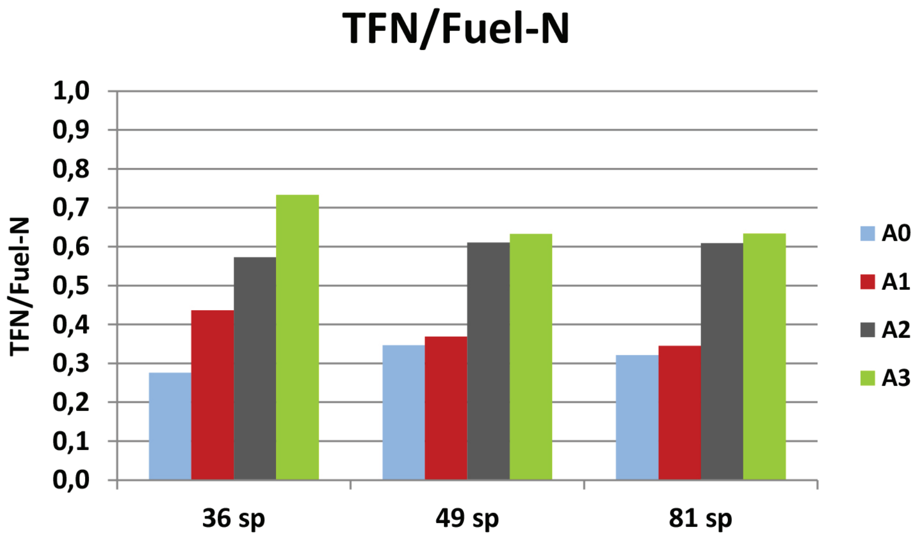

Figure 2: *TFN/Fuel-N ratio at the outlet for the three reaction mechanisms, 36, 49 and 81 species. A0-N in NO, A1-N in NO/HCN/NH_3, A2-N in NO/NO_2/N2O, A3- N in NO/NO_2/N_2O/HCN/NH_3*

It can be seen that the results for the 49 species mechanism correspond well with the detailed reaction mechanism (81 species). For the A3 and A2 assumption, the results are nearly identical (less than 0.5 % deviation), while the NO emission is slightly overpredicted for the skeletal mechanism (~8 %).

The results for the 36 species mechanism are less satisfactory. In this scenario the A3 assumption, emission of the major nitrogen species, is overpredicted with approximately 16 % compared to the detailed mechanism. This is mainly due to the over estimation of HCN, while the NO emissions are underpredicted. And hence, the 49 species mechanism could be used for prediction of NO_x emissions from woodstoves, while the 36 species mechanism is less suitable for the current problem.

Løvås et al. [04] found that the gas concentrations predicted with the 36 species mechanism were in agreement with the master mechanism (81 species) at higher temperatures (1073K), but the NO_x concentrations could be overpredicted at lower temperatures (873K). Gas concentrations predicted with the 49 species mechanism corresponded well with the master mechanism also at lower temperatures. In the present CFD study the temperatures are lower than 1073K in a significant part of the domain (Figure 2).

3.2. The effect of air distribution

Previous studies [11][12] have shown that air staging could be an efficient method to reduce NO_x emissions. Even if the present wood stove is not a classic air staged scenario as the mixing of fuel gas and primary air is far from complete before the secondary air is injected, some effect could be expected. The effect of air injection and distribution are studied. Simulations with primary air excess ratio of 0.8, 0.9 and 0.95 have been carried out. The total excess air ratio is 1.6 in all scenarios, and the ratio between flushing and secondary air is kept constant (1/4).

According to the simulations the NO emissions are nearly the same for the three scenarios (Figure 3). However, comparing the values of total fixed nitrogen (TFN) including NO_2, N_2O, HCN and NH_3 in addition to NO, the emissions (A3) are increasing when the primary air excess ratio increase, due to an increase in both the emissions of HCN+NH_3 as well as the emissions of NO_2+N_2O. The simulations show a significant reduction in TFN, with the largest reduction for a primary excess ratio of 0.8.

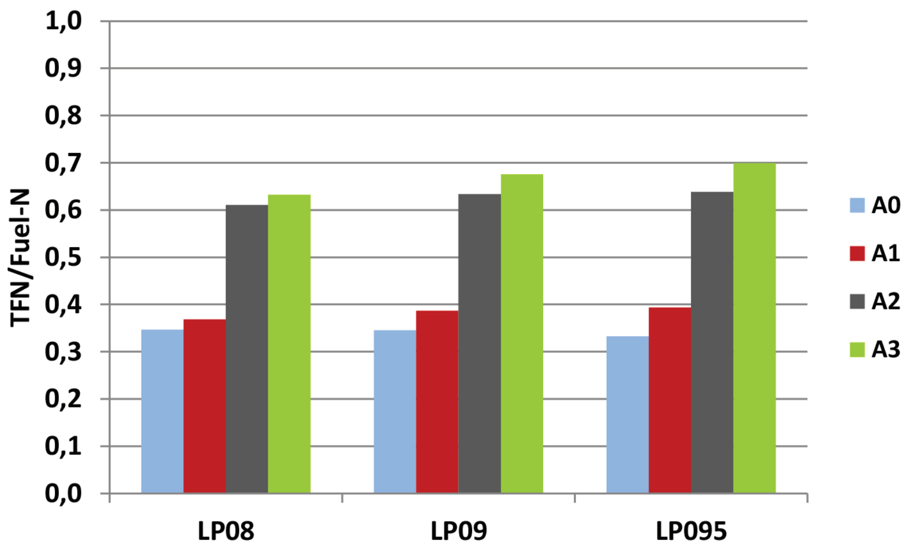

Figure 3: *TFN/Fuel-N ratio at the outlet for different air distributions.*
A0-N in NO, A1-N in NO/HCN/NH_3, A2-N in NO/NO_2/N_2O, A3- N in NO/NO_2/N_2O/HCN/NH_3

4. CONCLUSIONS

The simulations show that the skeletal mechanism with 49 species predicts results that correspond well with the detailed reaction mechanism while the one with 36 species overpredicts the NO_x formation at the conditions in this study, with relatively low temperatures in a significant part of the domain. The results give a significant NO_x reduction at a primary excess air ratio of 0.8, showing the potential of NO_x reduction by staged air combustion.

5. ACKNOWLEDGEMENTS

The authors acknowledge the financial support from the Research Council of Norway, and the four industrial partners in the StableWood project:

6. REFERENCES

[01] Regjeringen. Strategi for økt utbygging av bioenergi. 2008; Available from: http://www.regjeringen.no/nb/dep/oed/dok/rapporter/2008/strategi-for-okt-utbygging-av-bioenergi.html?id=505401

[02] Gran I, Magnussen B F (1996). A numerical study of a bluff-body stabilized diffusion flame. Part 2. Influence of combustion modeling and finite rate chemistry. Comb. Sci. Technol. 119, pp. 191–217.

[03] Ertesvåg I, Magnussen B F (2000). The Eddy Dissipation turbulence energy cascade model, Comb. Sci. Technol. 159, pp 213-236

[04] Løvås T, Houshfar E, Bugge M, Skreiberg Ø (2013). Automatic generation of kinetic skeletal mechanisms for biomass combustion, Energy & Fuels 27(11), pp. 6979-6991.

[05] Scharler R, Benesch H, Neudeck A, Obernberger I. (2009). CFD based design and optimization of wood log fired stoves, Proc. of 17th EU BC&E, Hamburg, pp. 1361-1367.

[06] Scharler R, Benesch H, Schulze K, Obernberger I. (2011). CFD simulations as efficient tool for the development and optimization of small-scale biomass furnaces and stoves, Proc. of 19th EU BC&E, Berlin, pp. 4-12.

[07] Huttunen M, Saastamoinen J, Kilpinen P, Kjäldman L, Oravainen H, Boström S. (2006). Emission formation during wood log combustion in fireplaces – part I: volatile combustion stage, Progress in Comp. Fluid Dynamics 6 (4-5), pp. 200-208.

[08] Saastamoinen J, Huttunen M, Kilpinen P, Kjäldman L, Oravainen H, Boström S. (2006). Emission formation during wood log combustion in fireplaces – part II – char combustion stage, Progress in Comp. Fluid Dynamics 6 (4-5), pp. 209-216.

[09] Menghini D, Marra F S, Allouis C, Beretta F. (2008). Effect of excess air on the optimization of heating appliances for biomass combustion, Experimental Thermal and Fluid Science 32.

[10] Bugge M, Haugen N E L, Skreiberg Ø. (2014). NOx emissions from wood stoves – a CFD modelling approach, Proc. of 22nd EU BC&E, Hamburg, pp. 674-679.

[11] Houshfar E, Skreiberg Ø, Løvås T, Todorovic D, Sørum L. (2011). Effect of excess air ratio and temperature on NOx emission from grate combustion of biomass in the staged air combustion scenario, Energy & Fuels, 25, pp. 4643-4654.

[12] Skreiberg Ø, Hustad J.E, Karlsvik E. (1996) In Developments in Thermochemical Biomass Conversion, Banff, Canada, A.V Bridgewater, D.G.B. Boocock, Eds. Blackie Academic & professional: London, UK, 1997, pp 1462-1478.

Laurent Georges (Norwegian University of Science and Technology), Øyvind Skreiberg (SINTEF), Norway

Simulation of the indoor thermal environment in passive houses heated using wood stoves: comparison between thermal dynamic simulations and CFD

Laurent Georges
Energy and Process Engineering Department, Norwegian University of Science and Technology (NTNU)
Kolbjørn Hejes vei 1b, NO-7491 Trondheim, Norway
laurent.georges@ntnu.no

Øyvind Skreiberg
Department of Thermal Energy, SINTEF Energy Research
Kolbjørn Hejes vei 1a, NO-7465 Trondheim, Norway
oyvind.skreiberg@sintef.no

The integration of wood stoves in passive houses (PH) is seen as problematic while this space-heating (SH) strategy is widespread in many countries. In practice, the integration of stoves in highly-insulated buildings faces two major challenges. Firstly, a good indoor air quality must be reached in an airtight building envelope. Secondly, the minimal combustion power of wood stoves currently available on the market is well above the SH power of PH. This power oversizing may lead to overheating in the room where the stove is placed. The present research aims at answering this second challenge dedicated to the indoor thermal environment. Numerical simulation is a powerful tool that enables to get a deep insight into these physical phenomena. Nevertheless, a major difficulty is to select between the modeling approaches: thermal dynamic simulations, computational fluid dynamics or the combination of both. Consequently, the present paper aims to discuss the advantages and limitations of these three approaches. It is shown that none of these methods is able to capture all the physical phenomena of interest using an acceptable computational time. On the contrary, they must be seen as three complementary methods that can span almost the complete range of physical problems.

KEYWORDS: All-year thermal comfort, Performance assessment, Passive House, nZEB.

1. INTRODUCTION

The integration of wood stoves in passive houses (PH) is seen as problematic while this space-heating (SH) strategy is widespread in many countries. In Norway, wood stoves provide about 20% of the SH needs of the residential building stock and about half of the bioenergy use. In parallel, Norway has decided to increase its share of biomass use whereas new building standards promote highly-insulated building envelopes, such as the passive house standard or future nearly-zero energy buildings (nZEB). In practice, the integration of stoves in highly-insulated buildings faces two major challenges. Firstly, a good indoor air quality (IAQ) must be reached although a wood combustion device is implemented within the airtight building envelope. Secondly, the minimal combustion power of wood stoves currently available on the market (typically 6-8 kW) is well above the SH power of PH (roughly < 3 kW). This power oversizing may lead to overheating in the room where the stove is placed. Furthermore, it is also worth investigating the heat transport between the room where the stove is placed and the neighboring rooms (such as bedrooms). The present research aims at answering this second challenge dedicated to the indoor thermal environment. Numerical simulation is a powerful tool that enables to get a deep insight into these physical phenomena. Nevertheless, a major difficulty is to select the proper level of modeling in order to perform this simulation work. Consequently, the present contribution aims to discuss the advantages and limitations of three common modeling approaches: thermal dynamic simulations, computational fluid dynamics (CFD) or their combination.

2. PHYSICAL PHENOMENA

2.1. Physical parameters

A large number of physical parameters are involved. As far as the building is concerned, its geometry and geographic/climatic location, as well as its thermal insulation and thermal mass are important factors. Obviously, the thermal insulation of external walls has a major influence. Nevertheless, the thermal transmittance of partition walls inside the building envelope should also be properly accounted for. This indeed influences the conductive heat transfer between the room where the stove is placed and its neighboring rooms. Furthermore, the SH power needed by highly-insulated houses is relatively low. The nominal SH power for a single-family passive house in Norway is typically ~3kW assuming extreme outdoor temperatures (i.e. a cold wave). During usual operating conditions within a heating season, the instantaneous SH power is well lower than this (< 1kW). Therefore, no steady-state regime can appear with the 6-8kW of heat produced by the wood stove and the much lower losses of the building envelope. The interaction of the stove with the building is thus by nature unsteady: the temperature in the room where the stove is placed is rising progressively during a combustion cycle of the stove. In this context, the building thermal mass stores the heat delivered by the stove and thus reduces the temperature increase in the room. In parallel, the hygienic ventilation system also has an important impact. Highly-insulated houses generally have balanced mechanical ventilation equipped with a heat recovery unit. In principle, the constant-air-volume (CAV) ventilation operates a cascade-flow: the fresh air is supplied in the living rooms and bedroom, and is extracted in so-called wet rooms (e.g. bathroom). Finally, it has also been shown that a significant amount of heat can flow between rooms through the open building doorways [01, 02]. A large bidirectional flow indeed takes place with flow rates having an order of magnitude higher than hygienic ventilation flow rates. As regards the wood stove, its nominal power (P_n) and power modulation capability are significant parameters. The thermal properties of the stove envelope should also be accounted for as it determines how the heat released from the combustion will subsequently be emitted to the room. The stove envelope flattens the heat release but also determines the ratio between heat emitted by convection and radiation: the convection will essentially heat the air of the room while the radiation will heat the internal surface of the walls facing the stove. Finally, a distinction should also be done between batch operated wood log stoves and continuous operated pellet stoves as their control possibilities and heat production profiles are very different.

The objective is to develop stoves that have the appropriate Pn but also that can operate correctly whatever the specific architectonic properties of a building. Given the large number of physical parameters involved, a suitable numerical simulation approach should then allow to perform large sensitivity analyses at an acceptable computational cost.

2.2. Physical timescales

A large spectrum of physical timescales is involved. This is known to be a challenge for time integration using numerical methods. The natural convection generated by the stove is unsteady with different timescales well below 1min. The stove control, if equipped with a power modulation, has also a reaction time of typically ~1min. The thermal storage of the stove may be saturated in some minutes to hours dependent on the storage capacity. One batch combustion cycle of wood log may last between ~40min and hours. On the contrary, the combustion timescale of pellets is often assumed negligible compared to the other physical timescales of the problem so that pellets combustion is often assumed instantaneous [03]. The building envelope (especially if well-insulated and with a high thermal mass) is characterized with relatively long timescales, from several hours to days. Finally, the boundary conditions of the building (i.e. the outdoor temperature, the user behavior, the internal gains and solar irradiation) change significantly throughout a heating season. A proper evaluation of the wood stove integration in a given building category would then require all-year simulations. An alternative is to define the most critical operating conditions (or periods of the heating season) and to limit the simulation for these specific periods. While this is in general a well-accepted methodology, these critical conditions have unfortunately not yet been established for highly-insulated buildings, such as PH.

2.3. Assessing the thermal comfort

The thermal comfort assessment may be evaluated with different levels of accuracy [04]. The most used approaches in building performance simulation (BPS) are global, such as the Fanger's and ISO 7730 methods [05], as the body is represented only using a single element. In this context, a simple comfort indicator is the operative temperature, T_{op}. For a given location in the room, T_{op} is often taken as the arithmetic mean of the local air temperature (T_s) and mean radiant temperature (T_{mrt}). By definition, this Tmrt requires computing the view factors of the walls as seen from the occupant's location. In the global thermal comfort model of the ISO 7730, the air velocity is also taken into account as well as the vertical temperature stratification. These values are far more computationally expensive to evaluate than T_{op}. Ultimately, if one is interested in the thermal comfort in the vicinity of the stove, a recent study has shown that a local thermal comfort assessment is required, where the body is divided into several segments (e.g. arms, head) [06].

3. COMPARING SIMULATION APPROACHES

3.1. Thermal dynamic simulations

Thermal dynamic simulations (TDS) are widespread in the BPS community. Common tools are TRNSYS [07], IDA-ICE, ESP-r or EnergyPlus. The building is often modeled using a thermal network approximation [08] and can be directly coupled to a simplified dynamic model of the stove [09], as shown in Figure 1. This stove model can include the stove control, its envelope and a combustion heat release model. Essentially, each room in the building model is represented by a single node (i.e. well-stirred tank approximation). Nevertheless, some software allow for splitting the room vertically in several air nodes to capture the thermal stratification. This method requires knowing the convective heat exchange between each vertical layer of air. This quantity is unfortunately not known nor approximated easily. Within each room, the flow is indeed not computed by thermal dynamic simulations. Only the airflows between rooms are usually evaluated using a ventilation network approach [10, 11] (e.g. using TRNFLOW [12]). All together, these rough approximations enable to perform all-year simulations at an acceptable computational cost, even if the stove control is taken into account. An approximation of the Top is reachable, based on the room average air temperature. Existing guidelines for the proper integration of wood stoves in passive houses have already been established using this approach [13, 14]. Nevertheless, the air velocity field within the room remains unknown as well as the temperature stratification. In ventilation network approaches, the bidirectional flow through an open door is modeled using the so-called *large opening approximation*. Using this last model, it has been proved that the temperature stratification in both rooms connected by the open door is an important input parameter in order to evaluate the convective heat exchange generated by the bidirectional flow [15].

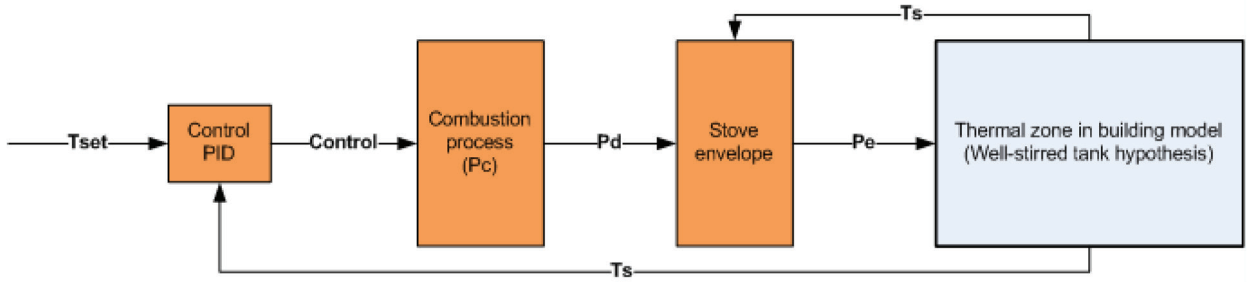

Figure 1: Simplified modeling procedure for the thermal comfort assessment using a wood stove (Pc is the combustion power, Pd the power delivered to the stove envelope, Pe the heat emitted to the room, Ts the sensible air temperature in the room and Tset the set-point temperature of the heating system).

3.2. Computational Fluid Dynamics

Computational Fluid Dynamics (CFD) is a powerful tool which is increasingly popular in BPS [16]. The radiation between walls as well as the unsteady turbulent flow can be properly modeled. The turbulence modeling of the flow in buildings is rather complex as the flow can be detached, laminar, transitional or turbulent. In this context, Reynolds-Averaged Navier-Stokes (RANS) approaches represent a good trade-off between computational speed and accuracy. Especially k-ε models are frequently used in building applications. Given high Rayleigh number of the buoyancy driven flow generated by the stove, unsteady simulations (URANS) should be applied to converge to a physical solution. On the one hand, the overall computational time for a CFD is way higher than for thermal dynamic simulations, which ultimately make full-building and all-year simulations unaffordable. On the other hand, the user has access to an estimate of the air velocity at different locations within a room as well as to the temperature stratification. Airflows through doorways are also better evaluated. Nevertheless, one should pay attention to the boundary conditions set to the computational domain of the CFD.

3.3. Coupled CFD with thermal dynamic simulations

In that respect, it is thus interesting to couple CFD with thermal dynamic simulations. The thermal dynamic simulation provides the boundary conditions of the CFD while the CFD provides the convection coefficients of walls for the thermal dynamic simulation. This method is as computationally expensive as CFD but boundary conditions are more consistently treated. Nevertheless, in the authors'opinion, no existing commercial software can provide a fully satisfactory tool for coupling CFD and thermal dynamic simulations. Some R&D tools exist, but suffer major limitations.

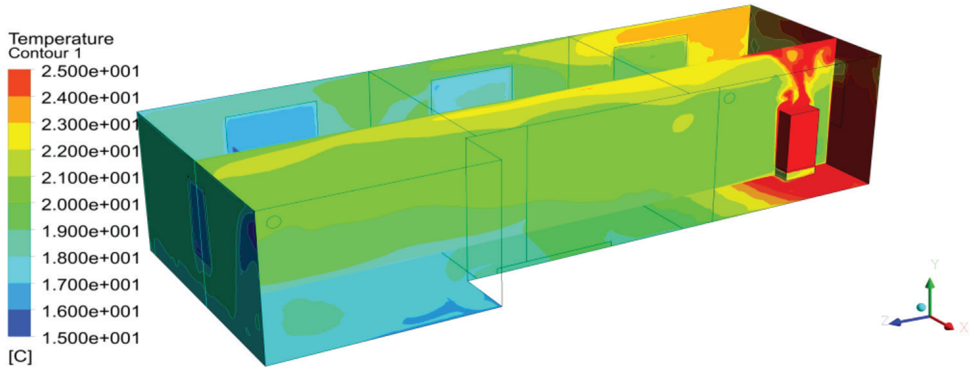

Figure 2: *Snapshot of the unsteady temperature field computed using CFD for a living room heated by a wood stove within a passive house [17]. The temperature is shown on the internal surfaces of the walls and along a longitudinal cut-plane (the colour scale is saturated outside the range of 15° to 25°C).*

Table 1: *Summary of the advantages and limitations of the three modelling approaches.*

Method	Δt imposed by	Tmin	Tmax	CPU time	Convection doors	Consistent BCS	Top	Stratification	Radiation asymmetry	Air velocity
TDS	Control/ Flow	1-cycle	1-year	Low-Medium	Simple	Yes	Yes	No	Yes	No
CFD	Flow	1-cycle	Few cycles	High	Accurate	No	Yes	Yes	Yes	Yes
TDS+CFD	Flow	1-cycle	Few cycles	High	Accurate	Yes	Yes	Yes	Yes	Yes

Tmin=minimal simulation time; Tmax=maximal simulation time

4. CONCLUSION

The present paper reviews three main modelling approaches to simulate the indoor thermal environment of buildings heated by wood stoves. They are especially discussed in the context of highly-insulated building envelopes, such as passive houses or nZEB. It is shown that none of these methods are able to capture all the physical phenomena of interest using an acceptable computational time. On the contrary, they must be seen as three complementary approaches that can span almost the complete range of physical problems. Furthermore, the present paper identifies the advantages and limitations of each modelling approach, as well as their range of applicability.

5. ACKNOWLEDGEMENTS

The authors want to acknowledge the Research Council of Norway for their support as this work was performed in the framework of the Research Centre on Zero Emission Buildings (ZEB, www.zeb.no) and the StableWood project.

6. REFERENCES

[01] Blumrich, F, Feist W, Hasper W, Krause H, Nitsch J, Pfluger R and Strauss R, Protokollband nr. 36: heizung mit biobrennstoffen für passivhäuser, P. Institut, Editor. 2007, Passivhaus Institut: Darmstadt.
[02] Feist W, Schnieders J, Dorer V, Haas A (2005). Re-inventing air heating: convenient and comfortable within the frame of the Passive house concept. Energy and Buildings 37, pp. 1186-1203.
[03] Persson T, Fiedler F, Nordlander S, Bales C, and Paavilainen J (2009). Validation of a dynamic model for wood pellet boilers and stoves. Applied Energy 86, pp. 645-656.
[04] Cheng Y, Niu J, Gao N (2012). Thermal comfort models: a review and numerical investigation. Building and Environment 47, pp 13-22.
[05] CEN, EN ISO 7730 : Ergonomics of the thermal environment: analytical determination and interpretation of thermal comfort using calculation of the PMV and PPD indices and local comfort criteria. 2005.
[06] Ghali K, Ghaddar N and Salloum M (2008). Effect of stove asymmetric radiation field on thermal comfort using a multisegmented bioheat model. Building and Environment 43, pp. 1241-1249.
[07] Klein et al., TRNSYS 17 : Volume 4, Mathematical Reference. 2010.
[08] TRANSSOLAR, TRNSYS 17: Volume 5, Multizone Building modeling with Type56 and TRNBuild. 2011.
[09] Georges L and Novakovic V. On the integration of wood stoves for the space-heating of passive houses: assessment using dynamic thermal simulations, in BSO 2012 conference. 2012: Lhouborough.
[10] Chen Q (2009). Ventilation performance prediction for buildings: a method overview and recent applications. Building and Environment 44, pp. 848-858.
[11] Wang L and Chen Q (2008). Evaluation of some assumptions used in multizone airflow network models. Building and Environment 43(10), pp. 1671-1677.
[12] TRANSSOLAR, TRNFLOW: a module of an air flow network for coupled simulation with TYPE 56 (multi-zone building of TRNSYS). 2009.
[13] Georges L, Skreiberg Ø and Novakovic V (2013). On the proper integration of wood stoves in passive houses: investigation using detailed dynamic simulations. Energy and Buildings 59, pp. 203-213.
[14] Georges L, Skreiberg Ø and Novakovic V (2014). On the proper integration of wood stoves in passve houses under cold climates. Energy and Buildings 72, pp. 87-95.
[15] Allard F, Bienfait D, Haghighat F, Liébecq G, Maas K V D, Pelletret R, Vandaele L et al. Air flow through Large Opening in Buildings, in Annex 20: Air flow patterns within Buildings, J. van der Maas, Editor. 1992, International Energy Agency.
[16] Srebric J, Ventilation performance prediction, in Building Performance Simulation for Design and Operation, Hensen J L M, Lamberts R, Editor. 2011, Spon Press: Oxon. p. 143-179.
[17] Georges L, Novakovic V. On the integration of wood stoves for the space-heating of passive houses: assessment using dynamic thermal simulations, in BSO 2012. 2012: Lhouborough.

Lars Seidel (BTU Cottbus, Germany)

CPU efficient modelling of biomass gasification using a stochastic reactor approach and chemistry guided reduction

Lars Seidel, Anna-Katharina Klaus, Fabian Mauss
Brandenburg University of Technology, Chair of Thermodynamics and Process Engineering
Siemens-Halske-Ring 8, 03046 Cottbus, Germany
Lars.Seidel@tdtvt.de, Anna-Katharina.Klaus@tu-cottbus.de, Fabian.Mauss@tdtvt.de

Cathleen Perlman, Karin Fröjd, Christian Klauer
LOGE AB – Lund Combustion Engineering
Scheelevägen 17, SE-223 70 Lund, Sweden
cperlman@loge.se, cklauer@loge.se

Timothy Laska, Jordan Jalving
Sundrop Fuels, Inc.
Longmont (CO), USA
Tim.Laska@sundropfuels.com

In this work a new developed model for biomass gasification using a series of partially stirred reactors is described. The model is validated against published measurements for different wood compositions and temperatures using a detailed reaction scheme for the solid and gas phase. In a further step the reaction mechanism was reduced to minimize the simulation time.

KEYWORDS: stochastic reactor model; gasification; model reduction; biomass

1. INTRODUCTION

The use of renewable biomass for energy generation, as feedstock for 2nd generation bio fuels and for chemical processes is of interest for a growing world population. The successful transition to a biomass based economy does depend on two major factors: the agricultural supply chain and the efficient use in the conversion process. This work focuses on the latter part and describes an efficient way of modelling the gasification process using detailed reaction chemistry. Due to its low computational cost the model is suitable for parameter studies in gasification devices resulting in deeper understanding and more efficient use of limited biomass resources.

2. STOCHASTIC GASIFICATION MODEL

The stochastic reactor model in LOGEsoft [01] is a probability density function (PDF) based approach for simulation of reactive systems. The gas in the reaction chamber is divided into a virtual number of particles, each representing a realisation of the discretised multidimensional mass density function (MDF):

$$F_{\Phi}(\psi_1, \dots, \psi_{\{S+1\}}, t)$$

where

$$\Phi(t) = (\Phi_1, \dots \Phi_N; t)$$

The time evolution of the MDF, assuming statistical homogeneity as proposed in the partially stirred plug flow reactor (PaSPFR) [02] [03], is given by

$$\frac{\partial}{\partial t}F_{\Phi}(\psi, t) + \frac{\partial}{\partial \psi_i}\left(Q_i(\psi)F_{\Phi}(\psi, t)\right) = mixing\ term$$

where Q_i denotes the source term for variable ψ, resulting from chemical reactions, heat transfer and volume work.

The gasifier is modelled as a series of partially stirred reactors, denoted cells, as displayed in Figure 1. Each gas particle in a cell is said to contain a certain amount of solid matter, moving with the gas. It is possible to have a number of different types of solid matter in each gas particle. All biomass particles contained within a gas particle are modelled by a single solid particle with a representative diameter, which may vary between different gas particles. The gas residing within the biomass particles' pores is set to the same temperature as that of the solid matter, which, in turn, is assumed to have uniform temperature.

An operator splitting technique is applied within each cell to evaluate particle mixing, reactor in- and outflow, chemistry and wall heat transfer whereas flow is calculated over the entire pipe. During the chemistry step, drying, biomass pyrolysis, tar formation, cracking, further particle breakdown, transport between gas and solid phase, gas phase chemistry and soot formation from PAH through the method of moments (bulk gas only) are considered.

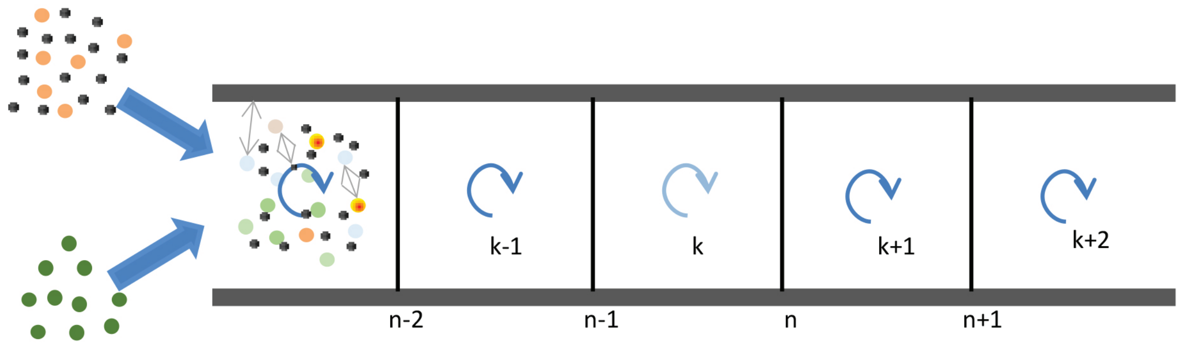

Figure 1: The gasifier is modelled as a series of partially stirred reactors where each gas phase particle contains a certain amount of solid matter

At each time step, the following equations are evaluated:

Bulk gas species fractions

$$Q_i(\psi) = \frac{\dot{\omega}_{i,g}}{\rho_g} - \frac{A_{s,total}}{m_g}W_i k_{m,i}\left(C_{i,g} - C_{i,p}\right) + Y_i\frac{A_{s,total}}{m_g}\sum_{j=1}^{n_g}W_j k_{m,j}\left(C_{j,g} - C_{j,p}\right), \quad i = 1, \dots, n_g$$

Bulk gas soot moments

$$Q_i(\psi) = \frac{\dot{\omega}_{soot,M_i}}{\rho_g}W_{soot}$$

Bulk gas temperature

$$\begin{aligned} Q_{T_g}(\psi) = \frac{1}{C_{p,soot+g}\rho_g}\Bigg(&\left(\sum_{i=1}^{n_g}h_i\dot{\omega}_i - \dot{\omega}_{M_1}W_{soot}h_{soot}\right) \\ &+ \frac{A_{s,total}}{V_{gas}}\left(\sum_{j=1}^{n_g}W_j k_{m,j}\left(C_{j,g} - C_{j,p}\right)\left(h_g - h_{j,g\leftrightarrow p}\right) + h_T\left(T_s - T_g\right)\right) + \dot{q}_{soot}\Bigg) \\ &- \frac{V}{C_p}\frac{dp}{dt} - \frac{h_g A_w}{C_p}(T - T_w) \end{aligned}$$

Gas mass

$$Q_{m_g}(\psi) = -A_{s,total}\sum_{j=1}^{n_g} W_j k_{m,j}\left(C_{j,g} - C_{j,p}\right) - \dot{\omega}_{M_1} W_{soot} V_g$$

Biomass pore gas species fractions

$$Q_i(\psi) = \frac{\dot{\omega}_{i,p}}{\rho_p} + \frac{\dot{\omega}_{i,s}}{\rho_s} - \frac{Y_i}{\rho_p}\sum_{j=1}^{n_g}\dot{\omega}_{j,p} + \frac{A_{s,total}}{m_p}\left(W_i k_{m,i}\left(C_{i,g} - C_{i,p}\right) - Y_i\sum_{j=1}^{n_g} W_j k_{m,j}\left(C_{j,g} - C_{j,p}\right)\right),\ i = n_{p,1}, \dots, n_{p,r}$$

Solid species fractions

$$Q_i(\psi) = V_{s,total}(1-\epsilon)\left(\dot{\omega}_{i,s} - Y_i\sum_{j=1}^{n_s}\dot{\omega}_{j,s}\right),\ i = n_{s,1}, \dots, n_{s,r}$$

Pore gas mass

$$Q_{m_p}(\psi) = V_{s,total}\epsilon\sum_{i=1}^{n_g}\dot{\omega}_{i,p} + A_{s,total}\sum_{j=1}^{n_g} W_j k_{m,j}\left(C_{j,g} - C_{j,p}\right)$$

Solid matter mass

$$Q_{m_s}(\psi) = V_{s,total}(1-\epsilon)\sum_{i=1}^{n_s}\dot{\omega}_{i,s}$$

Solid matter temperature

$$Q_{T_s}(\psi) = -\frac{1}{C_{p,s}\rho_{solid}}\left(\sum_{i=1}^{n_g} h_{i,p}\dot{\omega}_{i,p} + \sum_{i=1}^{n_s} h_{i,s}\dot{\omega}_{i,s}\right) + \frac{A_{s,total}}{C_{p,s} m_s}\left(\sum_{j=1}^{n_g} W_j k_{m,j}\left(C_{j,g} - C_{j,p}\right)\left(h_g - h_{j,g\leftrightarrow p}\right) - h_T\left(T_s - T_g\right) - \sigma\varepsilon_w\varepsilon_s\left(T_s^4 - T_w^4\right)\right)$$

Representative biomass particle diameter

$$Q_{d_s}(\psi) = \left(\frac{6}{\pi\rho_s} n_s\right)^{\frac{1}{3}} m_s^{-\frac{2}{3}} Q_{m_s}(\psi)$$

Representative biomass particle porosity

$$Q_\epsilon(\psi) = -\frac{(1-\epsilon)\,(1-\beta)}{\rho_s}\sum_{j=1}^{n_s}\dot{\omega}_{j,s}$$

In all equations above, subscripts *g*, *p* and s denote gas, pore and solid, respectively and *r* is the number of different solid particle ensembles. β is a tuning factor, meant to let the user capture the difference in speed with which solid mass, particle diameter and porosity changes and $V_{s,total}$ is the total biomass particle volume, including both solid matter and pore gas. Solid matter source terms are calculated either by mass or by surface depending on what type of process the reactions describe. In the expression above, unit conversions are applied where appropriate.

Heat transport between solid and bulk gas is calculated using Nusselt and Sherwood numbers for gas-to-particle convection.

Pressure is considered to be constant throughout the pipe and flow is assumed to be constant over the time step, which gives the following equation for the gas flow velocity:

$$\frac{\partial v}{\partial x} = \frac{1}{2\rho v}\left(\frac{f_r}{2}\frac{v|\rho v|}{e\ l}\right)$$

where f_r is the friction fanning factor, *l* the length of the cell and *e* and roughness indicator.

The stochastic gasification reactor is implemented in the LOGEsoft [01] suite which features an easy to use graphical user interface and allows for time efficient parameter studies due to the full parallelisation of the code. The implemented reduction tools are used in the next step.

3. CHEMICAL MODEL

For the chemistry modelling, the biomass reaction scheme from Ranzi et al. was used [04] together with a PAH formation model extension. In a first step the experiments were modelled with the detailed chemistry and compared to published experiments from Dupont et al. [05] for soft wood and hard wood gasification with different inlet temperatures. For the reduction of the gas phase mechanism, simulations with inactive gas phase chemistry were performed. The obtained gas phase mixtures were used as inlet composition in 0D constant pressure reactors where species and reactions were removed following the proposed strategy of "chemistry guided reduction" developed by Zeuch et al. [06].

3.1. MECHANISM REDUCTION

For the reduction the final time in each reactor was set to a value which ensures equilibrium (no further change concentration of key species). The profiles for key species such as CO, CO_2, H_2, H_2O, CH_4, C_2H_2, C_2H_4 and C_2H_6 were chosen as targets for the further reduction, meaning that in each reduction step it was made sure that those species profiles were preserved.

To ensure that the resulting mechanism was to be valid over a broad parameter range, a matrix for 0-D cases was set up. For each obtained gas phase mixture a variation in inlet temperature and pressure was applied. The actual reduction process can be described as follows:

1. For each matrix point the necessity of all species, relative to a species target, is calculated in constant pressure reactors.
2. The species/reaction with the lowest necessity over all matrix points is removed.
3. The reduced mechanism is validated against all targets and if the result is within the defined error tolerance the next species/reaction will be removed.

Using this technique, the original mechanism was reduced from 327 species and more than 10 000 reactions down to about 60 species and 150 reactions.

4. RESULTS

Table 1 shows a comparison between the experimentally obtained species fractions in the reactor outlet and the prediction with the stochastic model using the detailed and the reduced reaction scheme. Comparison is done for two different inlet temperatures (1073 K and 1223 K) and particle sizes (0.4 mm and 0.45 mm). Reactor conditions and composition for soft wood were chosen according to the data provided in [05].

Table 1: Measured species concentrations [05] and model prediction for soft wood mixture at T=1073 K / d=0.4 mm and beech wood at T=1223 K / d=0.45

Species	Experiment Soft wood [m%]	Detailed scheme [m%]	Reduced scheme [m%]	Experiment Beech wood [m%]	Detailed scheme [m%]	Reduced scheme [m%]
H_2	1.2	2.5	3.0	1.9	2.6	2.7
CO	43.0	52.8	59.6	49.0	42.5	42.6
CO_2	7.0	9.7	10.8	10.0	7.8	7.5
CH_4	4.4	7.7	7.8	6.6	4.7	4.2
C_2H_4	5.0	5.3	5.9	3.0	1.7	1.6
C_2H_2	1.1	1.5	1.9	3.3	4.2	5.0
C_2H_6	Not meas.	0.4	0.6	0.0	0.1	0.1
H_2O	11.0	8.7	9.5	12.0	6.8	6.8

A good agreement with the experiment was found for both the detailed and the reduced scheme and an overall speed up factor of 25 was obtained. Typical CPU times are about 10 minutes on an 8 core workstation (AMD Opteron 2389) using the reduced gas phase mechanism and representing the gasifier by 10 stochastic cells and 8 particles.

5. CONCLUSION

An efficient, fully parallelised stochastic reactor model for biomass gasification was developed and its predictive ability was compared to experimental data available in literature, using a published reaction scheme. Overall a good agreement between the published detailed reaction scheme and the measured experimental data was found for most of the species. For some species however the model under predicts the measurement which leaves room for improvement.

Applying the reduced reaction scheme resulted in 25 times faster CPU time while maintaining the prediction of the measured gas phase species. Such short CPU times enable users to efficiently study the gasification process in detail and to perform extensive parameter studies in the design process of biomass gasifiers. The impact of the biomass feedstock and physical process parameters are also easily investigated.

6. REFERENCES

[01] LOGEsoft - Software suite www.loge.se
[02] Kraft M. Stochastic Modelling of Turbulent Reacting Flow in Chemical Engineering VDI Verlag – Fortschrittsberichte des VDI, Reihe 6 pp. 1-109. 1998
[03] Perlman C, Fröjd K, Seidel L, Tunér M, Mauss F. A Fast Tool for Predictive IC Engine In-Cylinder Modelling with Detailed Chemistry, SAE 2012-01-1074
[04] Ranzi E, Cuoci A, Faravelli T, Frassoldati A, Migliavacca G, Pierucci S, Sommariva S (2008). Chemical Kinetics of Biomass Pyrolysis, Energy and Fuels 22 (6), pp. 4292-4300.
[05] Dupont C, Chen L, Cances J, Commandre J M, Couci A, Pierucci S and Ranzi E (2009). Biomass pyrolysis: Kinetic modelling and experimental validation under high temperature and flash heating rate conditions. Journal of Analytical and Applied Pyrolysis 85, pp. 260–267.
[06] Zeuch T, Moréac G, Mauss F (2008). A comprehensive skeletal mechanism for the oxidation of n-heptane generated by chemistry-guided reduction. Combustion and Flame 155(4), pp. 651-674.

Nils Erland L. Haugen (SINTEF, Norway)

Transient simulations of biomass char gasification

Nils Erland L. Haugen
SINTEF Energy Research
Trondheim, Norway
nils.e.haugen@sintef.no

Jonas Kruger, Terese Løvås
Department of Energy and Process Engineering,
Norwegian University of Science and Technology, Trondheim, Norway
jonas.kruger@ntnu.no

Reginald E. Mitchell and Matthew B. Tilghman
Department of Mechanical Engineering, Stanford University, Stanford, USA
remitche@stanford.edu

Results of simulations of gasification of corn-stover char in environments similar to the ones established in a full scale gasification reactor are presented. The heterogeneous reaction mechanism employed in the model takes into account char gasification via CO_2 and H_2O as well as char oxidation via O_2 to account for the low levels of oxygen added to gasifiers to drive the endothermic gasification reactions. Reactions that account for CO and H_2 inhibition are included in the reaction mechanism. When H_2 and CO are not present in the ambient gas, the inhibition of the gasification rate is found *not* to be due to adsorbed H or CO species occupying carbon sites.

In the model, account is also made for radiation exchange between char particles and between particles and the surrounding wall. It is shown that for many applications, inter-particle radiation, which is neglected in most gasification models, can be quite significant in influencing the char-particle cooling rate.

KEYWORDS: Biomass, gasification, heterogeneous reactions, adsorbed species.

1. INTRODUCTION

The gasification process consists of the devolatilization phase, followed by reactions of the volatiles, and then the char burnout phase. The char burnout proceeds through heterogeneous reactions between the gas and the solid phase. Single particle char burnout can be modelled using transient, zero dimensional models, i.e. with no spatial discretization, which is done by e.g. Qiao et al. (2012) [01] and references therein. These zero dimensional models are fast and can potentially be used as sub-models for heterogeneous reactions in higher dimensional CFD tools. In this work, gasification of biomass char is studied in a simulation code that includes a detailed heterogeneous reaction mechanism for char reactivity to CO_2, H_2O and O_2 and uses GRI-Mech 3.0 as the chemical kinetic mechanism that describes the impact of homogeneous reactions. The code is transient and zero dimensional in space, and is designed to be used both as a stand-alone gasification/combustion code and as a sub-model for heterogeneous reactions of solid particles in a CFD code when the particle evolution is described by Lagrangian particle tracking as well as when an Eulerian-Eulerian methodology is chosen. A newly developed sub-model [02] that accounts for gradients inside the particle in the zero dimensional representation is used to determine the mode of combustion.

2. METHOD

Let V define a volume enclosed by the surface S, containing a gas mixture with a constant number of N_p embedded char particles. Let the surface S be impermeable such that there is no mass flux over S and let it be flexible such that the volume V is allowed to change in order to keep the gas pressure of the enclosed gas constant. The total mass inside S is then constant and equal to $m = m_pN_p + mg$ where m_p is the mass of each particle while m_g is the mass of the gas. It is clear that the gas density is given by $\rho_g = m_g/V$ while the particle number density is $n_p = N_p/V$.

The heterogeneous particle-to-gas reactions are determined by the set of reactions listed in Table 1 [03], while the homogeneous gas phase reactions are determined by the GRI-3.0 reaction mechanism. The governing conservation equations for the gas phase are solved for the gas density, composition and temperature, while for the biomass char particles, the differential equations that describe the transport of mass and energy are solved to yield the particle mass, temperature and adsorbed species concentrations during char conversion. The effectiveness factor approach of Thiele [04] is used to account for the concentration gradients that exists inside char particles at high-temperatures and is also used in the mode of conversion sub-model in which the evolution of the particle radius and apparent density are handled by the method described in Haugen et al. (2014) [02]. The simulation code utilized in the current work is the same as previously described elsewhere [05,06].

Table 1: Heterogeneous reaction mechanism

	Reaction	Pre-Exponential	Activation Energy (kJ/mol)	Std Dev (kJ/mol)
R1	$2C_f + H_2O \leftrightarrow C(OH) + C(H)$	$7.3 \bullet 10^7$	106	
R2	$C(OH) + C_f \leftrightarrow C(O) + C(H)$	$1.5 \bullet 10^{12}$	150	
R3	$C(H) + C(H) \leftrightarrow H_2 + 2C_f$	$1.0 \bullet 10^{12}$	100	
R4	$C(O) + C_b \rightarrow CO + C_f$	$1.0 \bullet 10^{13}$	353	28
R5	$C(OH) + C_b \leftrightarrow HCO + C_f$	$1.0 \bullet 10^{13}$	393	28
R6	$C_b + C_f + C(H) + H_2O \leftrightarrow CH_3 + C(O) + C_f$	$1.0 \bullet 10^{13}$	300	
R7	$C_b + C_f + C(H) + H_2 \leftrightarrow CH_3 + 2C_f$	$1.0 \bullet 10^{13}$	300	
R8	$C_f + C(H) + CO \rightarrow HCO + 2C_f$	$1.0 \bullet 10^{13}$	300	
R9	$C(H) + C(H) \rightarrow CH_2 + C_f$	$3.0 \bullet 10^{11}$	426	
R10	$CO_2 + C_f \leftrightarrow C(O) + CO$	$8.6 \bullet 10^4$	188	
R11	$C_b + CO_2 + C(O) \rightarrow 2CO + C_f$	$3.26 \bullet 10^{12}$	367	
R12	$C(CO) \leftrightarrow CO + C_f$	$1.0 \bullet 10^{13}$	455	53
R13	$CO + C(CO) \rightarrow CO_2 + 2C_f$	$3.36 \bullet 10^6$	266	
R14	$2C_f + O_2 \rightarrow C(O) + CO$	$7.0 \bullet 10^{10}$	150	
R15	$2C_f + O_2 \rightarrow C_2(O_2)$	$3.0 \bullet 10^8$	103	
R16	$C_f + C_b + C(O) + O_2 \rightarrow CO_2 + C(O) + C_f$	$1.5 \bullet 10^7$	78	
R17	$C_f + C_b + C(O) + O_2 \rightarrow CO + 2C(O)$	$2.1 \bullet 10^7$	103	
R18	$C_b + C_2(O_2) \rightarrow CO_2 + 2C_f$	$1.0 \bullet 10^{13}$	304	33

3. RESULTS

In the following discussion, simulations of corn stover char particles exposed to the conditions given in Table 2 are presented. When comparing results of simulations, these conditions and the full reaction mechanism shown in Table 1 define the base case simulation.

Table 2: Properties of the simulations

Property	Value	Units
Carbon to gas mass ratio	0.4	-
Particle radius	50	µm
Particle number density	10^9	m^{-3}
Pressure	24	bar
Initial temperature	1640	K
Reactor size	1	m
Initial mass fraction of H_2O	0.6	-
Initial mass fraction of O_2	0.29	-
Initial mass fraction of CO_2	0.1	-
Initial mass fraction of N2	0.01	-

From Figure 1, it can be seen that for the base case simulation (black line) full conversion is reached after about 2.4 seconds, while the peak particle and gas temperatures reach 2450 K and 2800 K, respectively. In order to investigate the effect of H_2 inhibition on the heterogeneous reactions, reactions R3 reverse and R7 forward are turned off by temporarily setting their pre-exponential factors to zero. By this approach all other aspects of the simulations, e.g. transport data and gas phase reactions, are kept un-changed. These results are presented by the red lines in Figure 1, which show that full conversion is reached slightly earlier than for the base case. A weak temperature dependence is also observed. This means that there is indeed some inhibition of the heterogeneous reactions due to the hydrogen present in the gas phase, but the effect is not very strong. Inhibition due to CO can be examined in the same manner, by turning off reactions R8, R10 reverse, R12 reverse and R13. This is visualized by the blue line in Figure 2. Like for H_2 inhibition, it can be seen that CO does inhibit the reactions by yielding full conversion in a shorter time than the base case, but the effect is still not very strong.

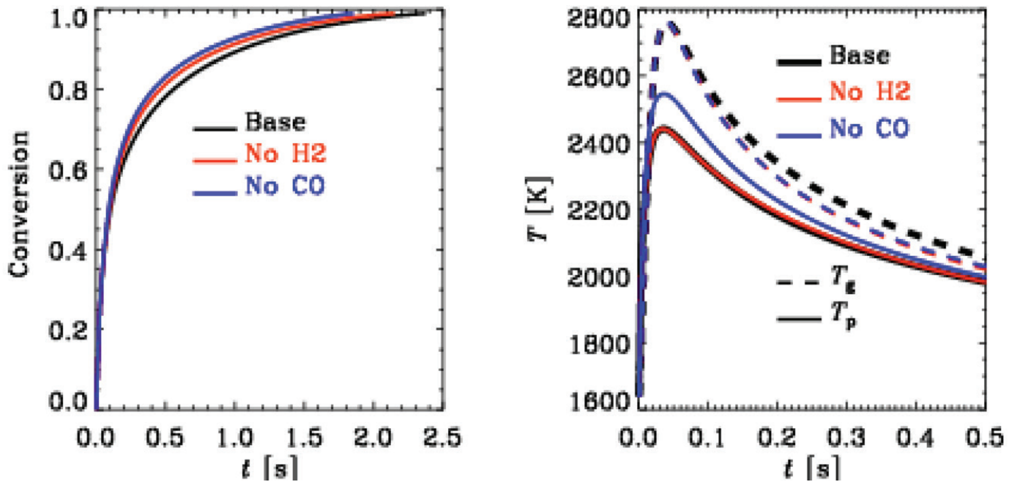

Figure 1: Conversion (left panel) and particle and gas temperatures (right panel) as a function of time for the base case (black line), the case with no H_2 heterogeneous reactants (red line) and the case with no CO heterogeneous reactants (blue line).

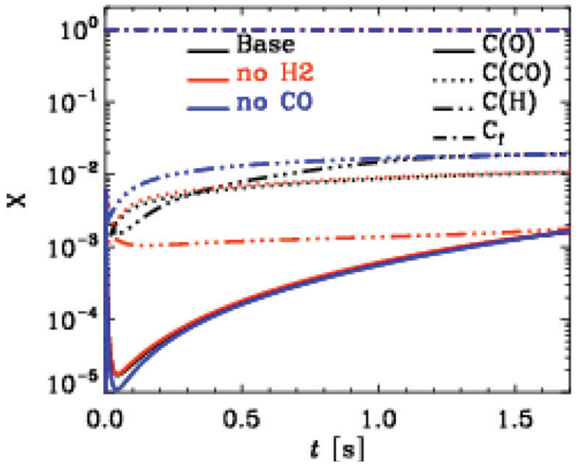

Figure 2 : Surface coverage fractions of adsorbed species as a function of time. The solid line represents adsorbed oxygen, the dotted line adsorbed CO and the dashed-triple-dotted line adsorbed H, while the dashed-dotted line represents the free carbon sites.

In Figure 2 the fraction of adsorbed species on the surface is shown for the base case (black lines) together with the cases with no H_2 reactions (red lines) and no CO reactions (blue lines). The amount of H adsorbed on the surface is found to decrease strongly when the hydrogen reactions are neglected. In the same way, the amount of adsorbed CO vanishes when CO reactions are neglected. It is clear however, that due to the low fraction of surface sites being occupied by adsorbed species, the fraction of available sites (C_f) is always close to unity. This means that both H_2 and CO inhibition must be due to a change in the reverse rates of these heterogeneous reactions, and *not* due to adsorbed species filling up the free sites and by this "clogging" the heterogeneous reaction paths.

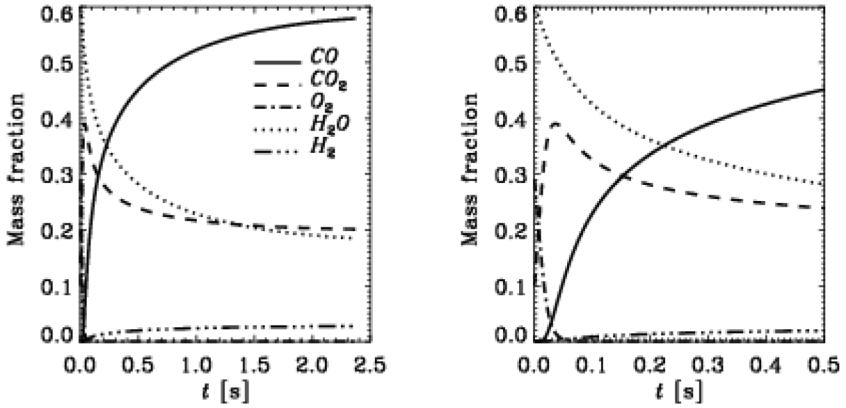

Figure 3: Mass fraction of gas phase species (ambient) as a function of time for the base case.

The mass fraction of the species in the ambient are shown in Figure 3, where one can see that the mass fraction of CO reaches almost 0.6. From the right plot it can be seen that the mass fraction of CO_2 starts to decrease when the O_2 mass fraction reaches zero. By comparison with the right hand plot of Figure 1, the time when O_2 has been consumed is also found to roughly correspond to the time when the gas and particle temperatures start to decrease.

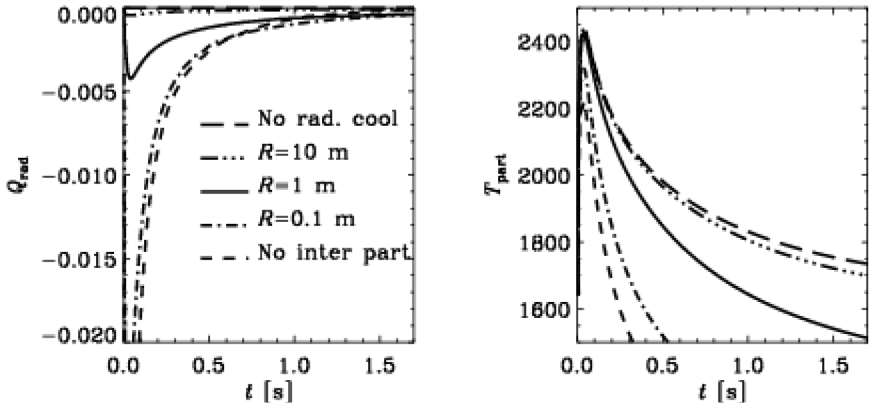

Figure 4: Radiative cooling of particles (left panel) and particle temperature (right panel) as a function of time for different treatments of radiation and reactor sizes.

It is common to see that particle-particle radiation is neglected for gasification environments. For the conditions presented here (see Table 2) the radiative particle cooling is represented by the solid line in the left panel of Figure 4. If inter particle radiation is neglected, it can be seen by the dashed line that the radiative cooling increases strongly, and is a good approximation only for reactors of sizes less than 10 cm (dashed-dotted line). When increasing the reactor size to 10 m (dashed-triple-dotted line) the radiative cooling becomes very low and approaches the situation when radiative cooling is neglected. The reason behind this is that for large reactors the optical depth is larger than unity for the majority of the particle cloud. This means that just a small fraction of the radiation emitted from the particles reaches the reactor walls. In the right hand panel of Figure 4, the particle temperature is shown to vary strongly with the reactor size and particle radiation model. As expected, the larger reactor sizes yields higher temperatures.

4. CONCLUSION

It is found that for the conditions used in this paper, there is inhibition of the gasification rate due to both hydrogen and carbon monoxide. The inhibition is not very strong at the high temperatures studied. It is concluded that in the absence of H_2 and CO in the gas phase, inhibition is not due to adsorbed H or CO filling up the free carbon sites for there are ample free sites available.

It is also found that for large enough reactors, it is crucial to include particle-particle radiation in the energy transport equation. Particle-particle radiation can be neglected only when the entire volume has an optical depth well below unity. For very large particle enclosures, the neglect of radiative cooling is an adequate assumption.

5. ACKNOWLEDGEMENTS

This work forms part of the CAMPS project supported by the Research Council of Norway (215707). The work has additionally been produced with support from the BIGCCS Centre, performed under the Norwegian Research Program Centres for Environment-Friendly Energy Research (FME). The authors acknowledge the following partners for their contributions: Aker Solutions, ConocoPhillips, Gassco, Shell, Statoil, TOTAL, GDF SUEZ and the Research Council of Norway (193816/S60).

The research leading to these results has received funding from the Polish-Norwegian Research Programme operated by the National Centre for Research and Development under the Norwegian Financial Mechanism 2009-2014 in the frame of Project Contract No Pol-Nor/232738/101/2014

NELH also acknowledges the Research Council of Norway under the FRINATEK grant 231444.

6. REFERENCES

[01] Qiao L, Xu J, Sane A and Gore J (2012). Combustion and Flame 159, pp. 1693.

[02] Haugen N E L, Tilghman M and Mitchell R E (2014). Combustion and Flame 161, pp. 612.

[03] Tilghman M and Mitchell R E. Coal and Biomass Char Reactivities in Gasification and Combustion Environments, Submitted for publication in Combustion & Flame, May 2014

[04] Thiele E W (1939). Ind. Eng. Chem 31, pp. 916 .

[05] Haugen N E L, Mitchell R E and Tilghman M. 8th US National Combustion Meeting, May 19-22, 2013.

[06] Haugen N E L, Mitchell R E and Tilghman M. A comprehensive model for char particle conversion in environments containing O_2 and CO_2, Submitted for publication in Combustion & Flame, August 2014

POSTER

Mette Bugge (SINTEF, Norway)

CFD simulations of staged biomass grate fired combustion with an emphasis on NO_x emissions

Mette Bugge, Øyvind Skreiberg, Nils Erland L. Haugen
SINTEF Energy Research
Kolbjørn Hejes vei 1A, Trondheim, Norway
Mette.Bugge@sintef.no, Oyvind.Skreiberg@sintef.no, Nils.E.Haugen@sintef.no

Ehsan Houshfar
ENERGOS AS
Kvenildmyra 5, Trondheim, Norway
Ehsan.Houshfar@energos.com

Terese Løvås
Norwegian University of Science and Technology
Kolbjørn Hejes vei 1B, Trondheim, Norway
Terese.Lovas@ntnu.no

The present paper addresses NO_x emissions from biomass combustion, and the objective is to demonstrate the applicability of stationary CFD simulations, including a detailed representation of the gas phase chemistry, to a multi-fuel lab-scale grate fired reactor using biomass as fuel.

In biomass combustion applications, the most significant route for NO_x formation is the fuel NO_x mechanism. The formation of fuel NO_x is very complex and sensitive to fuel composition and combustion conditions. And hence, accurate predictions of fuel NO_x formation from biomass combustion rely heavily on the use of chemical kinetics with sufficient level of details. The computational fluid dynamics (CFD) simulations in this work were performed using the realizable k-ε turbulence model and the Eddy Dissipation Concept (EDC) by Magnussen [01][02] for turbulent combustion in conjunction with a detailed chemical reaction mechanism and a skeletal mechanism recently developed for biomass combustion [03].

The results give a significant NO_x reduction at a primary excess air ratio of 0.8, showing the potential of NO_x reduction by staged air combustion.

KEYWORDS: Biomass, combustion, CFD simulations, NO_x emissions, reaction mechanism.

1. INTRODUCTION

Computational Fluid Dynamics (CFD) is a very useful tool to study flow and mixing behaviour, combustion and emissions from furnaces. CFD simulations can provide useful information in parts of combustion devices and furnaces where optical access and measurements are impossible. In addition, modifications and possible improvements can rather inexpensively be investigated. Normally, only a simplified description of the gas phase chemistry is used in simulations involving combustion. Such simplified descriptions, e.g. one-step reaction chemistry, are tuned to match combustion characteristics at certain conditions; hence, the accuracy may drop dramatically outside the valid state and composition window. Thus, by adopting a simplified treatment of the chemical processes, the possibility to capture ignition and extinction together with pollutant formation and reduction is very limited. For many applications it is therefore important to use detailed chemical kinetics.

In biomass combustion applications, the most significant route for NO_x formation is the fuel NO_x mechanism. The formation of fuel NO_x is very complex and sensitive to fuel composition and combustion conditions. And hence, accurate predictions of fuel NO_x formation from biomass combustion rely heavily on the use of chemical kinetics with sufficient level of details. The CFD simulations in this work were performed using the realizable k-ε turbulence model and the Eddy Dissipation Concept (EDC) by Magnussen [01][02] for turbulent combustion in conjunction with a detailed chemical reaction mechanism and a skeletal mechanism recently developed for biomass combustion [03].

The objective of this work is to demonstrate the applicability of stationary CFD simulations, including a detailed representation of the gas phase chemistry, to a multi-fuel lab-scale grate fired reactor using biomass as fuel.

2. THE MODELLING APPROACH

2.1. General

Computational Fluid Dynamics (CFD) is the analysis of systems involving fluid flow by means of computer-based simulations. These systems may also involve heat transfer and associated phenomena such as chemical reactions. CFD simulations are based upon a numerical solution of the basic equations of the fluid dynamics; conservation of mass, momentum, and energy, together with mathematical sub-models. The equations can be solved time-dependent and in three-dimensions. Comprehensive modelling of combustion in general requires simulation of turbulent fluid dynamics, chemical kinetics as well as their interactions.

In the current study, the ANSYS FLUENT software is used for the simulations. FLUENT 15 is a general-purpose CFD code, which is based on finite volumes. When using the finite volume method, the region of interest is divided into small sub-regions called control volumes. The equations are discretized and solved iteratively, providing the value of each variable (velocity, temperature, mass fractions etc.) for each control volume throughout the calculation domain. A description of the CFD tool can be found on the ANSYS website (www.ansys.com), and a short description of the various models used is given in the section below.

2.2. Physical models

The CFD simulations were performed using the realizable k-ε turbulence model and the Eddy Dissipation Concept (EDC) by Magnussen [01][02] for turbulent combustion in conjunction with chemical reactions from two different reaction mechanisms developed for biomass combustion [03]. The detailed reaction mechanism includes 81 species, while the skeletal mechanism reduced from the detailed one includes 36 species. In this work the discrete ordinates method (DO) is used to model the radiative transfer, and the soot model chosen is the Moss & Brookes model with the soot precursors acetylene and ethylene (C_2H_2 and C_2H_4). The physical models used are described in more detail in previous work [04].

2.3. Geometry and boundary conditions

The objective of this work is to study combustion of biomass in a grate fired lab-scale multi-fuel reactor (Figure 1). The reactor is located in the SINTEF Energy Research laboratory. The reactor has an electrically heated ceramic inner tube with a diameter of 100 mm and a length of 2 m. The reaction section located above the grate is 1.6 m long. The reactor is fitted with a unique two-level grate system, as shown in Figure 1, which allows for two-stage fuel burning. There are rotating blades on each level that move the unburned fuel particles on the grates, from the upper grate to the lower grate and from the lower grate to the ash bin through a slot in the grates. Air can be fed to the reactor at two levels; below the lower grate and at a level above the second grate. A more detailed description of the reactor can be found in a study by Khalil et al. [05].

Experiments studying the effect of excess air ratio on NO_x emissions were performed by Houshfar et al. [06] for staged and non-staged air combustion. The experiments were carried out using 6-mm-diameter pellets of demolition wood fed to the reactor at a set rate. Their experiments carried out at 1123 K were selected as a basis for comparison in this numerical study.

In the simulations the geometry model includes the 1.6 m high reaction section above the grate. The model is 3-dimensional and in full scale. The geometry has been gridded with the ANSYS meshing Platform (AMP). The mesh consists of approximately 202 100 hexahedral elements.

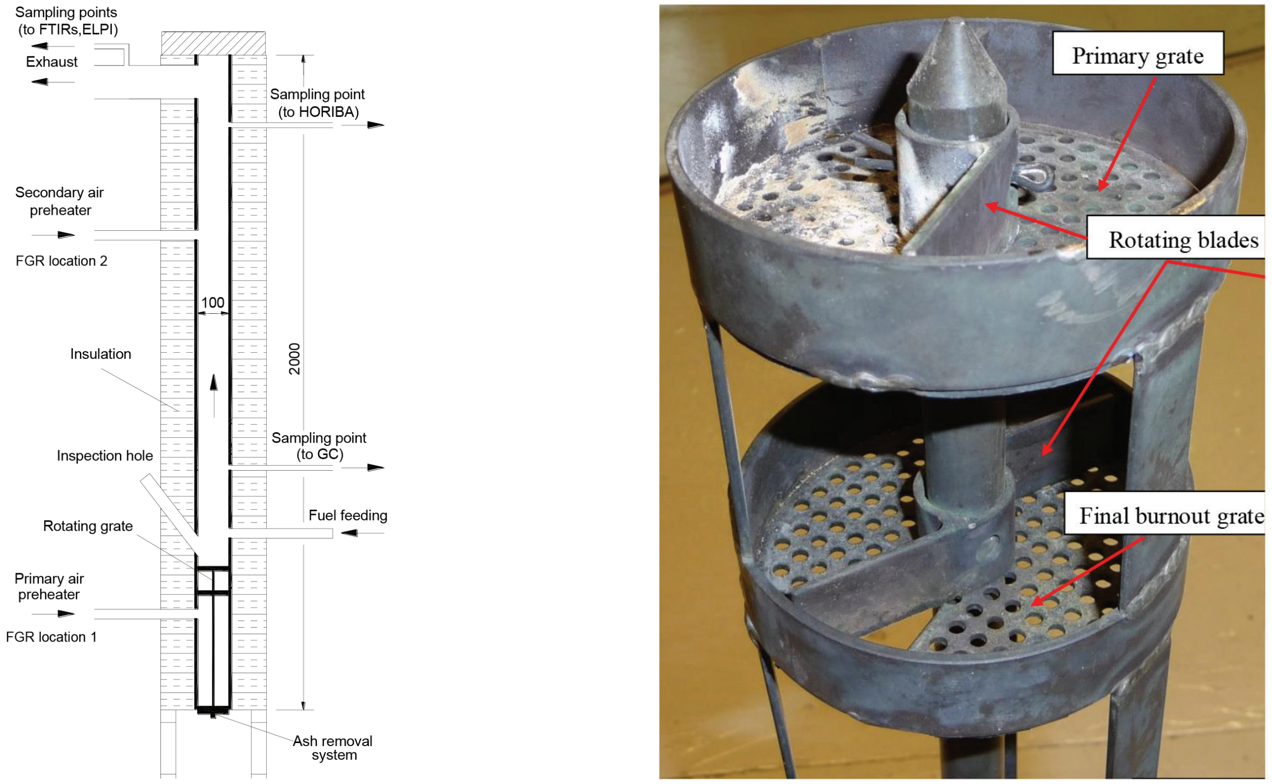

Figure 1: Left: Schematic drawing of the multi-fuel reactor of SINTEF Energy Research. Right: The two-level grate system

Table 1 : Composition of fuel gas/air mixture for primary excess air ratio (λ_p) of 0.8

	wt%	g
CO_2	13.8483	275.79
H_2O	5.3929	107.40
O_2	9.9429	198.01
N_2	60.7130	1209.10
CO	6.3018	125.50
H_2	0.2561	5.10
CH_4	1.3307	26.50
C_2H_2	0.0552	1.10
C_2H_4	0.5825	11.60
C_2H_6	0.3113	6.20
NO	0.0151	0.30
HCN	0.1105	2.20
NH_3	0.1054	2.10
Ar	1.0344	20.60
Total gas	100.0000	1991.50
Ash		8.70
Total		2000.20

The thermochemical conversion of the solid fuel is not included in the CFD-simulations. An inlet boundary is defined at the level of the upper grate, and a pyrolysis gas/air mixture is flowing into the reaction section. The gas composition and flow is based on demolition wood, a fuel feeding rate of 400 g/hr and the specific primary excess air ratio (λp=0.8). The gas composition has been optimized towards satisfying available relevant pyrolysis gas compositions and char gasification while maintaining the elemental balances for the solid fuel. The fact that burnout of the char will occur at the lower grate below the inlet boundary in the simulations is also taken into account. Table 1 shows the composition of the fuel gas/air mixture based on a primary excess air ratio of 0.8. The gas temperature is 1123 K. The secondary air is injected through an inlet with a diameter of 35 mm, located 417.5 mm above the upper grate. The secondary air temperature is 1123 K. Total excess air ratio is 1.6, while the primary excess air ratio is 0.8, which means that 50 % of the air is fed at each stage. The electrical heating elements serve to maintain a constant wall temperature. In the model the solid walls are specified as isothermal with a wall temperature of 1123 K.

3. RESULTS AND DISCUSSION

3.1. Simulations with master mechanism (81 sp)

Figure 2 shows the mean temperature and the mass flow rate of carbon in CO along the reactor length. The simulations show that the majority of the fuel conversion occurs in the primary zone, as expected. The final burn-out occurs when the secondary air is injected, giving elevated temperatures also in the secondary zone. The highest temperatures in the secondary zone are 1300-1400 K. The simulated mean outlet temperature is 1130 K, which corresponds well with the experimental results.

The mass flow rates [kg/s] of nitrogen in selected species along the reactor length are shown in Figure 2 (lower left). It can be seen that NO is produced in the primary zone. In the secondary zone there is a net reduction of HCN, NH_3 and NO, and it can be mentioned that there is a minor increase in NO_2 and N_2O.

The TFN (total fixed nitrogen)/Fuel-N ratio at the outlet are compared in Figure 3. Four assumptions are used for the TFN; in A0 only the nitrogen in NO is included, while in A3 the TFN includes all the major nitrogen species NO_2, N_2O, HCN and NH_3 in addition to NO. The two other assumptions are A1 including NO, HCN and NH_3, and A2 including NO, NO_2 and N_2O.

According to the simulations, there is a reduction in total fixed nitrogen (TFN) found in all the major nitrogen components; NO, HCN and NH_3, NO_2 and N_2O, from the fuel gas (at the inlet) to the sample surface (z=0.4 m) before the secondary air injection level, and a further reduction towards the flue gas outlet. At the outlet the TFN/Fuel-N ratio is 0.175 (see Figure 3), i.e. a high NO_x reduction level is achieved, comparable to the NO_x emission reduction level achieved in the corresponding experiment. Nearly 98 % of the TFN is the contribution from NO, the remaining is mainly NO_2. This means that the major part of the fuel-nitrogen is converted to molecular nitrogen instead of NO_x. Removing the nitrogen components (NO, HCN and NH_3) from the fuel gas, prevents the formation of fuel NO_x and allows to check the contribution from the other NO_x formation mechanisms to the NO_x emission level. As the temperatures are below 1700 K, the production of thermal NO_x is negligible. The predicted emissions of NO_x, which then will be prompt NO_x, is 1.3 % of the base case level. When including all the major nitrogen components it increases to 1.5 %. Hence, prompt NO_x formation is negligible compared to fuel NO_x formation.

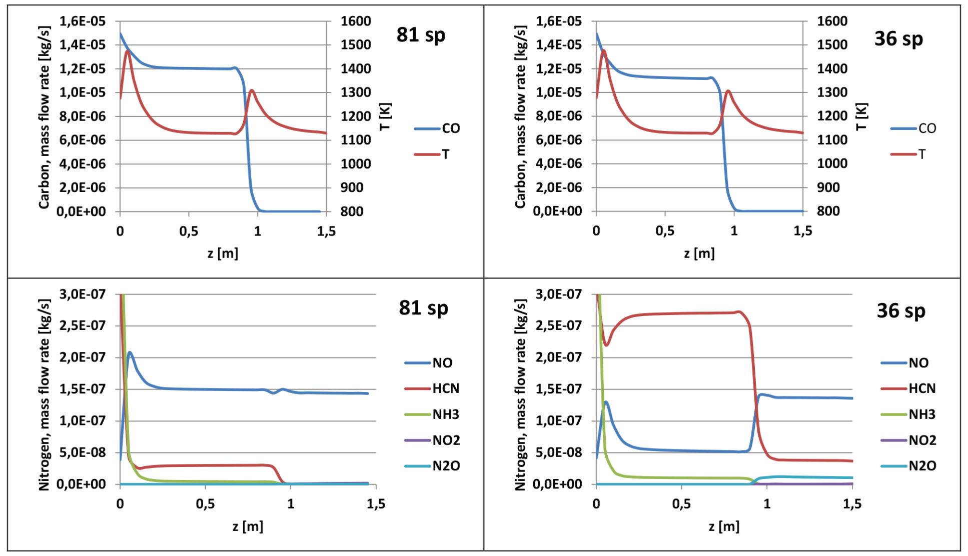

Figure 2: Mean temperature [K] and mass flow rate of selected species [kg/s] along the reactor length. Left: 81 species mechanism, Right: 36 species mechanism

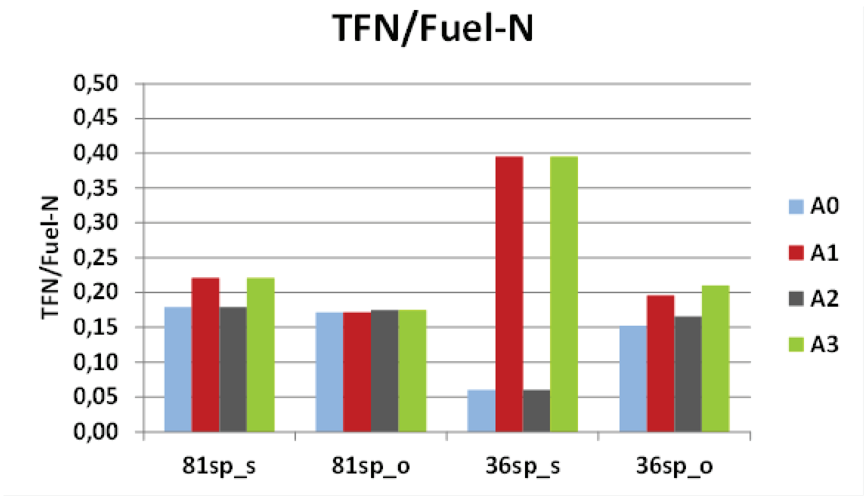

Figure 3: *TFN/Fuel-N ratio at the sample surface (s) and the outlet (o) for the two reaction mechanisms, 81 (left) and 36 (right) species. A0-N in NO, A1-N in NO/HCN/NH_3, A2-N in NO/NO_2/N2O, A3- N in NO/NO_2/N_2O/HCN/NH_3*

3.2. Simulations with skeletal mechanism (36 species)

Figure 2 and Figure 3 show results from the simulations with the skeletal mechanism compared with the full detailed mechanism. It can be seen that the mean temperatures along the reactor correspond well, while the predicted CO concentration before the injection of secondary air is slightly lower for the skeletal mechanism.

For the 36 species case a much lower reduction of HCN in the primary zone is predicted compared to the full detailed mechanism, resulting in also a higher HCN concentration at the reactor outlet than for the base case. Some NO is produced early in the primary zone, and in the secondary zone only some of the remaining HCN but all of the NH_3 are converted to NO, while in the base case all HCN and NH_3 is reduced in the primary zone and there is also a slight net reduction of NO in the secondary zone. Figure 3 shows that compared to the full detailed mechanism NO at the sample surface is underpredicted, while TFN/Fuel-N at the sample surface is significantly overpredicted mainly due to the overprediction of HCN. The trend is the same at the outlet, however the deviation is reduced. The TFN/Fuel-N at the outlet is overpredicted by 20 %. This overprediction of NO is also reported in Løvås et al [03]. However, a somewhat larger reduced mechanism also discussed in this paper does not have this feature

Removing the nitrogen components (NO, HCN and NH_3) from the fuel gas, investigating the prompt NO contribution, shows that the skeletal mechanism predicts a significantly higher NO value than the 81 species mechanism. The prompt NO contribution is overpredicted 20 times compared to the full detailed mechanism.

4. CONCLUSION

Using the full detailed mechanism (81 species), the results give a high NO_x reduction at a primary excess air ratio of 0.8, comparable to the NO_x emission reduction level achieved in the corresponding experiment, showing the potential of NO_x reduction by staged air combustion.

There are deviations in the prediction of the concentrations of the nitrogen components especially in the primary zone for the two chemical mechanisms compared. The skeletal mechanism overpredicts the concentration of HCN and underpredicts the concentration of NO in the primary zone, as well as overpredicts the prompt NO_x contribution, indicating that an improved or less reduced skeletal mechanism is needed.

5. ACKNOWLEDGEMENTS

The authors acknowledge the financial support by the Bioenergy Innovation Centre (CenBio), which is funded by the Research Council of Norway, a large number of industry partners and seven R&D institutions.

6. REFERENCES

[01] Gran I, Magnussen B F (1996). A numerical study of a bluff-body stabilized diffusion flame. Part 2. Influence of combustion modeling and finite rate chemistry. Comb. Sci. Technol. 119, pp. 191-217.

[02] Ertesvåg I, Magnussen B F (2000). The Eddy Dissipation turbulence energy cascade model, Comb. Sci. Technol. 159, pp. 213-236.

[03] Løvås T, Houshfar E, Bugge M, Skreiberg Ø (2013). Automatic generation of kinetic skeletal mechanisms for biomass combustion, Energy & Fuels 27(11), pp. 6979-6991.

[04] Bugge M, Haugen N E L, Skreiberg Ø (2014). NO_x emissions from wood stoves – a CFD modelling approach, Proc. of 22nd EU BC&E, Hamburg, pp. 674-679.

[05] Khalil R A, Houshfar E, Musinguzi W, Becidan M, Skreiberg O, Goile F, Lovas T, Sorum L (2011). Experimental Investigation on Corrosion Abatement in Straw Combustion by Fuel Mixing. Energy & Fuels 25(6), pp. 2687-2695.

[06] Houshfar E, Skreiberg O, Lovas T, Todorovic D, Sorum, L (2011). Effect of excess air ratio and temperature on NO_x emission from grate combustion of biomass in the staged air combustion scenario. Energy & Fuels 25(10), pp. 4643-4654.

Khadidja Safer (Université ’Oran Mohamed Boudiaf, Algeria)

Investigations of optimum operating conditions of Syngas Combustion in regards to NO_x Emissions

Khadidja Safer, Mériem Safer
Laboratoire des Carburants Gazeux et de l’Environnement/Faculté du Génie Mécanique, Université des Sciences et de la Technologie d’Oran Mohamed Boudiaf,
BP1505, Elmanouar,Oran, Algeria
khsafer@gmail.com, safer.meriem@gmail.com

Fouzi Tabet
DBFZ Deutsches Biomasseforschungszentrum gemeinnützige GmbH,
Torgauer Strasse 116, 04347 Leipzig, Germany
fouzi.tabet@dbfz.de

Syngas is a hydrogen-rich fuel mainly composed of H_2 and CO. One of the challenges when using syngas for energy production is the high level of NO_x emissions. The aim of this study is to identify optimum operating conditions of syngas combustion to minimize NO_x emissions. The analysis is performed in counter-flow diffusion flame configuration over a wide range of operating conditions (ambient pressure from 1 to 10 atm, flame strain rate from near equilibrium to near extinction and H_2/CO molar fraction ratio from 0.4 to 2.0).

Results show that H_2-rich syngas flames produce more NO at low strain rates while NO emissions increase for H_2-lean syngas at high strain rates. Also, thermal route is the dominant NO formation path. Practical burners like gas turbines should operate at low scalar dissipations (near 1 s^{-1}) with H_2-lean fuel or at very high scalar dissipations (100 to 1000 s^{-1}) with H_2-rich syngas in order to minimize NO emissions. Pressure increase involves more NO emissions and thermal route remains dominant at high pressures.

KEYWORDS: Syngas, Syngas composition, Diffusion flames, NO_x emissions, Ambient pressure.

1. INTRODUCTION

Syngas is a hydrogen-rich fuel, mainly composed of H_2 and CO and may contain other gases such as CH_4, CO_2, N_2 and H_2O. Syngas can be produced from various raw materials such as natural gas, biomass or municipal wastes. This variability of syngas sources induces variability in syngas composition [01]. Syngas is expected to play an increasing role in energy production. However, prior to its implementation, its environmental impact needs to be fully established. In particular, NO_x emissions should comply with the current and future emission regulations.

Several studies have been reported about NO_x emissions of syngas combustion. Giles et al. [02] examined the effect of air-stream dilution on flame structure and NO emissions of syngas diffusion flames with two representative syngas mixtures and three diluents, N_2, H_2O and CO_2 in air. Results indicated that syngas flames with CO_2 and H_2O dilution are more effective in reducing NO emission. Shih et al. [03] numerically studied NO_x emissions characteristics of 1D counterflow syngas flames with radiation. Two representative syngas compositions have been chosen: 20 % H_2, 80 % CO and 80 % H_2, 20 % CO. The effect of pressure (lower than 10atm) and dilution have also been studied. They conclude that both H_2-lean and H_2-rich flames produce more NO at high pressures and that thermal route is the main formation path. Results also indicated that for H_2-lean syngas flame, the NO emissions for CO_2 dilution are higher than that with H_2O dilution. A numerical study led by Chun et al. [04] investigated the effect of N_2 and CO_2 dilution and stretch rate on NO_x formation in non-premixed syngas flames, using a quasi-one-dimensional counterflow configuration. The results showed that $EINO_x$ decreases with stretch rate but the decreasing rate is different between the cases of N_2 and CO_2 and that thermal NO mechanism is weakened for high dilution cases. Safer et al. [05] studied the effect of syngas composition and ambient pressure on counter-flow diffusion flame and NO_x emissions. They found that NO formation is strongly dependant on temperature, thereby, thermal NO is the prominent NO formation path. Their results also indicated that NO increases with pressure and strain rate increasing. Although the above survey manifests substantial efforts that have been devoted to investigate NO_x emissions of syngas diffusion flames, a comprehensive characterization of NO_x emissions over a wide range of operating conditions have not been yet consummated.

The objective of the present work is to perform numerical simulations over a wide range of operating conditions (H_2/CO ratio from 0.4 to 2.0, ambient pressure from 1 to 10 atm and strain rate from near equilibrium to near extinction) and extract information from the numerical databases to analyse NO_x emissions. The emphasis is put on optimum operating conditions in regards to NO_x emissions. The investigation is conducted in counter-flow diffusion flame configuration in mixture fraction space using flamelet equations with the consideration of radiation.

This article consists of four parts. After the introduction of the simulation methodology, including the laminar flamelet model equations and the simulation details, the results are presented in two parts. The first part concerns the effects of syngas composition on NO emissions while the second part is dedicated to the effects of pressure.

2. METHODOLOGY

2.1. The laminar flamelet model

In laminar flamelets, all scalars are functions of the mixture fraction and the scalar dissipation rate. Their balance equations for species n and energy are written as [06]:

$$\rho\frac{\partial Y_n}{\partial t}=\frac{1}{2}\rho\chi\frac{\partial^2 Y_n}{\partial Z^2}+\dot{\omega}_n \tag{1}$$

$$\rho\frac{\partial T}{\partial t}=\frac{1}{2}\rho\chi\frac{\partial^2 T}{\partial Z^2}-\frac{1}{c_p}\sum_k H_n\dot{\omega}_n+\frac{1}{2c_p}\rho\chi\left[\frac{\partial c_p}{\partial Z}+\sum_n c_{p,n}\frac{\partial Y_n}{\partial Z}\right]\frac{\partial T}{\partial Z} \tag{2}$$

The notation in equations (1) and (2) is as follows: Y_n, T, ρ are the nth species mass fraction, temperature and density, respectively. ω_n is the *n*th species reaction rate and χ is the instantaneous scalar dissipation rate defined by: $\chi= 2D_Z\,(\Delta Z.\Delta Z.)$ Its modelling is based on the relation below which is taken from the counter-flow geometry [06] :

$$\chi=\chi_{st}\frac{\Phi}{\Phi_{st}}\frac{g(Z)}{g(Z_{st})} \tag{3}$$

χ_{st} is the scalar dissipation rate at stoichiometry and Φ is a factor introduced in order to include the effect of density variation [07]:

$$\Phi=\frac{1}{4}\frac{3(\sqrt{\rho_\infty/\rho}+1)^2}{2\sqrt{\rho_\infty/\rho}+1} \tag{4}$$

The subscript ∞ means the oxidizer stream. The function *g*(Z) is given as follows [07]:

$$g(Z)=\exp\left[-2(erfc^{-1}(2Z))^2\right] \tag{5}$$

where $erfc^{-1}$ is the inverse of the complementary error function. The last term in Equation (2) is an optically thin model for radiative energy loss from the flamelet. Here, σ is the Stefan-Boltzmann constant, *P* is the pressure, X_n is the nth species mole fraction, a_i are polynomial coefficients for the Planck mean absorption coefficients [08], and T_b is the far-field (background) temperature. The two input parameters in Equations (1) and (2) are mixture fraction *Z* and stoichiometric scalar dissipation rate χ_{st}.

2.2. Simulation details

CO and H_2 are considered as the dominant syngas components. Syngas oxidation chemistry is modelled by using the GRI Mech-3.0 [09] mechanism that involves 53 species and 325 reactions. The GRI 3.0 mechanism and its earlier versions have been extensively validated in previous studies using a variety of configurations including perfectly stirred reactors, autoignition and shock-tube ignition delay times, extinction limits, laminar flame speeds, and nonpremixed and partially premixed flames [10].

The flamelet Equations (1) and (2) are solved for several values of H_2/CO ratio until steady state is achieved assuming Le_n = 1 for all the species involved in the chemical mechanism. The calculations are carried out with PrePDF 4 code [11]. The radiation participating gaseous species included are CO, CO_2, and H_2O.

Five H_2/CO molar fractions are considered : 0.4, 0.8, 1, 1.4 and 2.0 at the pressure range between 1 and 10 atm as shown in Table 1. Scalar dissipation values are taken from 1 s^{-1} until flame extinction. The NO concentrations are obtained directly from the flamelet calculation. The incorporation of NO_x chemistry into fuel chemistry allows the prediction of detailed NO_x formation.

Table 1: Syngas composition and operating conditions

H_2/CO molar rate	H_2 molar rate	CO molar rate	Pressure (atm)	Scalar dissipation rate (s^{-1})
0.4	0.29	0.71	1 to 10	from 1 to flame extinction
0.8	0.44	0.56		
1.0	0.50	0.50		
1.4	0.58	0.42		
2.0	0.67	0.33		

3. RESULTS

3.1. Effects of syngas composition on NO emissions

The global NO emission index EINO as a function of scalar dissipation for different H_2/CO molar rates at P = 1 atm is depicted in Figure 1. *EINO* index exhibits a non-monotonic variation with syngas composition. It increases to a maximum value and then decreases. The scalar dissipation rate, at which the maximum EINO peaks, shifts toward lowest values with H_2 enrichment. The peak of EINO index increases with hydrogen enrichment.

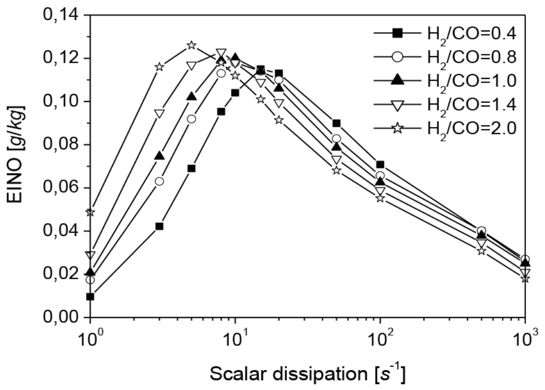

Figure 1: NO emission Index as a function of scalar dissipation for different H_2/CO molar rates at 1 atm

Figure 2 indicates NO formation routes as a function of H_2/CO molar rate. The analysis concerns Thermal path, prompt NO and N_2O path. Thermal route is found to be the most important in syngas flames and its contribution to the NO production continually increases with hydrogen enrichment. The take-off of the NO production curve from thermal route is the consequence of the thermal runaway from hydrogen reaction, which promotes the reactions of NO formation at high flame temperature region [03]. The contributions to NO production from N_2O intermediate route exhibit a non-monotonic behavior. It increases to a maximum at $H_2/CO \approx 1.4$ and then begins to drop. These results demonstrate that, due to higher flame temperature, H_2-rich syngas flame has more NO production through thermal route compared to N_2O and prompt-intermediate routes. These findings are consistent with the predictions of [03].

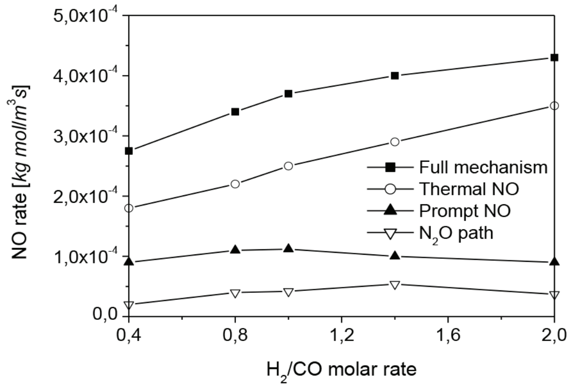

Figure 2: NO formation paths as a function of H_2/CO molar rates at 1 atm

3.2. Effects of pressure on NO emissions

Figure 3 depicts EINO as a function of scalar dissipation for H_2-lean and H_2-rich syngas at different pressures lower than 10atm. The trends are the same as figure 1 but with more production of NO. NO production increases when pressure increases for both H_2-lean and H_2-rich syngas.

NO production routes at 10atm as a function of H_2/CO molar rate are depicted in Figure 4. Thermal NO remains the most important NO formation path at high pressures. It represents more than 90 % of total NO. Pressure increasing raises the contribution of thermal NO in comparison to other paths.

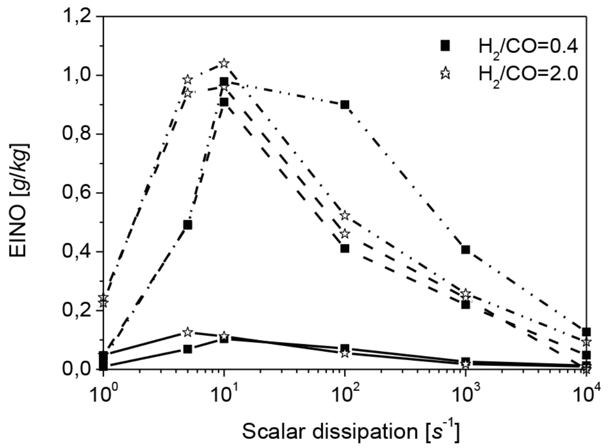

Figure 3: NO emission index as a function of scalar dissipation at different pressures for H_2-lean and H_2-rich syngas : solid : P=1atm, dash : P=5atm and dash dot dot : P=10atm.

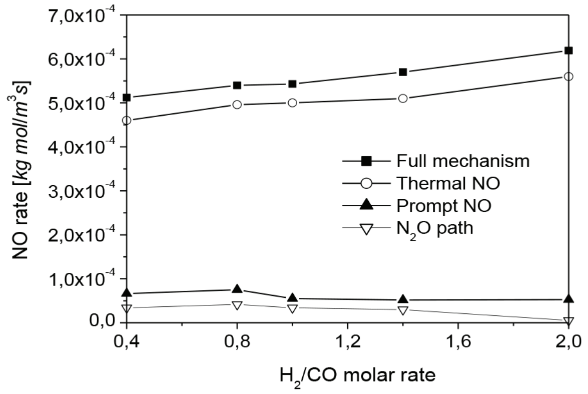

Figure 4: NO formation routes as a function of syngas composition at P=10 atm.

4. CONCLUSION

This work is intended to provide some understanding of the effects of fuel variability and operating pressure on NO emissions of syngas flames. Optimum conditions corresponding to acceptable levels of NO emissions are also investigated. It was found that:

- H_2-rich syngas flames produce more NO at low strain rates while NO levels increase towards H_2-lean syngas at high strain rates
- NO is mainly produced by thermal route
- Pressure increasing involves more NO emissions and thermal NO remains the dominant formation route at high pressures.
- Practical burners like gas turbines should operate at low scalar dissipations (near 1 s^{-1}) with H2-lean fuel at any pressure or at very high scalar dissipations (100 to 1000 s^{-1}) with H_2-rich syngas in order to minimize NO emissions.

5. REFERENCES

[01] Gökalp I, Lebas E. (2004). Alternative fuels for industrial gas turbines (AFIUR). Appl Therm Eng. 24, pp. 1655.
[02] Giles D E et al. (2006). NO_x emission characteristics of counterflow syngas diffusion flames with airstream dilution. Fuel 85, pp. 1729.
[03] Shih H Y, Hsu J R (2012). Computed extinction limits and flame structures of opposed-jet syngas diffusion flames. Applied Mechanics and Material 110, pp. 4899.
[04] Chun KW et al. (2011). A numerical study on extinction and NO_x formation in nonpremixed flames with syngas fuel. J. Mech. Sci. Tech 25, pp. 2943.
[05] Safer et al. (2013). Combustion characteristics of hydrogen-rich alternative fuels in counter-flow diffusion flame configuration. Energ. Convers. Manag. 74, pp. 269.
[06] Pitsch H and Peters H N (1998). Consistent flamelet formulation for nonpremixed combustion considering differential diffusion effects. Combust. Flame. 114, pp. 26.
[07] Peters N (2000). Turbulent combustion. Cambridge University Press.
[08] Barlow R S et al. (1999). Nitric Oxide formation in dilute hydrogen jet flames: isolation of the effects of radiation and turbulence-chemistry submodels, Combust. Flame 117, pp. 4.
[09] Smith et al. GRI Mech-3.0, Available from: http://www.me.berkeley.edu/grimech/
[10] Barlow R S et al. (2001). Scalar profiles and NO formation in laminar opposed-flow partially premixed Methane/Air flames, Combust. Flame 127, pp. 2102.
[11] FLUENT Inc. (2005), Fluent User's Guide Ver. 6.2.

Quingang Xiong, Song-Charng Kong (Iowa State University, USA)

Development and application of a computer code for simulating biomass fast pyrolysis

Qingang Xiong, Song-Charng Kong
Department of Mechanical Engineering, Iowa State University
2025 Black Engineering, Ames, IA 5001, USA
xiong@iastate.edu, kong@iastate.edu

A numerical framework was developed and applied to simulate biomass fast pyrolysis in this study. In this framework, a multi-fluid model was employed to model the multi-phase hydrodynamics and global reaction kinetics was used to describe the physicochemical conversion. The coupling of these two methodologies was realized by a time-splitting method. The models were validated using experimental data from fast pyrolysis reactors. Good levels of agreement were obtained in the product distribution including tar, biochar, and syngas. Various submodels to account for the interphase transport phenomena, i.e., drag force and heat transfer, were also implemented to characterize their effects on the predicted results. Comparisons between the simulated and experimental results showed that the drag coefficient model considering detailed sub-grid structures predicted lower drag forces and performed better than the homogeneity-based drag correlation models. Lower drag forces on solid biomass particles resulted in lower solid biomass outflux, higher gas velocities, and shorter tar residence time, all resulting in higher tar yields. On the other hand, heat transfer correlations had less effect on the temperature distributions and final product yields.

KEYWORDS: Biomass fast pyrolysis, fluidized bed, multiphase flow, biomass thermochemical conversion.

1. INTRODUCTION

Bio-oil, derived from fast pyrolysis of biomass, has the advantages of high energy density, low transportation cost, and direct applications in combustion devices [01]. With the increasing concern regarding availability and environmental impacts of fossil fuels, bio-oil has attracted increased interest in recent years [02]. Fast pyrolysis, a thermochemical conversion process in the absence of oxygen, has served as the dominant means of converting lignocellulosic biomass to bio-oil. Developing highly efficient fast pyrolysis technologies, crucial to bio-oil production, has therefore received extensive interest [03].

Experimental study has been the main approach to developing advanced technologies for biomass fast pyrolysis [04]. However, performing experiments at different scales (e.g., laboratory scale, pilot scale, and industry scale) is usually time-consuming, making this approach cost ineffective. The accuracy of measurements in the hostile reactor environment also poses great challenges. In contrast, numerical simulation can complement experiments into the fundamental details of the reactor processes. An accurate numerical model can be used to investigate the effects of operating variables on the reactor performance and can shorten the development cycle considerably. As a result, numerical simulations are increasingly conducted to study phenomena inside the biomass pyrolysis reactors [05].

In this study, a computational framework is developed and different correlations for the interphase transport coefficients are investigated and their effects on the performance of a fluidized-bed reactor for biomass pyrolysis are characterized. A comprehensive multi-fluid model (MFM) that describes the hydrodynamics of gas, sand, and solid biomass is coupled with chemical reactions for simulating biomass fast pyrolysis in the reactor. The results are compared with experimental data to assess the performance of various correlations.

2. MODEL FORMULATION

Table 1: Drag force coefficient correlations

Base equations	$C_{Dm}=\begin{cases}\frac{24}{\mathrm{Re}_m}(1+0.15\mathrm{Re}_m^{0.687}) & (\mathrm{Re}_m<1000)\\ 0.44 & (\mathrm{Re}_m\ge 1000)\end{cases}$; $\mathrm{Re}_m=\frac{\rho_g d_{sm}\lvert\boldsymbol{U}_g-\boldsymbol{U}_{sm}\rvert}{\mu_g}$
D1: Gisaspow [9]	$\beta_{gsm}=\begin{cases}\frac{3}{4}C_{Dm}\frac{\rho_g\alpha_g\alpha_{sm}\lvert\boldsymbol{U}_g-\boldsymbol{U}_{sm}\rvert}{d_{sm}}\alpha_g^{-2.65} & (\alpha_g\ge 0.8)\\ 150\frac{\alpha_{sm}^2\mu_g}{\alpha_g d_{sm}^2}+\frac{7}{4}\frac{\rho_g\alpha_{sm}\lvert\boldsymbol{U}_g-\boldsymbol{U}_{sm}\rvert}{d_{sm}} & (\alpha_g<0.8)\end{cases}$
D2: Syamlal-O’Brien [10]	$\beta_{gsm}=\frac{3}{4}\frac{\alpha_g\alpha_{sm}\rho_g\lvert\boldsymbol{U}_g-\boldsymbol{U}_{sm}\rvert}{V_{rm}^2 d_{sm}}\left(0.63+4.8\sqrt{\frac{V_{rm}}{Re_m}}\right)^2,$ $V_{rm}=\frac{1}{2}(a-0.06Re_m+\sqrt{(0.06Re_m)^2+0.12Re_m(2b-a)+a^2})$ $a=\alpha_g^{4.14}\qquad b=\begin{cases}0.8\alpha_g^{1.28} & (\varepsilon_g\le 0.85)\\ \alpha_g^{2.65} & (\varepsilon_g>0.85)\end{cases}$
D3: EMMS [12]	$\beta_{gsm}=\frac{3}{4}C_{Dm}\frac{\rho_g\alpha_g\alpha_{sm}\lvert\boldsymbol{U}_g-\boldsymbol{U}_{sm}\rvert}{d_{sm}}\alpha_g^{-2.65}H_{Dm},$ $H_{Dm}=a(\mathrm{Re}_m+b)^c,$ $\begin{cases}a=0.7008-\frac{0.5174}{1+(\alpha_g/0.437)^{19.8015}}\\ c=0\end{cases}\qquad(\alpha_g<0.465)$ $\begin{cases}a=0.01786+\frac{0.6252}{1+(\alpha_g/0.5069)^{32.3483}}\\ b=19.5897-\frac{19.6031}{1+\exp((0.4393-\alpha_g)/0.00575)}(1-\frac{1}{1+\exp((0.6701-\alpha_g)/0.00999)})\\ c=0.4036-\frac{0.4358}{1+(\alpha_g/0.5216)^{21.1039}}\end{cases}\qquad(0.465<\alpha_g<0.61)$ $\begin{cases}a=\frac{1}{61.9321-622783\alpha_g{}^{6.7883}}\\ -0.2923+\frac{1.5321}{1+\exp((0.9703-\alpha_g)/0.2682)}(1-\frac{1}{1+\exp((0.9703-\alpha_g)/0.0322)})\\ c=(0.00029-0.00029\alpha_g)^{0.1037}\end{cases}\qquad(0.61<\alpha_g<0.9898)$ $\begin{cases}a=0.00657+\frac{1.9134}{1+\exp((0.9966-\alpha_g)/0.00399)}(1-\frac{1}{1+\exp((0.9999-\alpha_g)/0.00057)})\\ b=\frac{\alpha_g-0.9912}{0.05377-15.9492(\alpha_g-0.9912)+1444.8906(\alpha_g-0.9912)^2}\\ c=13.08817-13.01786\exp(-0.5(\frac{\alpha_g-0.9975}{0.0533})^2)\end{cases}\qquad(0.9898<\alpha_g<0.9997)$ $a=1,\quad c=0\qquad(\alpha_g>0.9997)$

A comprehensive multi-fluid model is employed to simulate the hydrodynamics of a fluidized-bed reactor [06, 07]. MFM models gas and solid phases as inter-penetrating continua and describes each phase by a set of volume fraction incorporated conservation equations. The conservation equations for mass, momentum, energy, and species in each phase can be found from previous literature. The modified multi-component multi-stage Broido-Shafizadeh reaction kinetics is chosen for the biomass fast pyrolysis reactions [08]. In this reaction mechanism, biomass is assumed to be composed of cellulose, hemicellulose and lignin, and the mass fraction of each component is specified. When fast pyrolysis starts, each component is activated into an intermediate stage, followed by two competitive decomposition reactions that yield tar, char and gas. At appropriate temperature and reactor conditions, some portion of tar further decomposes into gas. The rate of each reaction is controlled by first-order Arrhenius kinetics. The above conservation equations and the chemical reaction kinetics are solved using our developed open-source code, BIOTC (BIOmass Thermochemical Conversion) [06] developed based on the OpenFOAM® platform.

The hydrodynamic coupling between the gas and solid phases is realized by the interphase transport coefficients appearing in both the momentum and energy conservation equations. As the drag force plays a dominant role in the gas-solid momentum transfer, only drag correlations are considered in the phase momentum equations. For the gas-solid heat transfer, only convective heat transfer is accounted for. Three typical correlations for the gas-solid drag force and three typical correlations for gas-solid heat transfer are considered in this study. The formulations of these interphase transport coefficients are listed in Table 1 and 2. For convenience, these interphase models are referred to as D1 for the Gisaspow model [09], D2 for the Syamlal-O’Brien model [10], D3 for the EMMS model [11], H1 for the Ranz-Marshall model [12], H2 for the Gunn model [13], and H3 for the Li-Mason model [14].

Table 2: Heat transfer coefficient correlations

Base equations	$h_{gsm}=\frac{6\alpha_{sm}\kappa_g Nu_m}{d_{sm}^2};\quad \mathrm{Pr}=\frac{C_{pg}\mu_g}{\kappa_g}$
H1: Ranz-Marshall [12]	$Nu_m=2+0.6\mathrm{Re}_m^{1/2}\mathrm{Pr}^{1/3}$
H2: Gunn [13]	$Nu_m=(7-10\alpha_g+5\alpha_g^2)(1+0.7\mathrm{Re}_m^{0.2}\mathrm{Pr}^{1/3})+(1.33-2.4\alpha_g+1.2\alpha_g^2)\mathrm{Re}_m^{0.7}\mathrm{Pr}^{1/3}$
H3: Li-Mason [14]	$Nu_m=\begin{cases}2+0.6\alpha_g^{3.5}\mathrm{Re}_m^{1/2}\mathrm{Pr}^{1/3} & (\mathrm{Re}_m<200)\\ 2+0.5\alpha_g^{3.5}\mathrm{Re}_m^{1/2}\mathrm{Pr}^{1/3}+0.02\alpha_g^{3.5}\mathrm{Re}_m^{0.8}\mathrm{Pr}^{1/3} & (200<\mathrm{Re}_m<1500)\\ 2+0.000045\alpha_g^{3.5}\mathrm{Re}_m^{1.8} & (\mathrm{Re}_m>1500)\end{cases}$

3. RESULTS AND DISCUSSION

3.1. Reactor operating conditions

A lab-scale bubbling fluidized-bed reactor located in the Agricultural Research Service (ARS) of the U.S. Department of Agriculture (USDA) was simulated [15]. The fluidization medium was silica sand, initially packed to a height of 17 cm and porosity of 0.45. The biomass feedstock, switchgrass, was fed from the side injector at the left, located 5 cm from the bottom, at a feed rate of 2.22 kg/h. The initial composition of switchgrass is assumed to be 42 % cellulose, 34 % hemicellulose, and 24 % lignin. Fluidization nitrogen was supplied from the bottom of the reactor at a fixed rate of 4.81 kg/h. The sidewall was heated and maintained at a fixed temperature of 773 K.

3.2. Results

To allow for direct comparison with experimental results, the simulated product yields averaged from the last 50 s in each case are shown in Figure 1. All product yields are presented as their weight fractions (wt%) at the reactor exit. It can be seen that the maximum and minimum differences between numerical prediction and experimental measurement for tar yield are about 22.1 % and 1.8 %, respectively. The best prediction was obtained with use of the combination of D3 and H2 and the largest deviation with a combination of D2 and H1. An important observation is that the drag coefficient model has a pronounced effect on the predictions for tar, gas and unreacted biomass, compared with the heat transfer coefficient model.

The outflux of solid biomass at the reactor exit is directly linked to the tar yield; a high outflux of solid biomass implies a low tar yield. The temporal evolutions of solid biomass outflux in all cases are plotted in Figure 2. It can be seen that whatever heat transfer model is used, D2 gives the highest solid biomass outflux and D3 the lowest outflux. This is because, with the same solid volume fraction and interphase slip velocity, D2 gives the highest β_{gsm} overall, while D3 gives the lowest. As a result, the overall drag force experienced by biomass particles when D2 is used will be the highest, resulting in more biomass particles being carried out of the reactor. In contrast, D3 predicts the lowest drag force and a large portion of biomass particles cluster inside the reactor. To further elaborate the effects of the drag model, the axial distributions of the time-averaged solid biomass volume fractions are presented in Figure 3.

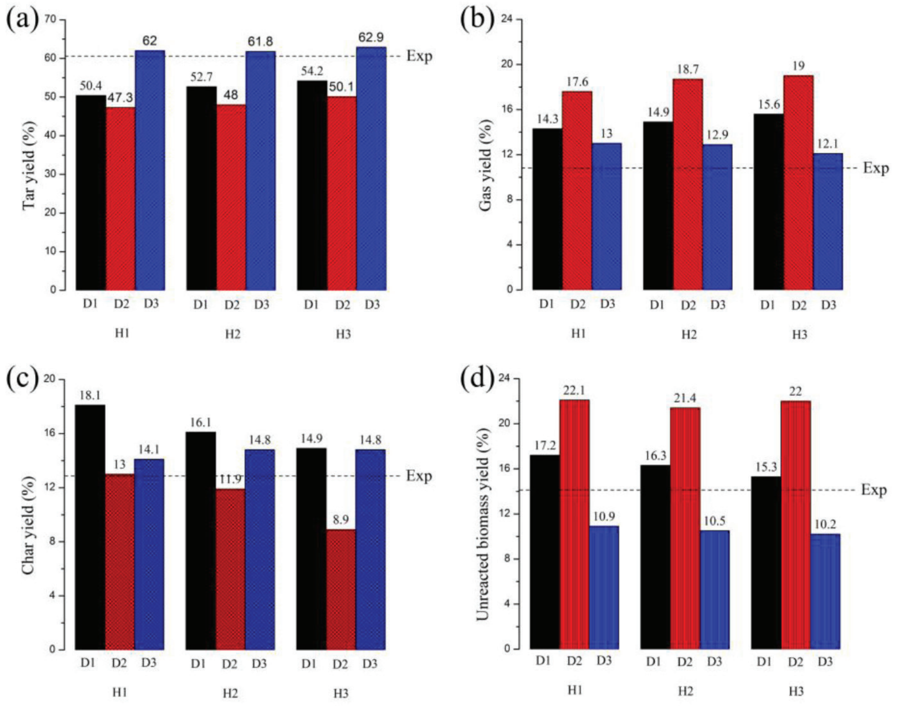

Figure 1: Product yields from simulation and experiment for (a) tar, (b) gas, (c) char, and (d) unreacted biomass

The high drag force predicted by D2 implies that more biomass particles are carried out by the gas and evenly distributed inside the reactor, resulting in the most dilute volume fraction of the biomass particles. The low drag force predicted by D3 prevents biomass particles from moving effectively along with the gas flow, resulting in high concentrations of biomass particles near the injector. This is consistent with the instantaneous snapshots of the spatial distributions of solid biomass, as shown in Figure 4. Additionally, because of the low drag force predicted by D3, the residence time of the biomass particles is long, causing more consumption of biomass particles. As can be seen from Figure 3, the D3 model predicts a pronounced S-shape distribution of the biomass particles, i.e., high solid volume fraction in the middle but low at the exit. It should be mentioned that though the magnitude of volume fraction of solid biomass near the exit is about two orders lower than that near the middle, the predicted differences by different interphase transport coefficient models in the enlarged window of Figure 3 correspond to the differences of solid biomass outflux as shown in Figure 2. In fact, the solid biomass outflux, Qout, can be estimated as follows

$$Q_{out} = 900\pi \times \alpha_{out} \times V_{out} \times \rho_{out} \times D_f^2 . \tag{2}$$

where α_{out}, V_{out}, and ρ_{out}, are the volume fraction of solid biomass near the exit, the outlet velocity of solid biomass, and the superficial density of solid biomass, respectively. Choosing α_{out} to be 0.0015 as shown in Figure 3, the calculated Q_{out} is about 1 kg/h which matches the results in Figure 2 very well. As shown in Figure 1, if the drag coefficient model considers the effects of sub-grid structures to a greater extent (e.g., D3), the percentage of unreacted solid biomass is lower. Lower drag force predicted by D3 will cause a longer residence time of solid biomass particles and result in conversion of a larger portion of raw biomass. On the basis of experimental validation, the detailed formulation for the drag coefficient with use of D3 appears to perform better.

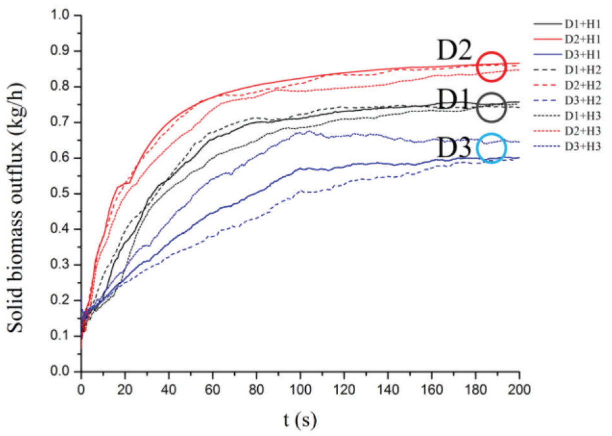

Figure 2: Temporal evolutions of solid biomass outfluxes

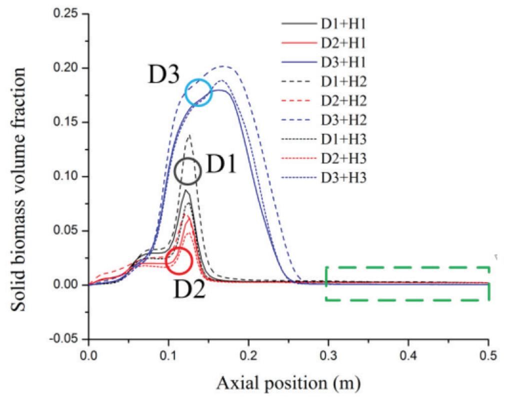

Figure 3: Axial distributions of volume fraction of biomass particles

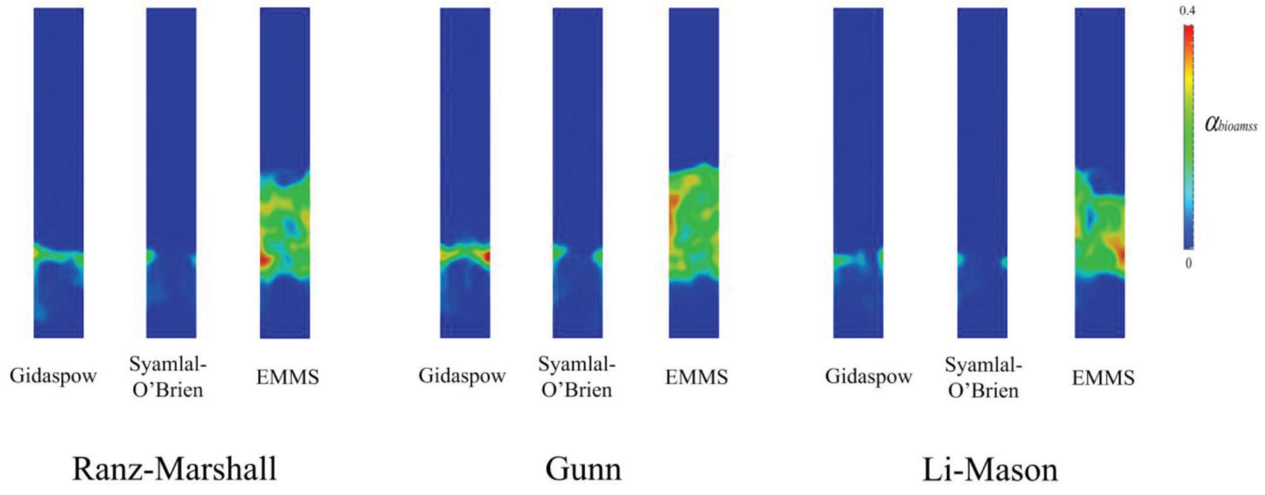

Figure 4: Snapshots of biomass particle volume fractions using different models

4. CONCLUSION

Different models for interphase transport coefficients were tested in the numerical simulation of a fluidized-bed reactor for biomass fast pyrolysis. Continuum descriptions of both gas and solid phases were applied to simulate the in-bed hydrodynamics and the modified multi-component multi-stage Broido-Shafizadeh reaction kinetics was utilized to predict biomass fast pyrolysis. The numerical results were compared with experimental data on product yields. The comparisons show that the choice of the drag coefficient model significantly influences the product yields, particularly tar. A longer residence time of solid biomass coupled with higher gas velocity, both resulting from lower drag coefficients, are responsible for higher tar yields, lower gas production, and less unreacted biomass. Among the drag models tested, the EMMS model that considers more detailed sub-grid structures generally predicted better product yields.

The sensitivity to the formulation of the drag coefficient is attributed to the long response time for the adjustment of the interphase slip velocity. Because of the relatively short response time for the adjustment of the interphase temperature difference, heat transfer between two phases takes place immediately. As a result, nearly the same temperature profiles were predicted with use of different heat transfer models. Overall, this study shows that to simulate a fluidized-bed reactor using coarse-grid CFD, the effects of sub-grid structures on drag coefficient need to be taken into account.

5. REFERENCES

[01] Brown R C. Biorenewable resources: engineering new products from agriculture. Iowa State Press, 2003.
[02] Panwar N, Kothari R, Tyagi V (2012). Thermo chemical conversion of biomass–Eco friendly energy routes. Renewable and Sustainable Energy Reviews 16, pp. 1801-1816.
[03] Babu B (2008). Biomass pyrolysis: a state of the art review. Biofuels, Bioproducts and Biorefining 2, pp. 393-414.
[04] Bridgwater A V (2012). Review of fast pyrolysis of biomass and product upgrading. Biomass and Bioenergy 38, pp. 68-94.
[05] Di Blasi C (2008). Modeling chemical and physical processes of wood and biomass pyrolysis. Progress in Energy and Combustion Science 34, pp. 47-90.
[06] Xiong Q, Kong S C, Passalacqua A (2013). Development of a generalized numerical framework for simulating biomass fast pyrolysis in fluidized-bed reactors. Chemical Engineering Science 99, pp. 305-313.
[07] Xiong Q, Aramideh S, Kong S C (2013). Modeling effects of operating conditions on biomass fast pyrolysis in bubbling fluidized bed reactors. Energy & Fuels 27, pp. 5948-5956.
[08] Miller R, Bellan J (1997). A generalized biomass pyrolysis model based on superimposed cellulose, hemicelluloseand liqnin kinetics. Combustion science and technology 126, pp. 97-137.
[09] Gidaspow D. Multiphase flow and fluidization: continuum and kinetic theory descriptions, Access Online via Elsevier, 1994.
[10] Syamlal M, Rogers W, O'Brien T J. MFIX documentation: Theory guide, Technical Note, DOE/METC-94/1004, NTIS/DE94000087, National Technical Information Service, Springfield, VA, (1993).
[11] Lu B, Wang W, Li J (2009). Searching for a mesh-independent sub-grid model for CFD simulation of gas–solid riser flows. Chemical Engineering Science 64, pp. 3437-3447.
[12] Ranz W, Marshall W (1952). Evaporation from drops. Chem. Eng. Prog 48, pp. 141-146.
[13] Gunn D (1978). Transfer of heat or mass to particles in fixed and fluidised beds. International Journal of Heat and Mass Transfer 21, pp. 467-476.
[14] Li J, Mason D (2000). A computational investigation of transient heat transfer in pneumatic transport of granular particles. Powder Technology 112, pp. 273-282.
[15] Boateng A A, Daugaard D E, Goldberg N M, Hicks K B (2007). Bench-scale fluidized-bed pyrolysis of switchgrass for bio-oil production. Industrial & Engineering Chemistry Research 46, pp. 1891-1897.

Daniel Laska, Andrea Dernbecher, Fouzi Tabet (DBFZ, Germany)

Investigation of internal flow in a domestic wood pellet stove

Daniel Laska, Andrea Dernbecher, Fouzi Tabet
DBFZ Deutsches Biomasseforschungszentrum gemeinnützige GmbH,
Torgauer Strasse 116, 04347 Leipzig, Germany
daniel.laska@dbfz.de, andrea.dernbecher@dbfz.de, fouzi.tabet@dbfz.de

Stefan Wollny
Anhalt University of Applied Science
Bernburger Strasse 55, 06366 Köthen, Germany
s.wollny@bwp.hs-anhalt.de

In this paper, an investigation of the internal flow of a domestic wood pellet stove is presented. A workflow only with Open Source-tools is tested to keep costs low. A CAD model is being rebuilt and an amount of simplifications are made to generate a mesh of sufficient quality. A cold flow is simulated to receive an overview of mixing processes and utilization of burning chamber and heat exchanger. Shortcomings in the design are detected and proposals for remedy are made.

KEYWORDS: domestic pellet stove, cold flow, design investigation.

1. INTRODUCTION

Optimal utilization of the combustion chamber is a prerequisite for effective combustion in plants. Experiments which offer only a limited insight into the internal processes are very time-consuming and often don't have the desired effects as they are based on trial-and-error. Often the problems of emission of ashes, CO and NO_x are caused by poor mixing of primary and secondary air. Zones of high flow rates lead to incomplete combustion and dead zones are not available as region for combustion, so residence time is too small. Recent progression in numerical techniques and computing efficiency has advanced CFD (Computational Fluid Dynamics) as a widely used approach to provide efficient design solutions and analysis tool to increase efficiency, reduce pollutant emissions, and improve the system's overall performance. Simulation of combustion processes is very time consuming and thus expensive, but an overview of the mixing process between primary and secondary air can be achieved even by investigation of cold flow. Dead zones and recirculation zones as well as areas of high flow rates can be identified, so that already at an early stage of construction problems can be identified. This makes investigation of changes in the geometry fairly easy and ideas can be tested prior to building a prototype, as time needed for calculation can be relatively small.

2. DESCRIPTION OF THE STOVE

The stove is made by manufacturer SUPRA and has a power output of 8 kW. Its feedstock is pellets made from wood, e.g. DIN+ or EN+. The presented stove has an efficiency factor of only 85 % at full load which makes it not suitable for some european markets. Figure 1 shows a CAD model of the stove. Air enters on the lower right side, passes the holes in the burner and leaves combustion chamber via the five holes in the deflector. After passing the heat exchangers on top and on the left side, flue gas leaves the stove on the lower left side. The stove is equipped with a fan which sucks the flue gas through the stove such that fresh air for combustion enters the distribution box. The burner (Figure 2) has several holes for primary air in the cup and eight holes for secondary air on its shoulder. Secondary air should mix with primary air to burn the fuel completely. Secondary air is pre-heated by touching the burner from the outer side. As both primary and secondary air come from the same distribution box, the ratio of both air flows is only controlled by the size of the holes inside the burner and the height of the pellet bed. Pellets are fed to the burner via the slide on the right side.

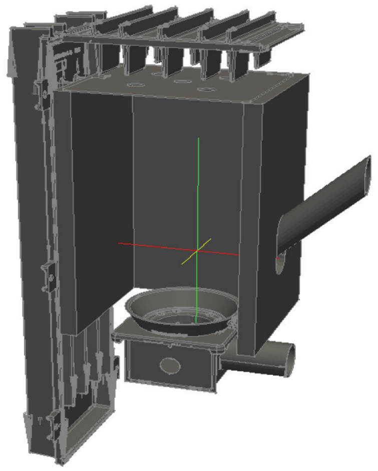

Figure 1: CAD-model of the stove

Figure 2: CAD-Model of the burner

3. METHODS

The chosen geometry is very complex, so there is need for simplifications to generate a geometry which provides a basis for a mesh which allows CPU-efficient simulation. In this work, all tasks are carried out with Open Source Tools. The work is based on the CAD-data which is provided by the manufacturer. Preprocessing is carried out with Blender [01], a tool which is normally used for producing 3D-models which can be animated and rendered to produce films or computer games. Objects are generated from geometric bodies which are being joined with or subtracted from each other. For the generation of a usable geometry, all parts of the stove had to be measured and rebuilt.

A number of simplifications are made to reduce complexity. Chamfered boreholes are implemented as straight holes and some radii are implemented as angles. The ash box is left out as it is not expected that it will be part of the flow region and the feeding device is shortened for the same reason. The second heat exchanger is implemented as a simple box.

Blender is scriptable via python, so the modelling of the geometry is carried out with extensive parametrization which allows easy changes for further investigations. Meshing and simulation utilize tools from the OpenFOAM library.

Meshing is conducted with snappyHexMesh [02] which produces structured hex-dominated meshes. As the stove consists of very large elements (the burning chamber) and very fine elements (the holes in the burner itself), there is a need for regions with large cells and smaller cells if number of cells should be kept as low as possible. So a relatively coarse background mesh is created which consists of about 50×50×100 cells for the burning chamber. Refinements of the mesh are made near edges and surfaces.

Additionally, boundary layers are added where necessary to gain y+ values below 10. The final mesh consists of 1.4 million cells. Simulation is carried out with pimpleFoam [03], as flow is assumed to be incompressible and doesn't change temperature. K-ω-SST is chosen as turbulence model. The simulation is done for 7 seconds of simulated time. For the simulation, the vacuum the fan produces is replaced by an inlet condition which inserts a volumetric airflow which corresponds to approximately 50 % load of the stove. The simulation is carried out at 293 K. Additionally, the residence time of the air inside the chamber is determined by means of a scalar function object.

The simulation needs about 3 days per second of simulated time on a system equipped with two four-core Xeon(R) CPU E5462 at 2.80 GHz.

4. RESULTS

Two shortcomings of the design of the stove are identified: First there is a large part of the burning chamber which is effectively unused by combustion processes. Second, the upper heat exchanger is not evenly passed by the air.

4.1. Recirculation and dead zones

Streamlines show large recirculation zones in the burning chamber (Figure 3). Large parts of the burning chamber remain unused or are not used very well because the main flow is confined into a high-speed narrow stream which crosses the chamber diagonally. At the lower part beside the burner zones are identified where there is recirculation directly after air leaves the burner. The crownring on top of the burner doesn't show the desired effect of broadening and slowing down the flow (Figures 3 and 4). As a result of these phenomenon, residence time is shortened, mixing of primary and secondary air becomes worse, and finally the performance of the wood stove is degraded.

4.2. Residence time in the heat exchanger

Figure 4 shows the age of air inside the stove. It can be seen that a non-negligible part of the upper heat exchanger is not used properly. Residence time in the heat exchanger is very unevenly distributed. Air enters the heat exchanger mainly on the left side and in the middle (Figure 3). It flows mainly from the holes in the deflector more or less straight towards the left heat exchanger and so the part on the other side is filled with aged air. In a case where heat transfer would occur, there would be a very little gradient between flue gas and the wall in this region, so heat transfer would not be good

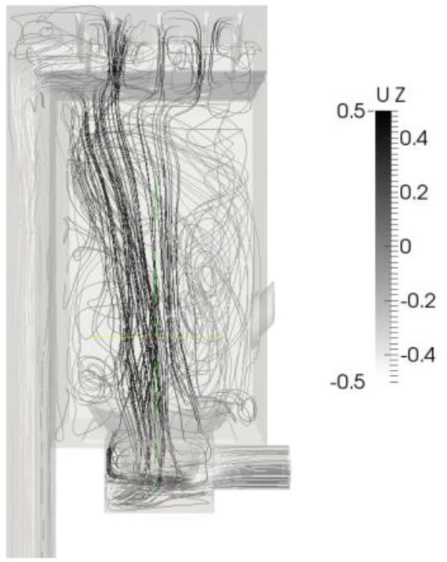

Figure 3: Streamlines inside the stove

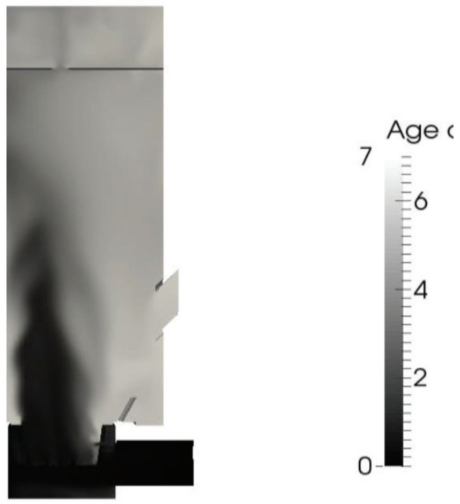

Figure 4: Age of air inside the stove on an x-normal plane

4.3. Future investigations

There are two approaches which may lead to a better utilization of the burning chamber and the heat exchanger: For better utilization of the burning chamber and for better mixing of primary and secondary air, air supply holes of the burner should be rearranged together with their angle to ensure good mixing. The narrow stream should broaden and combustion behaviour would be improved if mixing of primary and secondary air could be controlled better. For improved utilization of the heat exchanger, holes in the deflector should be rearranged to align the upward stream more to the center of the chamber. Together, these two construction measures should help to avoid dead zones and ensure a better utilization of the whole construction.

5. CONCLUSIONS

Time-consuming and thus expensive simulations of combustion is often out of range for small or mid-sized companies which need to analyse their designs of stoves to increase efficiency and reduce pollution. Software packages like Fluent do cost several thousand € per year and are often unaffordable. In this work the cold flow of a domestic wood pellet stove is simulated only with Open Source tools to keep costs low.

A good overview of the processes inside the stove has been achieved only by simulation of cold flow. Dead zones, recirculation zones and shortcomings in utilization of the system have been identified. This knowledge allows for development of ideas for improvements of the design. As only Open Source tools were utilized and the construction of the geometry is extensively parameterized, it is quite easy, fast and not expensive to test them prior to building prototypes. Simulation can be carried out with relatively weak equipment like the six year old computer used in this work. However, for reasonably fast computations, equipment should be upgrade, as the computational time is still very large. Additionally, the preparation of the model in Blender is quite time-consuming, so the construction has to be well-prepared.

6. REFERENCES

[01] www.blender.org
[02] http://www.openfoam.org/docs/user/snappyHexMesh.php
[03] http://www.openfoam.org/features/standard-solvers.php

Andrea Dernbecher, Fabian Findeisen, Fouzi Tabet (DBFZ, Germany)

Investigation of combustion processes in small-scale furnaces with a flamelet solver in OpenFOAM

Andrea Dernbecher, Fabian Findeisen, Fouzi Tabet
DBFZ Deutsches Biomasseforschungszentrum gemeinnützige GmbH
Torgauer Straße 116, 04317 Leizpig, Germany
andrea.dernbecher@dbfz.de, fouzi.tabet@dbfz.de

The results of numerical investigation of a wood log stove combustion chamber using OpenFOAM are shown in this paper. Opportunities for the geometry improvement are identified. The numerical model applied is based on RANS (Reynolds Averaged Navier-Stokes) technique including RNG-k-ε turbulence model and SLFM (Steady laminar flamelet model) approach for turbulence / combustion interactions.

KEYWORDS: Downdraft stove, design investigation, steady laminar flamelet model

1. INTRODUCTION

Thermal energy generated from biomass is widely used for domestic heating, with tendency to rise. However, wood combustion in small-scale furnaces may lead to ecologically harmful emissions. The formation of pollutants can be prevented by optimizing the combustion chamber and the operating parameters of domestic heating appliances. Computational fluid dynamics (CFD) has been recognized as a reliable tool to optimize the operating conditions of existing systems and the design of new efficient appliances. OpenFOAM [01] is used, in this study, to analyse the reacting flow inside the lower combustion chamber of a downdraft stove. The main focus of this study is on mixing between the primary stream and secondary air. The present work is the basis for future investigations with additional models for particle emissions.

2. METHODS

The investigated stove is a Xeoos Twinfire stove designed by Specht Modulare Ofensysteme GmbH & Co. KG with a nominal power output of 8 kW. It is divided into two compartments. In the upper combustion chamber, solid fuel reacts with primary air in a gasification process. The resulting gases are drawn downwards into the lower combustion chamber, where they are burned with secondary air.

For this study, the lower burning chamber is modelled. The mesh is shown in figure 1 cut along the symmetry plane. Fuel gas enters at the top of the connecting piece between upper and lower combustion chamber, secondary air is drawn in through the channels on the side. The mesh in the mixing zone is strongly refined, as high turbulence is expected in this area.

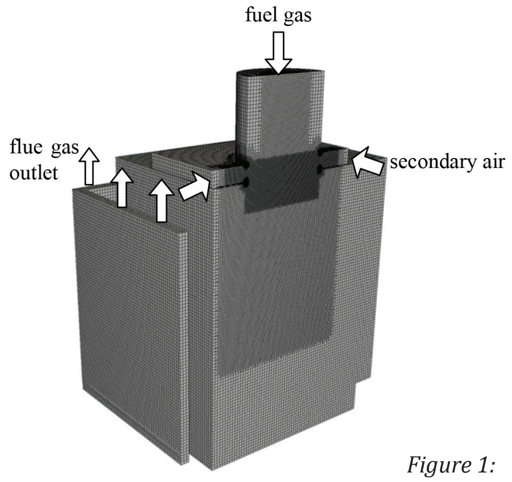

Figure 1: Mesh of the simulated combustion chamber

The governing equations for the turbulent flow field are the Favre-averaged continuity, Navier-Stokes and energy equations coupled with the RNG-k-ε model for turbulence closure. Flamelet approach is applied for combustion / turbulence interactions, being an efficient way to reduce computational time in industrial configurations.

The solver flameletFoam [02] is chosen in this study. Flamelet equations are solved with Cantera software [03] using GRI-mech 3.0 [04] in a pre-processing step. Mean scalar values (temperature and species mass fractions) are obtained using a presumed probability density function (PDF) and stored in a library. OpenFOAM calculates the flow field and accesses the flamelet library solution for each computational cell. Three parameters are needed to couple CFD software and look-up-tables: The scalar dissipation rate χ, the mean mixture fraction Z and its variance Z''^2. OpenFOAM receives sensible enthalpy h_s and species mass fractions Y_k in return. To account for heat loss due to radiation and heat transfer through walls, an enthalpy defect needs to be considered by the flamelet model. This enthalpy defect would be the fourth variable in the tables of the flamelet library. This is not implemented yet, therefore the simulated case is adiabatic.

A semi-empirical bed model is chosen to calculate the composition of the fuel gas at the inlet of the lower firing chamber. A method introduced by Thunman [05] is applied for the calculation based on the composition of beech wood. Fuel gas enters the combustion chamber at 973 K, as it is heated by the gasification reaction. Secondary air is preheated when it flows along the combustion chamber and has a temperature of 473 K at the inlet. The flue gas is assumed to have a constant mass flow rate, which is calculated based on the amount of fuel used during experiments. Thermal boundary conditions are adiabatic because of the missing enthalpy defect.

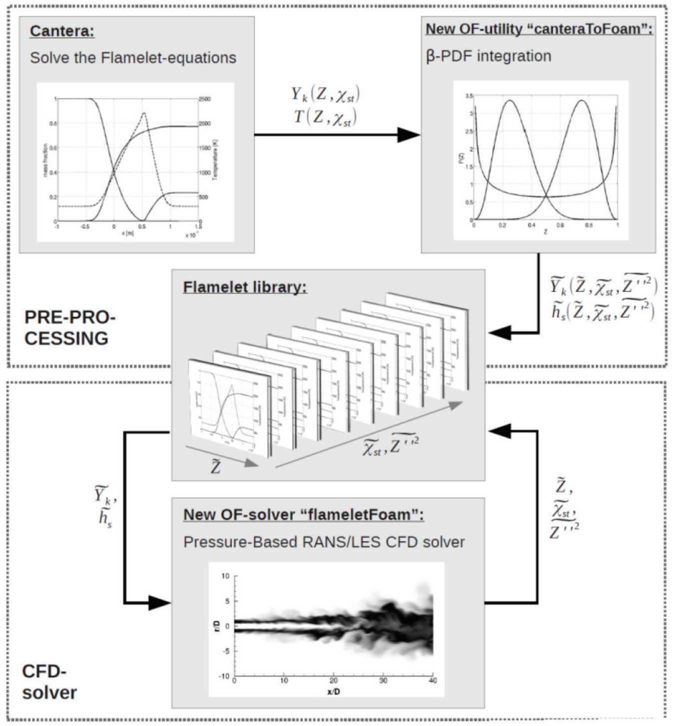

Figure 2: Scheme of flameletFoam [02]

3. RESULTS

The calculation is significantly faster than simulations with other combustion models available in OpenFOAM. The temperature field computed by the flamelet solver is almost uniform due to the missing enthalpy defect. This is also the reason for the high temperatures, which exceed the expected values. Enhancement is planned by Frank et al. [06] for the new version of the solver.

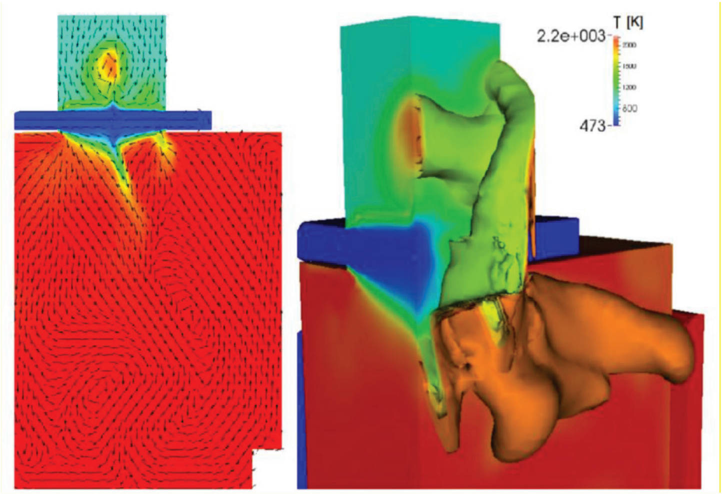

Figure 3: Temperature field, isothermal surfaces and velocity vectors inside the stove [07]

The velocity vectors in figure 3 show an issue inside the combustion chamber at the secondary air inlet. The secondary air enters with high flow rate and causes a backflow of unburned air into the fuel bed. The unwanted backflow could be avoided by enlarging the area of the inlet openings to reduce the inlet velocity or by directing the flow downwards. The flames reach the base plate during combustion, as it is also observed in experiments. This leads to cooling of the flame and causes emissions. Also ash from the bottom of the stove is entrained and discharged by flue gas. These issues can be avoided by lengthening the combustion chamber.

4. CONCLUSION

The combustion processes inside the downdraft stove were successfully modelled and analysed. Based on the findings of this study proposals for an enhanced stove design were made. To improve mixing of fuel gas and secondary air, the secondary air inlet will be enlarged and the direction of the flow will corrected. In addition, the combustion chamber will be lengthened to avoid cooling of the flame at the base plate. The application of the solver flameletFoam reduced the computational effort compared to conventional combustion models, but improvements concerning the enthalpy defect are still needed.

5. ACKNOWLEDGEMENTS

The research was partly funded by "Deutsche Bundesstiftung Umwelt (DBU)" in the framework of the project NEKO. The contribution of Ingo Hartmann, Frank Werner and University of Leipzig is also gratefully acknowledged.

6. REFERENCES

[01] OpenFOAM; http://www.openfoam.org/.
[02] Müller H. Implementation of a Steady Laminar Flamelet Model for non-premixed combustion in LES and RANS simulations, 8th Internation OpenFOAM Worhshop, Jeju and Korea 2013.
[03] Cantera; http://www.cantera.org/.
[04] Smith P. et al.: GRI-Mech 3.0. http://www.me.berkeley.edu/gri_mech.
[05] Thunman H, Niklasson F, Johnsson F, Leckner B (2001). Composition of Volatile Gases and Thermochemical Properties of Wood for Modeling of Fixed or Fluidized Beds. Energy & Fuels 15, pp. 1488–1497.
[06] Frank G, Pohl S, Pfitzner M. Heat Transfer in Reacting Cooling Films Part II: Modelling Near-Wall Effects in Non-Premixed Combustion with OpenFoam. Proceedings of ASME Turbo Expo 2014: Turbine Technical Conference and Exposition, Düsseldorf 2014.
[07] Findeisen F (2014). Modell zur Optimierung von Verbrennungsvorgängen in Kleinfeuerungsanlagen mittels OpenFOAM; Masterthesis; DBFZ.

ANNEX

The DBFZ

Organizer of the CFD-Workshop is the DBFZ Deutsches Biomasseforschungszentrum gemeinnützige GmbH.

Our Mission

The DBFZ was established by the former German Federal Ministry of Food, Agriculture and Consumer Protection (BMELV) with the aim of establishing a central scientific research institution covering all the fields relevant to bioenergy, to bring together the findings of the highly diverse German research community in the sector. The scientific mission of the DBFZ is to support the efficient integration of biomass as a valuable resource for sustainable energy supply based on wide-ranging applied research. The mission incorporates technical, ecological, economic, social policy and energy business aspects all along the process chain, from production, through supply, to use. The DBFZ drives and supports the development of new processes, methodologies and concepts in close cooperation with industrial partners. It also maintains close links with public-sector research bodies in Germany in the agricultural, forestry and environmental sectors, as well as with European and global institutions. Working from this broad research base, the DBFZ is also tasked to devise scientifically sound decision-making aids for government policy-makers.

DBFZ Deutsches Biomasseforschungszentrum gemeinnützige GmbH
Torgauer Straße 116
04347 Leipzig
Phone: +49 (0)341 2434-112
Fax: +49 (0)341 2434-133
info@dbfz.de

List of Participants

Nº	First name	Name	Institution
1.	Øyvind	Skreiberg	SINTEF, Norway
2.	Morten	Seljeskog	SINTEF, Norway
3.	Mateusz	Szubel	AGH University of Science and Technology, Krakow, Poland
4.	Mariusz	Filipowicz	AGH University of Science and Technology, Krakow, Poland
5.	Mette	Bugge	SINTEF, Norway
6.	Nils Erland L.	Haugen	SINTEF, Norway
7.	Martin	Miltner	Institute of Chemical Engineering, Vienna University of Technology, Austria
8.	Florian	Sudbrock	Ruhr University of Bochum, Department of Energy Plant Technology (LEAT), Bochum, Germany
9.	Laurent	Georges	Energy and Process Engineering Department, Norwegian University of Science and Technology (NTU), Norway
10.	Harold	Garcia	Institut für Feuerungs- und Kraftwerkstechnik – IFK, Stuttgart
11.	Lars	Seidel	Brandenburg University of Technology, Chair of Thermodynamics and Process Engineering
12.	Fabian	Mauss	Brandenburg University of Technology, Chair of Thermodynamics and Process Engineering
13.	Serban	Bruma	DOVRE, Belgium
14.	Anke	Schwark	-
15.	Abdallah	Elorf	ICARE - CNRS, France
16.	Torsten	Schröder	SL - Grossenhain, Germany
17.	Daniel	Wohter	TEER-RWTH, Aachen, Germany
18.	Markus	Schmitt	DEKRA, Arnhem, The Netherlands
19.	Arthur F.	Stam	DEKRA, Arnhem, The Netherlands
20.	Andrea	Dernbecher	TK - DBFZ
21.	Andreas	Ortwein	TK - DBFZ
22.	Volker	Lenz	TK - DBFZ
23.	Fouzi	Tabet	TK - DBFZ
24.	Polina	Sorjanaja	TK - DBFZ
25.	Daniel	Laska	TK - DBFZ
26.	Saad	Butt	TK - DBFZ
27.	Elias	Grasemann	BR - DBFZ
28.	Fabian	Findeisen	TK - DBFZ
29.	Manfred	Eiden	TK - DBFZ
30.	Schliermann	Thomas	BR - DBFZ

Scientific Committee

- Fouzi Tabet, DBFZ Deutsches Biomasseforschungszentrum gemeinnützige GmbH, Leipzig, Germany
- Andreas Ortwein, DBFZ Deutsches Biomasseforschungszentrum gemeinnützige GmbH, Leipzig, Germany
- Øyvind Skreiberg, SINTEF („Stiftelsen for industriell og teknisk forskning“) Energy Research, Trondheim, Finland
- Martin Miltner, Technical University of Vienna, Vienna, Austria
- Brahim Sarh, University of Orleans, Orleans, France

Organization committee

- Fouzi Tabet, DBFZ Deutsches Biomasseforschungszentrum gemeinnützige GmbH, Leipzig, Germany
- Andrea Dernbecher, DBFZ Deutsches Biomasseforschungszentrum gemeinnützige GmbH, Leipzig, Germany

Organizer:

DBFZ Deutsches Biomasseforschungszentrum
gemeinnützige GmbH
Torgauer Straße 116
04347 Leipzig
Phone: +49 (0) 341 2434-112
Fax: +49 (0) 341 2434-133
E-Mail: info@dbfz.de
www.dbfz.de

With support from

Federal Ministry
of Food
and Agriculture

by decision of the
German Bundestag